

ISSN : 2165-4069(Online)

ISSN : 2165-4050(Print)



IJARAI

International Journal of  
Advanced Research in Artificial Intelligence

Volume 2 Issue 8

[www.ijarai.thesai.org](http://www.ijarai.thesai.org)

A Publication of  
The Science and Information Organization



INTERNATIONAL JOURNAL OF  
ADVANCED RESEARCH IN ARTIFICIAL INTELLIGENCE



THE SCIENCE AND INFORMATION ORGANIZATION  
[www.thesai.org](http://www.thesai.org) | [info@thesai.org](mailto:info@thesai.org)



## Editorial Preface

### *From the Desk of Managing Editor...*

"The question of whether computers can think is like the question of whether submarines can swim." — Edsger W. Dijkstra, the quote explains the power of Artificial Intelligence in computers with the changing landscape. The renaissance stimulated by the field of Artificial Intelligence is generating multiple formats and channels of creativity and innovation.

This journal is a special track on Artificial Intelligence by The Science and Information Organization and aims to be a leading forum for engineers, researchers and practitioners throughout the world.

The journal reports results achieved; proposals for new ways of looking at AI problems and include demonstrations of effectiveness. Papers describing existing technologies or algorithms integrating multiple systems are welcomed. IJARAI also invites papers on real life applications, which should describe the current scenarios, proposed solution, emphasize its novelty, and present an in-depth evaluation of the AI techniques being exploited. IJARAI focusses on quality and relevance in its publications.

In addition, IJARAI recognizes the importance of international influences on Artificial Intelligence and seeks international input in all aspects of the journal, including content, authorship of papers, readership, paper reviewers, and Editorial Board membership.

The success of authors and the journal is interdependent. While the Journal is in its initial phase, it is not only the Editor whose work is crucial to producing the journal. The editorial board members, the peer reviewers, scholars around the world who assess submissions, students, and institutions who generously give their expertise in factors small and large— their constant encouragement has helped a lot in the progress of the journal and shall help in future to earn credibility amongst all the reader members.

I add a personal thanks to the whole team that has catalysed so much, and I wish everyone who has been connected with the Journal the very best for the future.

**Thank you for Sharing Wisdom!**

**Managing Editor**  
**IJARAI**  
**Volume 2 Issue 8 August 2013**  
**ISSN: 2165-4069(Online)**  
**ISSN: 2165-4050(Print)**  
**©2013 The Science and Information (SAI) Organization**

# Editorial Board

**Peter Sapaty - Editor-in-Chief**

**National Academy of Sciences of Ukraine**

Domains of Research: Artificial Intelligence

**Alaa F. Sheta**

**Electronics Research Institute (ERI)**

Domain of Research: Evolutionary Computation, System Identification, Automation and Control, Artificial Neural Networks, Fuzzy Logic, Image Processing, Software Reliability, Software Cost Estimation, Swarm Intelligence, Robotics

**Antonio Dourado**

**University of Coimbra**

Domain of Research: Computational Intelligence, Signal Processing, data mining for medical and industrial applications, and intelligent control.

**David M W Powers**

**Flinders University**

Domain of Research: Language Learning, Cognitive Science and Evolutionary Robotics, Unsupervised Learning, Evaluation, Human Factors, Natural Language Learning, Computational Psycholinguistics, Cognitive Neuroscience, Brain Computer Interface, Sensor Fusion, Model Fusion, Ensembles and Stacking, Self-organization of Ontologies, Sensory-Motor Perception and Reactivity, Feature Selection, Dimension Reduction, Information Retrieval, Information Visualization, Embodied Conversational Agents

**Liming Luke Chen**

**University of Ulster**

Domain of Research: Semantic and knowledge technologies, Artificial Intelligence

**T. V. Prasad**

**Lingaya's University**

Domain of Research: Bioinformatics, Natural Language Processing, Image Processing, Robotics, Knowledge Representation

**Wichian Sittiprapaporn**

**Maharakham University**

Domain of Research: Cognitive Neuroscience; Cognitive Science

**Yaxin Bi**

**University of Ulster**

Domains of Research: Ensemble Learning/Machine Learning, Multiple Classification Systems, Evidence Theory, Text Analytics and Sentiment Analysis

---

## Reviewer Board Members

- **Alaa Sheta**  
Electronics Research Institute (ERI)
- **Albert Alexander**  
Kongu Engineering College
- **Amir HAJJAM EL HASSANI**  
Université de Technologie de Belfort-Monbéliard
- **AmitVerma**  
Department in Rayat&Bahra Engineering College,Mo
- **Antonio Dourado**  
University of Coimbra
- **B R SARATH KUMAR**  
Lenora College of Engineering
- **BabatundeOpeoluwaAkinkunmi**  
University of Ibadan
- **BestounS.Ahmed**  
UniversitiSains Malaysia
- **Chien-PengHo**  
Information and Communications Research Laboratories, Industrial Technology Research Institute of Taiwan
- **David M W Powers**  
Flinders University
- **DimitrisChrysostomou**  
Democritus University
- **Dr.DhananjayR Kalbande**  
Mumbai University
- **Francesco Perrotta**  
University of Macerata
- **Frank Ibikunle**  
CovenantUniversity
- **Grigoras Gheorghe**  
"Gheorghe Asachi" Technical University of Iasi, Romania
- **GuandongXu**  
Victoria University
- **Haibo Yu**  
Shanghai Jiao Tong University
- **Jatinderkumar R. Saini**  
S.P.College of Engineering, Gujarat
- **Krishna Prasad Miyapuram**  
University of Trento
- **Luke Liming Chen**  
University of Ulster
- **Marek Reformat**  
University of Alberta
- **Md. Zia Ur Rahman**  
NarasaraopetaEngg. College, Narasaraopeta
- **MokhtarBeldjehem**  
University of Ottawa
- **MonjiKherallah**  
University of Sfax
- **Nitin S. Choubey**  
Mukesh Patel School of Technology Management &Eng
- **Rajesh Kumar**  
National University of Singapore
- **Rajesh K Shukla**  
Sagar Institute of Research & Technology-Excellence, Bhopal MP
- **RongrongJi**  
Columbia University
- **Said Ghoniemy**  
Taif University
- **Samarjeet Borah**  
Dept. of CSE, Sikkim Manipal University
- **Sana'a WafaTawfeek Al-Sayegh**  
University College of Applied Sciences
- **Saurabh Pal**  
VBS Purvanchal University, Jaunpur
- **ShahaboddinShamshirband**  
University of Malaya
- **ShaidahJusoh**  
Zarqa University
- **ShrinivasDeshpande**
- **SUKUMAR SENTHILKUMAR**  
UniversitiSains Malaysia
- **T C.Manjunath**  
HKBK College of Engg
- **T V Narayana Rao**  
Hyderabad Institute of Technology and Management
- **T. V. Prasad**

Lingaya's University

- **Vitus S.W Lam**  
Domains of Research
- **VUDA Sreenivasarao**  
St. Mary's College of Engineering &  
Technology
- **Vishal Goyal**
- **Wei Zhong**  
University of south Carolina Upstate
- **WichianSittiprapaporn**  
Mahasarakham University
- **Yaxin Bi**

University of Ulster

- **Yuval Cohen**  
The Open University of Israel
- **Zhao Zhang**  
Deptment of EE, City University of Hong  
Kong
- **Zne-Jung Lee**  
Dept. of Information management, Huafan  
University
- **Zhigang Yin**  
Institute of Linguistics, Chinese Academy of  
Social Sciences

# CONTENTS

**Paper 1: Comparison between Rayleigh and Mie Scattering Assumptions for Z-R Relation and Rainfall Rate Estimation with TRMM/PR Data**

*Author: Kohei Arai*

**PAGE 1 – 6**

**Paper 2: Comparative Study on Sea Surface Temperature Estimation with Thermal Infrared Radiometer Data among Conventional MCSST, Split Window and Conjugate Gradient Based Methods**

*Author: Kohei Arai*

**PAGE 7 – 15**

**Paper 3: Prediction Method of El Nino Southern Oscillation: ENSO by Means of Wavelet Based Data Compression with Appropriate Support Length of Base Function**

*Author: Kohei Arai*

**PAGE 16 – 20**

**Paper 4: Multi Spectral Image Classification Method with Selection of Independent Spectral Features through Correlation Analysis**

*Authors: Kohei Arai*

**PAGE 21 - 27**

**Paper 5: Access Fee Charging System for Information Contents Sharing Through P2P Communications**

*Authors: Kohei Arai*

**PAGE 28 – 33**

**Paper 6: Wearable Computing System with Input-Output Devices Based on Eye-Based Human Computer Interaction Allowing Location Based Web Services**

*Author: Kohei Arai*

**PAGE 34 - 39**

**Paper 7: Algorithm for Design of Digital Notch Filter Using Simulation**

*Authors: Dr.AmitVerma, Naina, Mrs.C.S. Vinitha*

**PAGE 40 – 43**

**Paper 8: Memetic Algorithm with Filtering Scheme for the Minimum Weighted Edge Dominating Set Problem**

*Authors: Shada N. Abdel-Aziz, Abdel-RahmanHedar, Adel A. Sewisy*

**PAGE 44 – 49**

# Comparison between Rayleigh and Mie Scattering Assumptions for Z-R Relation and Rainfall Rate Estimation with TRMM/PR Data

Kohei Arai

Graduate School of Science and Engineering  
Saga University  
Saga City, Japan

**Abstract**— Comparison of the rain rate estimated with the assumptions of Rayleigh and Mie scattering is made. We analyzed the different relationships between the radar reflectivity factor and rain rate (so-called Z-R relationship) with both scattering models for different DSD (droplet size distribution) and rainfall types as the wavelength is 2.2cm which is in accord with the band of TRMM/PR. Meanwhile we introduced a discrete ordinates method to retrieve the Z-R relationship for Mie scattering assumption. It is found that the retrieval result can be represented as the sum of some simple Z-R relationships. By the analysis of the Z-R relationships estimated from Rayleigh and Mie scattering assumptions in the rain types, we found that the difference of Z-R relationships between Rayleigh and Mie scattering in the thunderstorm that represents the larger raindrop size is larger than that in the drizzle that represents the smaller raindrop size.

**Keywords**—TRMM/PR; Precipitation; Z-R Relation; Rainfall Rate; Rayleigh scattering; Mie scattering; Droplet size distribution; Radar Reflectivity Factor;

## I. INTRODUCTION

Rainfall rate estimation of the Tropical Rainfall Measuring Mission: TRMM carries Precipitation Radar: PR is based on Z-R Relation (Z denotes radar reflectance factor, while R denotes rainfall rate)[1]. In order to estimate Z factor, attenuation due to rainfall and scattering due to raindrops is taken into account. Scattering due to raindrops depends on droplet size distribution under Rayleigh or Mie scattering assumptions. If the droplet size is greater than  $\lambda/8$  ( $\lambda$  denotes wavelength), then Mie scattering assumption is appropriate while that is less than  $\lambda/8$ , then Rayleigh scattering is assumed. Usually, Rayleigh scattering is assumed for rainfall rate estimation of TRMM/PR empirically [2], [3], [4].

It is reported that Mie scattering based Z factor estimation is better than that of Rayleigh scattering based estimation [5],[6]. Although these reports deal with influence due to different assumptions, Rayleigh and Mie scattering on Z factor estimation, there is no report which discusses the influence on rainfall rate estimation. The reason for this is difficulty on definition of Z-R Relation which is taken into account rainfall types [10], atmospheric conditions, topological effect, etc. There is a paper related to radar meteorology which deals with Z-R Relation based on empirical exponential law of 69 of different rainfall types, weather conditions, written by Battan

[7]. Also difficulty is caused by complicated computations of backscattered reflection factor based on Mie scattering assumption.

In this paper, rainfall rate estimation method based on Mie scattering is proposed together with some experimental background data for validation of the proposed method. Firstly, Z-R Relation based on Rayleigh and Mie scattering assumptions for three rainfall types, stratiform, drizzling, and thunder storm theoretically. Then both influences of the different scattering assumptions on Z-R Relation and rainfall rate estimations. There is mm order of droplet size according to Marshall and Palmer [9]. Wavelength of TRMM/PR is 22mm [8] so that Rayleigh limitation is situated at 2.75 mm. Therefore, it is better to adopt Mie scattering assumption for rainfall rate estimation for such large droplet size of rainfall.

The following section describes theoretical background of rainfall estimation followed by experimental data for validation of the proposed method. Then conclusion is described together with some discussions.

## II. THEORETICAL BACKGROUND

### A. Estimation of Rayleigh and Mie Scattering Based Z-R Relations

Averaged received reflectance can be represented as equation (1),

$$\eta = \int_{vol} \sigma_b N(D) dD = \frac{\pi^5}{\lambda^4} |K|^2 \int_0^{D_{max}} D^6 N(D) dD \quad (1)$$

where K denotes absorption coefficient of water and ice crystal while D denotes droplet radius, N(D) denotes size distribution and  $\sigma$  denotes backscattering cross section. Radar reflection factor, Z, then is represented in equation (2),

$$Z = \int_0^{D_{max}} D^6 N(D) dD \quad (2)$$

On the other hand, Mie scattering based Z factor is expressed as equation (3),

$$Z_{Mie} = \frac{\lambda^4}{\pi^5 |K|^2} \int_0^{D_{max}} \sigma_{Mie} N(D) dD \quad (3)$$

Then rainfall rate can be written in equation (4),

$$R = 6\pi * 10^{-4} \int_0^{D_{max}} D^3 N(D) \nu(D) dD \quad (4)$$

Where  $v(D)$  denotes droplet falling speed which is used to be represented as a function of droplet size. In this paper, exponential representation  $v(D) = cD^\gamma$  is used as usual. This is validated by Atlas and Ulbrich for the case,  $c=3.778$  and  $\gamma=0.67$  [11]. Gunn and Kitzner proves that this equation show a good coincidence with the calculation results of rainfall rate for the raindrop radius ranged from 0.5 to 5.0 mm [12].  $N(D)$  denotes droplet size distribution and is represented as equation (5) of gamma distribution proposed by Ulbrich [13],

$$N(D) = N_0 D^\mu \exp(-\Lambda D) \quad (5)$$

Where  $N_0$  denotes N axis cross section of droplet size distribution while  $D^*$  denotes the factorial of power law of raindroplet size distribution. Meanwhile,  $\mu$  denotes slope droplet size distribution in logarithmic-logarithmic expression. When  $\mu=0$ , then  $D^\mu=1$ . On the other hand,  $\Lambda$  defines exponential function based droplet size distribution,  $\Lambda = \alpha R^\beta$ . Thus Z factor can be represented as equation (6) and (7) using equations (2), (4) and (5) based on integral conversion of Gamma function [14].

$$Z = \int_0^{D_{max}} D^6 N_0 D^\mu \exp(-\Lambda D) dD = \frac{N_0}{\Lambda^{7+\mu}} \Gamma(7+\mu) \quad (6)$$

$$R = 6\pi * 10^{-4} \int_0^{D_{max}} D^3 N_0 D^\mu \exp(-\Lambda D) * 3.778 * D^{0.67} dD \quad (7)$$

$$= 6\pi * 10^{-4} * 3.778 * \frac{N_0}{\Lambda^{4.67+\mu}} \Gamma(4.67+\mu)$$

where  $\Gamma(x)$  denotes Gamma function.  $\Lambda$  can be obtained from the equation (7) the Z-R Relation can be reduced as follows,

$$Z = aR^b \quad (8)$$

Droplet size distribution is not so easy to estimated results in difficulty on determination of a, b coefficients. In general, droplet size distribution can be estimated with several actual observed data of Z factors based on iteration and /or regression [15], [16].

On the other hand, Mie scattering based Z-R Relation cannot be estimated with backscattering coefficients  $\sigma_{Mie}$  and droplet size distribution derived Gamma function of integral conversion.

Therefore,  $\sigma_{Mie}$  has to be expanded with Legendre function expansion as shown in equation (9),

$$\sigma_{Mie}(D) = r_0 P_0(D) + r_1 P_1(D) + r_2 P_2(D) + \dots + r_n P_n(D) \quad (9)$$

where

$$P_0(D) = 1, P_1(D) = D, P_2(D) = \frac{1}{2}(3D^2 - 1), P_3(D) = \frac{1}{2}(5D^3 - 3D), \dots$$

[17].  $\sigma_{Mie}$  for droplet size of D can be estimated based on Mie scattering theory [16]. The coefficients of  $\sigma_{Mie}$  of the equation (9)  $\{r_0, r_1, r_2, \dots, r_n\}$  can then be obtained through least square method with  $\sigma_{Mie}$  for each droplet size estimated based on Mie scattering theory.

Meanwhile, there is the following relation between Legendre function  $\{P_0, P_1, P_2, \dots, P_n\}$  and droplet size as follows,

$$Z_{Mie} = \frac{\lambda^4}{\pi^5 |K|^2} (a_0 \int_0^{D_{max}} N(D) dD + a_1 \int_0^{D_{max}} DN(D) dD + \dots + a_n \int_0^{D_{max}} D^n N(D) dD)$$

$$= \frac{\lambda^4 N_0}{\pi^5 |K|^2} \left( \frac{a_0}{\Lambda^{1+\mu}} \Gamma(1+\mu) + \frac{a_1}{\Lambda^{2+\mu}} \Gamma(2+\mu) + \dots + \frac{a_n}{\Lambda^{n+1+\mu}} \Gamma(n+1+\mu) \right) \quad (10)$$

Thus the equation (3) can be rewritten results in equation (11) of Z factor,

$$Z_{Mie} = p_0 R^{l_0} + p_1 R^{l_1} + \dots + p_n R^{l_n} \quad (11)$$

### B. Evaluation of Rainfall Rate Estimation based on Rayleigh and Mie Scattering Assumptions

F. Yoshino [7], Christian Matzler [6], and the others estimate parameters of droplet size distributions, stratiform (Marshall and Palmer), drizzling (Joss-Drizzle), thunderstorm (Joss-Thunderstorm) and realistic rainfall (Laws-Persons) by using Normalized distribution (Marshall-Palmer: MP, Joss-Drizzle: JD, Joss-Thunderstorm: JT and LP distributions). Typical parameters of these different types of rainfall are shown in Table 1. Droplet size distribution, on the other hand, is shown in Figure 1.

TABLE I. PARAMETERS FOR LP, MP, JD, JT DISTRIBUTIONS

Distribution Function	$N_0(R)$	$\Lambda(R)$
LP	1.98E-5R <sup>-(0.384)</sup>	5.38R <sup>^(-0.186)</sup>
MP	8.0E-06	4.1R <sup>^(-0.21)</sup>
JD	3.0E-05	5.7R <sup>^(-0.21)</sup>
JT	1.4E-06	3.0R <sup>^(-0.21)</sup>

Distribution Function	$\mu$	Z-R	Rain Type
LP	2.93	378R <sup>^1.43</sup>	realistic DSD
MP	0	298R <sup>^1.50</sup>	stratiform rain
JD	0	120R <sup>^1.49</sup>	Drizzle
JT	0	536R <sup>^1.48</sup>	Thunderstorm

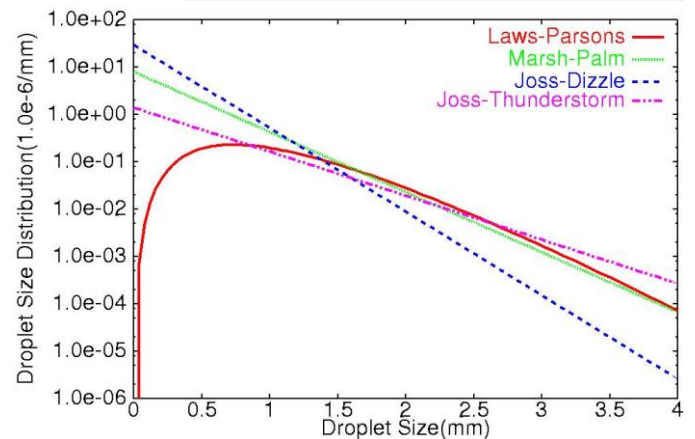


Fig.1. Droplet size distribution of four typical rainfall models

The parameters shown in Table 1 are estimated based on Rayleigh scattering assumption. Thunderstorm is

characterized as relatively large “a” and comparatively small “b” while stratiform is characterized as relatively small “a” and comparatively large “b”. These estimated results are coincident to Z-R Relation which is estimated by RemkoUijlenhoet et al. [14].

Next Mie scattering based Z-R Relation is estimated. In general, the number of droplets is decreasing in accordance with decreasing of droplet size [10]. From Figure 2, it is set that droplet size ranges from 1 to 6.4 mm while air temperature is assumed to be 20 degree centigrade under the standard atmospheric pressure.

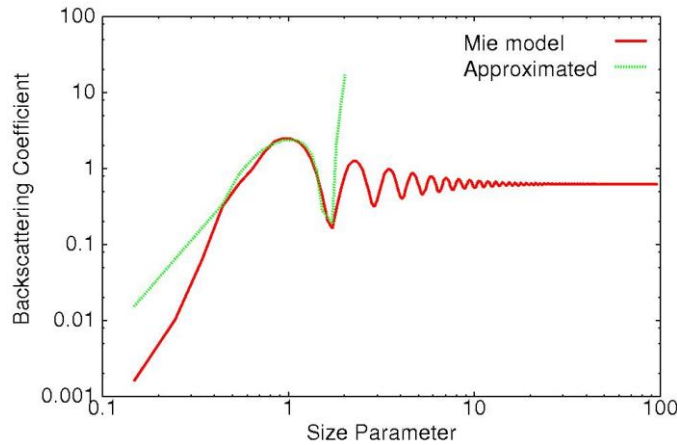


Fig.2. Mie scattering based backscattering coefficient and its approximated coefficient

Wavelength is assumed to be 22 mm as of TRMM/PR wavelength. According to F. Yoshino, droplet refractive index is assumed to be  $8.02 - i 2.00$  through linear interpolation [10]. Backscattering coefficient is calculated with Mie2New which is included in MODTRAN (Radiative transfer software code) [19]. The 6 coefficients in the equation (9) are estimated through least square method by using 5 Legendre functions with Mie scattering code. The estimated coefficients are shown in equation (12).

$$\{a_0, a_1, a_2, \dots, a_5\} = \{3.1927, -3.6439, 2.0386, 3.6681, -3.4678, 0.6950\} \quad (12)$$

Size parameter which is shown in Figure 2 is expressed as  $\pi D$  in unit of cm. Both Mie scattering based backscattering coefficient and its approximation shows coincidence for the range from 3 to 20 mm of size parameter. The corresponding droplet size ranges from 1 to 6.4 mm.

Thus Mie scattering based Z-R Relation can be estimated. These are shown in equations (13), (14) and (15)

$$Z_{strat} = (1.45R^{0.2293} + 6.34R^{0.4393} - 9.50R^{0.6493} + 1.78R^{0.8593} - 1.07R^{1.0693} + 5.64R^{1.2793}) * 100 \quad (13)$$

$$Z_{drz} = (4.86R^{0.2293} + 15.28R^{0.4393} - 16.47R^{0.6493} + 2.22R^{0.8593} - 0.96R^{1.0693} + 3.64R^{1.2793}) * 100 \quad (14)$$

$$Z_{thund} = (0.46R^{0.2293} + 2.75R^{0.4393} - 5.64R^{0.6493} + 1.44R^{0.8593} - 1.19R^{1.0693} + 8.54R^{1.2793}) * 100 \quad (15)$$

Figure 3 shows Z factors for three different rainfall types, drizzling, stratiform and thunderstorm under the assumptions of Rayleigh and Mie scatterings.

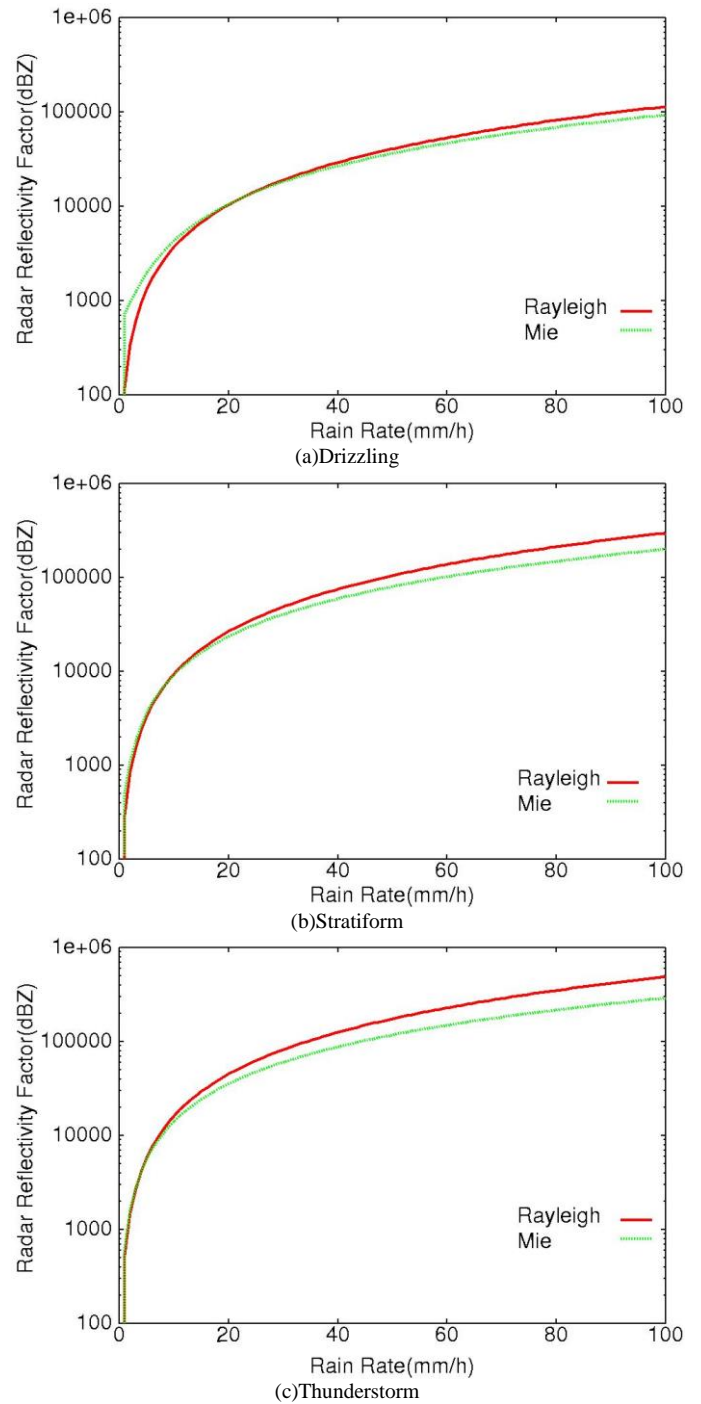


Fig.3. Rayleigh and Mie scattering based Z-R Relations

For relatively small rainfall rate, both Rayleigh and Mie scattering based Z-R Relations are coincident. Meanwhile, the difference between both is getting large in accordance with rainfall rate is increased. Also it is found that the difference between both is getting large in accordance with increasing of droplet size.

### III. EXPERIMENTS

#### A. Method for Experiment

TRMM/PR data of 2A25 product (Z value at ground surface after the rainfall attenuation correction) is used. Also ground based rain radar data (2.8GHz of radar frequency) is used for validation. The radar site is situated at Houston, Texas and Kwajalein Atoll. TRMM/PR data of Houston is acquired on October 24 2005 while that of Kwajalein Atoll is acquired on September 15 and 20 2008. These acquisition location and dates are selected from the TRMM/PR GV data for validation of TRMM/PR show heavy rainfall with much greater than 40 mm/hr in the year of 2008.

The radar data is a portion of GV data for validation of TRMM/PR. Rainfall rate obtained from the GV data are mapped onto longitude / latitude coordinate mesh. Therefore, it is easy to find the location through pattern matching between rainfall rate pattern derived from TRMM/PR and the GV data. Rainfall pattern of Houston derived from TRMM/PR data is compared to ground based radar data of Houston.

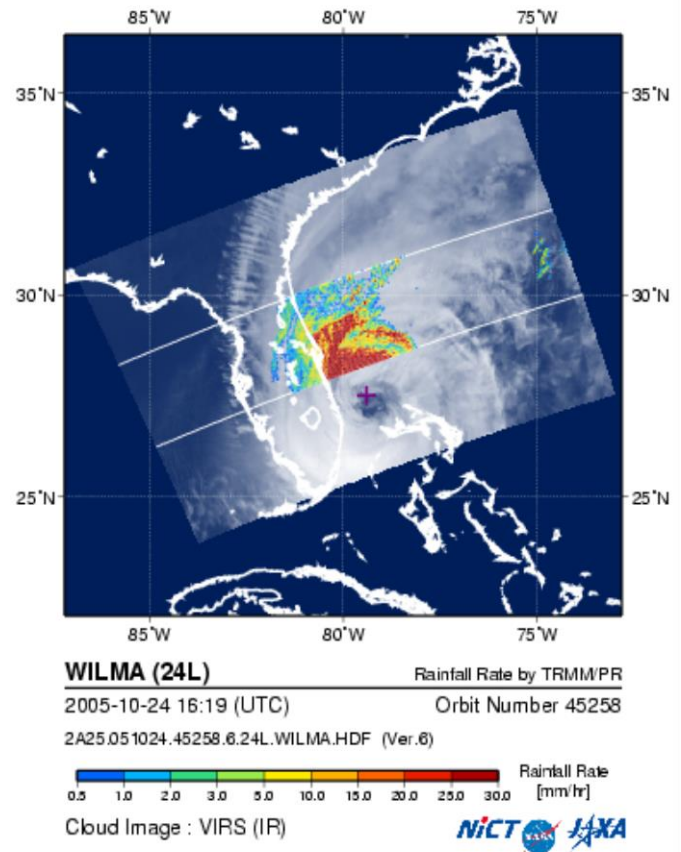
Meanwhile, the GV data of Kwajalein Atoll is used for comparison of Rayleigh and Mie scattering based rainfall rate. Rainfall rate of Kwajalein Atoll acquired on September 15 is heavier than September 20. TRMM/PR data at range bin number of 60 for the TRMM/PR data acquired on September 15 shows rainfall while that for September 20 does not show such rainfall. Equation (15) of Z-R Relation which is represented as Mie scattering based rainfall rate estimation is used.

#### B. Experimental Results

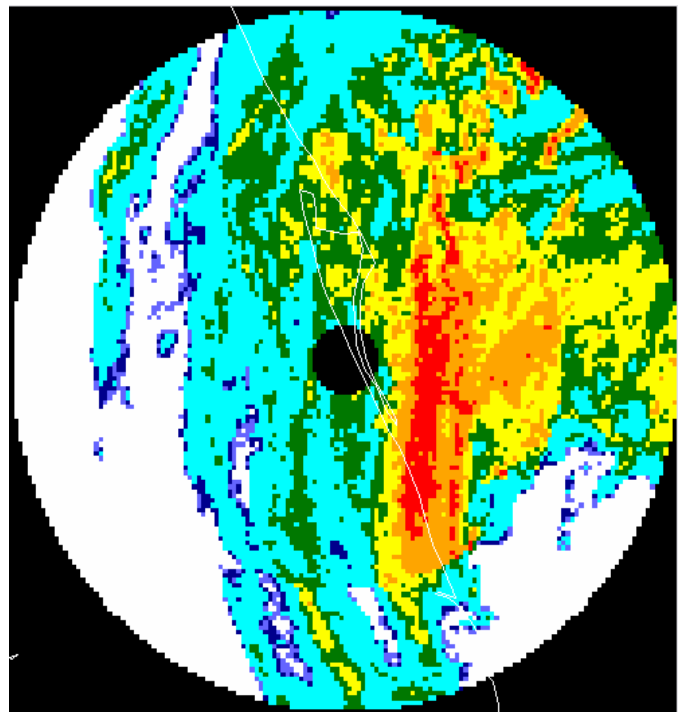
Figure 4 (a) shows TRMM/PR derived rainfall rate for hurricane Wilma while (b) shows ground based radar data derived rainfall rate acquired at around same time on 24 October 2005. Figure 4 (a) shows narrow swath of TRMM/PR data derived rainfall rate on the imagery data which is derived from VIRS (Visible to Infrared Radiometer which is onboard the same satellite of TRMM). Both rainfall rates show a good coincidence.

Figure 5 (a) and (b) shows vertical profiles of the estimated rainfall rate derived from TRMM/PR data of Kwajalein Atoll acquired on 15 September (a) and on 20 September (b), respectively. Figure 5 also shows comparison of the estimated rainfall rate between Rayleigh and Mie scattering assumption for relatively heavy rainfall (September 15) and comparatively light rainfall (September 20), respectively.  $R_{rayleigh}$  and  $R_{mie}$  denote the estimated rainfall rate under the Rayleigh scattering assumption and that under the Mie scattering assumption. On the other hand,  $\Delta R$  denotes the difference between both estimated rainfall rates.  $\Delta R$  near the surface is greater than that in the high altitude. Also  $\Delta R$  for heavy rain is greater than that for light rain.

Figure 6 (a) shows the relation between  $R_{rayleigh}$ ,  $R_{mie}$  as well as  $\Delta R$  and true rainfall rate derived from ground based radar data as GV data for relatively heavy rainfall while those for comparatively light rainfall is shown in Figure 6 (b). Figure 6 also shows linear approximation of relation between both.



(a)TRMM/PR



(b)Ground based radar

Fig.4. Comparison of estimated rainfall rate between TRMM/PR and ground based radar

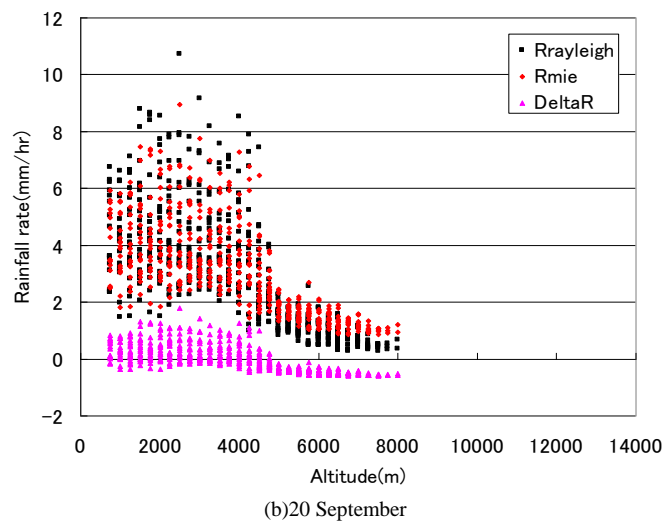
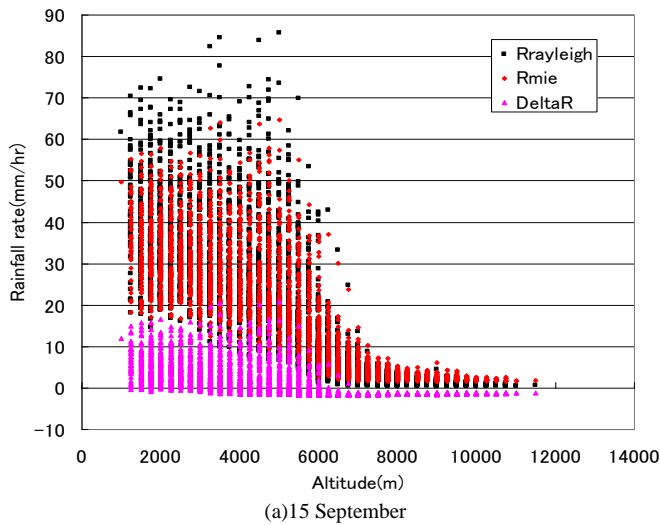


Fig.5. Estimated rainfall rate derived from TRMM/PR of Kwajalein Atoll acquired on 15 and 20 September 2008. Comparison of the estimated rainfall rate based on Rayleigh and Mie scattering assumptions.

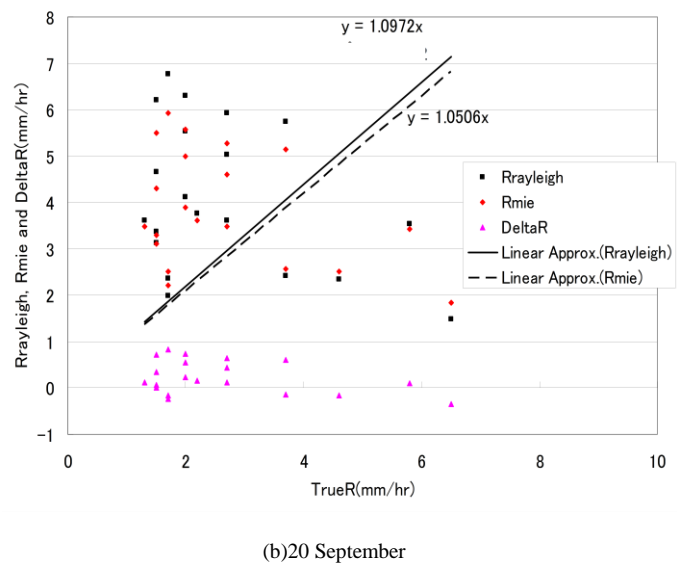
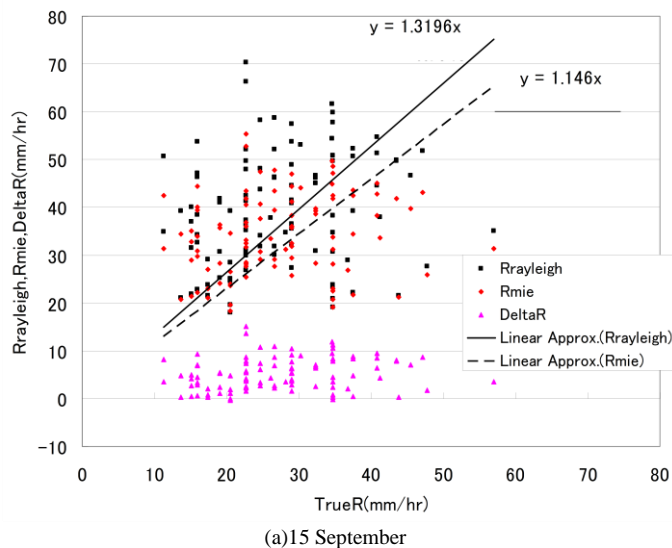


Fig.6. Relation between Rayleigh, Rmie as well as Delta R and true rainfall rate derived from ground based radar data as GV data for relatively heavy rainfall while those for comparatively light rainfall

#### IV. CONCLUSION

Comparison of the rain rate estimated with the assumptions of Rayleigh and Mie scattering is made. We analyzed the different relationships between the radar reflective factor and rain rate (so-called Z-R relationship) with both scattering models for different DSD (droplet size distribution) and rainfall types as the wavelength is 2.2cm which is in accord with the band of TRMM/PR. Meanwhile we introduced a discrete ordinates method to retrieve the Z-R relationship for Mie scattering assumption. It is found that the retrieval result can be represented as the sum of some simple Z-R relationships. By the analysis of the Z-R relationships estimated from Rayleigh and Mie scattering assumptions in the rain types, we found that the difference of Z-R relationships between Rayleigh and Mie scattering in the thunderstorm that represents the larger raindrop size is larger than that in the drizzle that represents the smaller raindrop size. The followings are concluded,

- 1) Estimation of Z-R Relation based on Mie scattering theory by using Legendre function of approximation has been conducted.
- 2) Z-R Relation based on Rayleigh scattering theory can be represented with exponential function while Z-R Relation based on Mie scattering theory can be represented with summation of exponential functions.
- 3) Z-R Relations based on both Rayleigh and Mie scattering theories are coincident when raindrop size is relatively large while these are not coincident when raindrop size is small through analysis with four types of size distributions of stratiform rain, drizzling and thunder storm as well as actual rain.
- 4) In particular, the difference of Z-R Relation between thunder storm and stratiform is greatest followed by between drizzling.

5) *Rainfall rate estimation based on Mie scattering theory is much closer to ground based rain radar derived rainfall rate rather than that based on Rayleigh scattering theory for the hurricane "Wilmer" which hit Florida peninsula on 24 October 2005 observed with TRMM/PR of which raindrop size is relatively large at the boundary layer. The reason for this would be the fact that backward scattering is relatively small and forward scattering is comparatively large for Mie scattering while backward and forward scattering are almost same for Rayleigh scattering.*

#### ACKNOWLEDGMENT

The author would like to thank Dr. Xing MingLiang of NOAA/NESDIS for his effort to conduct the experiments.

#### REFERENCES

- [1] K.Okamoto, edit. Earth Environment Observations, Ohm Publishing Co. Ltd., 1999.
- [2] R. Meneghini, et. al., Use of the surface reference techniques for path attenuation estimates from the TRMM precipitation radar, *Journal of Applied Meteorology*, 39, pp.2053-2070, 2000.
- [3] Meneghini, R., S. W. Bidwell, R. Rincon, and G. M. Heymsfield, Differential-frequency Doppler weather radar: Theory and experiment, *RADIO SCIENCE*, 38(3), 2003.
- [4] M. Šálek, J.L. Cheze, J. Handwerker, L. Delobbe and R. Uijlenhoet, Radar techniques for identifying precipitation type and estimating quantity of precipitation, Document of COST Action 717, WG 1, 2004.
- [5] K.K. Comstock, R. Wood, S.E. Yuter, C.S. Bretherton, Reflectivity and rain rate in and below drizzling stratocumulus, *Quarterly Journal of the Royal Meteorological Society*, 130:603603, pp.2891-2918, 2004.
- [6] C. Mätzler, Drop-Size Distributions and Mie Computations for Rain, Institut für Angewandte Physik, Research Report No. 2002-16, 2002
- [7] L.J. Battan, Radar Observation of the Atmosphere, Univ. of Chicago Press, Chicago, Illinois, 324p., 1973.
- [8] TRMM Precipitation Radar Team, Tropical Rainfall Measuring Mission (TRMM) Precipitation Radar Algorithm, Instruction Manual for Version 6, JAXA and NASA, 2005.
- [9] M. Marzoug, and P.Amayenc, A class of single frequency algorithms for rain rate profiling from a spaceborne radar, 1. Principle and tests from numerical simulations, *Journal of Atmospheric and Oceanic Technology*, 11, pp.1480-1506, 1994.
- [10] F.Yoshino, Radar Hydrology, MorikitaShuppan Publishing Co. Ltd, 2002.
- [11] D. Atlas, C.W. Ulbrich, Path- and Area-Integrated Rainfall Measurement by Microwave Attenuation in the 1–3 cm Band, *Journal of Applied Metrology*, 16(12), pp.1322-1331, 1977
- [12] R. Gunn, G.D. Kinzer, THE TERMINAL VELOCITY OF FALL FOR WATER DROPLETS IN STAGNANT AIR, *Journal of the Atmospheric Sciences*, 6(4), pp.243-248, 1949.
- [13] C.W. Ulbrich, Natural Variations in the Analytical Form of the Raindrop Size Distribution, *Journal of Applied Meteorology*, 22(10), pp.1764-1775, 1983.
- [14] U. Remko, Raindrop size distributions and radar reflectivity–rain rate relationships for radar hydrology, *Hydrology and Earth System Sciences*, 5(4), pp.615-627, 2001
- [15] T. Iguchi, and R. Meneghini, Intercomparison of single frequency methods for receiving a vertical rain profile from airborne and spaceborne radar data, *Journal of Atmospheric and Oceanic Technology*, 11, 1507-1516, 1994.
- [16] Iguchi, T., T.Kozu, R.Meneghini, J.Awaka and K.Okamoto, Rain-profiling algorithm for the TRMM precipitation radar, *Journal of Applied Meteorology*, 39, 2038-2052, 2000.
- [17] Murray R. Spiegel, McGraw-Hill Mathematical Formulas – Numerical Tables Handbook, Ohm Publishing Co. Ltd., 1998.
- [18] A.R. Jameson, and A. B. Kostinski, Spurious power-law relations among rainfall and radar parameters, *Q. J. R. Meteorol. Society*, 128, pp.2045–2058, 2002.
- [19] A. Berk, L.S. Bernstein, and D.C. Robertson, MODTRAN: A Moderate Resolution Model for LOWTRAN 7, Air Force Geophysics Laboratory Technical Report GL-TR-89-0122, Hanscom AFB, MA.
- [20] K.Okamoto, S. Kasane, Observed Results and Research and Development of TRMM/PR, Invited Paper of Journal of the Japanese Institute of Electronics, Information Communications, J91-B, 7,723-733,2008.

#### AUTHORS PROFILE

Kohei Aarai He received BS, MS and PhD degrees in 1972, 1974 and 1982, respectively. He was with The Institute for Industrial Science and Technology of the University of Tokyo from April 1974 to December 1978 and also was with National Space Development Agency of Japan from January, 1979 to March, 1990. During from 1985 to 1987, he was with Canada Centre for Remote Sensing as a Post Doctoral Fellow of National Science and Engineering Research Council of Canada. He moved to Saga University as a Professor in Department of Information Science on April 1990. He was a councilor for the Aeronautics and Space related to the Technology Committee of the Ministry of Science and Technology during from 1998 to 2000. He was a councilor of Saga University for 2002 and 2003. He also was an executive councilor for the Remote Sensing Society of Japan for 2003 to 2005. He is an Adjunct Professor of University of Arizona, USA since 1998. He also is Vice Chairman of the Commission-A of ICSU/COSPAR since 2008. He wrote 30 books and published 332 journal papers.

# Comparative Study on Sea Surface Temperature Estimation with Thermal Infrared Radiometer Data among Conventional MCSST, Split Window and Conjugate Gradient Based Methods

Kohei Arai

Graduate School of Science and Engineering  
Saga University  
Saga City, Japan

**Abstract**— Comparative study on Sea Surface Temperature: SST estimations among the conventional Multi-Channel Sea Surface Temperature: MCSST, split window method and the proposed Conjugate Gradient based method: CGM with Thermal Infrared Radiometer: TIR data through simulations is conducted. Utilizing the proposed linearized inversion of radiative transfer equation, SST can be estimated. SST estimation accuracy of the proposed method is compared to the conventional regression based method (Split Window and MCSST method). Through the simulation study, it is found that the proposed CGM based method is superior to the conventional regression based method.

**Keywords**— Sea Surface Temperature; radiative transfer equation; regression; conjugate gradient; MCSST; split window.

## I. INTRODUCTION

Sea Surface Temperature: SST estimation with thermal infrared radiometer onboard satellites is well known and widely used in a variety of research fields, in particular climate changes, global warming, etc. SST estimation methods are proposed [1]-[4]. Most of these are based on regressive analysis and use several spectral bands in Thermal Infrared: TIR wavelength region. The most dominant atmospheric factor is precipitable water. Using the different wavelength TIR bands whose influences due to water vapor are different, it is possible to reduce the influence. The most popular method is Multi Channel Sea Surface Temperature: MCSST [5]. Also previously proposed SST estimation methods are summarized by I. Barton [6]. In the same time, comparative study among the previously proposed methods is well reported [7].

Based on radiative transfer equation, inversion based SST estimation method is proposed [8]. Nonlinear radiative transfer equation is linearized then optimum combination of wavelength regions are selected [9]. Other than that, Geographic Information System: GIS based neural network is proposed for SST estimation method [10]. In this paper, linearized inversion based SST estimation method is utilized. Conjugate gradient method is applied to solve the linearized radiative transfer equation.

The following section describes the proposed SST estimation method with some theoretical background followed

by some experiments with the conventional regression based methods. Then conclusion is described together with some discussions.

## II. PROPOSED METHOD

### A. Theoretical Background on SST Estimation with Thermal Infrared Radiometer Data

Radiation from a blackbody with physical temperature of T is expressed in equation (1)

$$B_{\nu}(T) = \frac{2hc^2}{\lambda^5(\exp(\frac{hc}{\lambda kT}) - 1)} [W \cdot cm^{-2} \cdot sr^{-1} \cdot \mu m^{-1}] \quad (1)$$

Where

k : Boltzman constant [J/K]

h : Plank constant [J · s]

c : Light speed [m/s]

λ : Wavelength at wave number ν

The contribution from the atmosphere can be expressed as follows,

$$\tau(\theta, z_{\infty}, z) = \exp \left\{ - \int_z^{z_{\infty}} \frac{\rho(z)k(z)}{\cos(\theta)} dz \right\} \quad (2)$$

Where

θ : Observation zenith angle

ρ : Density of atmospheric constituents

k : Volume extinction coefficient

And

$$\int_z^{z_{\infty}} \frac{\rho(z)k(z)}{\cos(\theta)} dz$$

Is called as optical depth of the atmosphere.

### B. At Sensor Radiance of Thermal Infrared Radiometer

For sea surface observation with TIR radiometers onboard remote sensing satellites, radiance includes three components,

the contribution from sea surface, the contribution from the reflected radiance at sea surface and the contribution from the atmosphere.

$$I(\theta) = \int_{\lambda_1}^{\lambda_2} \Phi(\lambda) \left[ \{ \epsilon_{\lambda} B_{\lambda}(T_s) + (1 - \epsilon_{\lambda}) \int_{z_s}^{\infty} B_{\lambda}[T(z)] \frac{\partial \tau(\theta, z_{\infty}, z)}{\partial z} dz \} \cdot \tau(\theta, z_{\infty}, z_s) + \int_{z_s}^{\infty} B_{\lambda}[T(z)] \frac{\partial \tau(\theta, z_{\infty}, z)}{\partial z} dz \right] d\lambda \quad (3)$$

Where

$T_s$  : Sea surface temperature[K]

$\Phi$  : Spectral response function

$\epsilon$  : Emissivity

$\tau$  : Transparency

Spectral response function means spectral sensitivity function of spectral bands of TIR onboard satellites. In general, emissivity of sea surface in TIR wavelength region is almost 1. Therefore, the second term of the equation (3) can be neglected.

$$I(\theta) = \int_{\lambda_1}^{\lambda_2} \Phi(\lambda) \left\{ \epsilon_{\lambda} B_{\lambda}(T_s) \tau(\theta, z_{\infty}, z_s) + \int_{z_s}^{\infty} B_{\lambda}[T(z)] \frac{\partial \tau_{\lambda}(\theta, z_{\infty}, z)}{\partial z} dz \right\} d\lambda \quad (4)$$

### C. Approximation of At Sensor Radiance

Assuming spectral response function in the spectral wavelength region of spectral band is 1, then the equation (4) and be rewritten as follows,

$$I(\theta) = B_{\lambda}(T_s) \tau(\theta, z_{\infty}, z_s) + \int_{z_s}^{\infty} B_{\lambda}[T(z)] \frac{\partial \tau_{\lambda}(\theta, z_{\infty}, z)}{\partial z} dz \quad (5)$$

The second term of equation (5) can be approximated as follows,

$$\int_{z_s}^{\infty} B_{\lambda}[T(z)] \frac{\partial \tau_{\lambda}(\theta, z_{\infty}, z)}{\partial z} dz = [1 - \tau_i(\theta, z_{\infty}, z)] I_{ai} \quad (6)$$

Where  $I_{ai}$  denotes representative of spectral band  $i$  of radiance. Atmospheric transparency can be rewritten as follows,

$$\begin{aligned} \tau_i(u, \theta) &= c_{1i} \exp[-1(c_{2i} + c_{3i}m)u^{c_{4i}+c_{5i}m}] \\ &= c_{1i} \exp[-(c_{2i} + \frac{c_{3i}}{\cos \theta})u^{c_{4i} + \frac{c_{5i}}{\cos \theta}}] \\ m &\approx 1/\cos \theta \end{aligned} \quad (7)$$

Where  $u$  denotes precipitable water while  $m$  denotes slant length between sea surface and TIR instrument onboard satellites. In the TIR wavelength region, precipitable water is major absorbing continuants in the atmosphere. Through simulation studies with radiative transfer code of MODTRAN with six atmospheric models (Tropic, Mid. Latitude Summer, Mid. Latitude Winter, Sub Arctic Summer, Sub Arctic Winter

and 1976 US Standard Atmosphere), the coefficients are obtained as shown in Table 1.

TABLE I. COEFFICIENTS OF EQUATION (7) OBTAINED WITH MODTRAN OF ATMOSPHERIC SOFTWARE CODE

	$c_{n1}$	$c_{n2}$	$c_{n3}$
$c_{1i}$	0.8507924	0.9356485	0.9253728
$c_{2i}$	-0.0754923	-0.03505476	-0.03752114
$c_{3i}$	0.175898	0.08923810	0.1261287
$c_{4i}$	1.451688	1.739096	1.679308
$c_{5i}$	-0.2339985	-0.1563839	-0.1293923

Then  $I_{ai}$  is calculated as follows,

$$I_{ai} = F_i(I_{ak}) = A_{1i} + A_{2i}I_{ak} \quad (8)$$

The coefficients in the equation (8) are calculated with MODTRAN in the same manner which is mentioned above. Table 2 shows the results.

TABLE II. COEFFICIENTS OF EQUATION (8) OBTAINED WITH MODTRAN OF ATMOSPHERIC SOFTWARE CODE

	$A_{n1}$	$A_{n2}$	$A_{n3}$
$A_{1i}$	$-0.88610 \times 10^{-6}$	0.0	$0.75270 \times 10^{-6}$
$A_{2i}$	0.62180	1.0	1.0590

Consequently, radiance of spectral band  $i$  can be expressed as follows,

$$I_i = B_i[T_s] \tau_i(u, \theta) + [1 - \tau_i(u, \theta)] F_i(I_{ak}) \quad (9)$$

In order to avoid divergence of the solution, the following conditional equation is introduced.

$$X = \frac{X_{max} + X_{min}}{2} + \frac{X_{max} - X_{min}}{\pi} \arctan \xi \quad (10)$$

### D. Iteration Method for SST, Precipitable Water, and Representative Radiance

The unknown factors are as follows,

$$\mathbf{x} = (T_s, u, I_{ak}) \quad (11)$$

Namely, sea surface temperature, precipitable water, and representative radiance. The following cost function is introduced,

$$J(\mathbf{x}) = \sum_{i=1}^3 (I_i - \hat{I}_i)^2 \quad (12)$$

Then iteration is stopped when the cost function is below the designated value,

$$J(\mathbf{x}) \leq \varepsilon \quad (13)$$

Radiance of the spectral band  $i$  can be rewritten as follows,

$$\begin{aligned} I_i &= \frac{c1c_{1i}}{\lambda^3 \exp(\frac{c2}{\lambda T_s}) - 1} \exp \left\{ - \left( c_{2i} + \frac{c_{3i}}{\cos \theta} \right) u^{c_{4i} + \frac{c_{5i}}{\cos \theta}} \right\} \\ &+ \left[ 1 - c_{1i} \exp \left\{ - \left( c_{2i} + \frac{c_{3i}}{\cos \theta} \right) u^{c_{4i} + \frac{c_{5i}}{\cos \theta}} \right\} \right] (C_{1i} + C_{2i}I_{ak}) \end{aligned} \quad (14)$$

Then the following updating equation is introduced,

$$\mathbf{x}^{(n+1)} = \mathbf{x}^{(n)} + \beta^{(n)} A^{(n)} \nabla J[\mathbf{x}^{(n)}] \quad (15)$$

It is rewritten in matrix and vector as follows,

$$\begin{pmatrix} T_s \\ u \\ I_{ak} \end{pmatrix}^{(n+1)} = \begin{pmatrix} T_s \\ u \\ I_{ak} \end{pmatrix}^{(n)} + \beta^{(n)} \begin{pmatrix} \frac{\partial^2 J}{\partial T_s^2} & \frac{\partial^2 J}{\partial T_s \partial u} & \frac{\partial^2 J}{\partial T_s \partial I_{ak}} \\ \frac{\partial^2 J}{\partial u \partial T_s} & \frac{\partial^2 J}{\partial u^2} & \frac{\partial^2 J}{\partial u \partial I_{ak}} \\ \frac{\partial^2 J}{\partial I_{ak} \partial T_s} & \frac{\partial^2 J}{\partial I_{ak} \partial u} & \frac{\partial^2 J}{\partial I_{ak}^2} \end{pmatrix}^{-1} \begin{pmatrix} \frac{\partial J}{\partial T_s} \\ \frac{\partial J}{\partial u} \\ \frac{\partial J}{\partial I_{ak}} \end{pmatrix}^{(n)} \quad (16)$$

Where

$$\beta^{(n)} = 1/2^n \quad (17)$$

### E. Conjugate Gradient Method

In general,

$$\nabla f(\mathbf{x}) = \left( \frac{\partial f(\mathbf{x})}{\partial x_1}, \frac{\partial f(\mathbf{x})}{\partial x_2}, \dots, \frac{\partial f(\mathbf{x})}{\partial x_n} \right)^T \quad (18)$$

And

$$\nabla^2 f(\mathbf{x}) = \begin{pmatrix} \frac{\partial^2 f(\mathbf{x})}{\partial x_1^2} & \frac{\partial^2 f(\mathbf{x})}{\partial x_1 \partial x_2} & \dots & \frac{\partial^2 f(\mathbf{x})}{\partial x_1 \partial x_n} \\ \frac{\partial^2 f(\mathbf{x})}{\partial x_1 \partial x_1} & \frac{\partial^2 f(\mathbf{x})}{\partial x_2^2} & \dots & \frac{\partial^2 f(\mathbf{x})}{\partial x_2 \partial x_n} \\ \vdots & \vdots & \ddots & \vdots \\ \frac{\partial^2 f(\mathbf{x})}{\partial x_n \partial x_1} & \frac{\partial^2 f(\mathbf{x})}{\partial x_n \partial x_2} & \dots & \frac{\partial^2 f(\mathbf{x})}{\partial x_n^2} \end{pmatrix} \quad (19)$$

Therefore, the cost function can be rewritten as follows,

$$J = f(\mathbf{x}), H_n = \nabla^2 f(\mathbf{x}) \quad (20)$$

Where

$$H_n = \begin{pmatrix} \frac{\partial^2 J}{\partial T_s^2} & \frac{\partial^2 J}{\partial T_s \partial u} & \frac{\partial^2 J}{\partial T_s \partial I_{ak}} \\ \frac{\partial^2 J}{\partial u \partial T_s} & \frac{\partial^2 J}{\partial u^2} & \frac{\partial^2 J}{\partial u \partial I_{ak}} \\ \frac{\partial^2 J}{\partial I_{ak} \partial T_s} & \frac{\partial^2 J}{\partial I_{ak} \partial u} & \frac{\partial^2 J}{\partial I_{ak}^2} \end{pmatrix} \quad (21)$$

is called Hessian or Hesse matrix.

Equation (1) can be rewritten as follows,

$$B_\nu(T_s) = \frac{c_i}{\exp(\frac{c_0 i}{T_s}) - 1}$$

$$B_\nu(T) = \frac{c1}{\lambda^3 (\exp(\frac{c2}{\lambda T}) - 1)} \quad (22)$$

where

$$c_i : 2hc^2/\lambda_i^5$$

$$c_{0i} : ch/\lambda_i k$$

$$c1 : 2hc = 1.191126^{-12}$$

$$c2 : ch/k = 1.43889 \quad (23)$$

Then the unknown variables are estimated through iterations.

### F. Estimation of Hessian

The first derivatives of the cost function are expressed as follows,

$$\frac{\partial J}{\partial T_s} = -2 \sum_{i=1}^3 (I_i - \hat{I}_i) \frac{\partial \hat{I}_i}{\partial T_s}$$

$$\frac{\partial J}{\partial u} = -2 \sum_{i=1}^3 (I_i - \hat{I}_i) \frac{\partial \hat{I}_i}{\partial u}$$

$$\frac{\partial J}{\partial I_{ak}} = -2 \sum_{i=1}^3 (I_i - \hat{I}_i) \frac{\partial \hat{I}_i}{\partial I_{ak}} \quad (24)$$

Also the second derivatives are represented as follows,

$$\frac{\partial^2 J}{\partial T_s^2} = 2 \sum_{i=1}^3 \left\{ \frac{\partial \hat{I}_i}{\partial T_s} \frac{\partial \hat{I}_i}{\partial T_s} - (I_i - \hat{I}_i) \frac{\partial^2 \hat{I}_i}{\partial T_s^2} \right\}$$

$$\frac{\partial^2 J}{\partial T_s \partial u} = 2 \sum_{i=1}^3 \left\{ \frac{\partial \hat{I}_i}{\partial u} \frac{\partial \hat{I}_i}{\partial T_s} - (I_i - \hat{I}_i) \frac{\partial^2 \hat{I}_i}{\partial T_s \partial u} \right\}$$

$$\frac{\partial^2 J}{\partial T_s \partial I_{ak}} = 2 \sum_{i=1}^3 \left\{ \frac{\partial \hat{I}_i}{\partial I_{ak}} \frac{\partial \hat{I}_i}{\partial T_s} - (I_i - \hat{I}_i) \frac{\partial^2 \hat{I}_i}{\partial T_s \partial I_{ak}} \right\}$$

$$\frac{\partial^2 J}{\partial u \partial T_s} = 2 \sum_{i=1}^3 \left\{ \frac{\partial \hat{I}_i}{\partial T_s} \frac{\partial \hat{I}_i}{\partial u} - (I_i - \hat{I}_i) \frac{\partial^2 \hat{I}_i}{\partial u \partial T_s} \right\}$$

$$\frac{\partial^2 J}{\partial u^2} = 2 \sum_{i=1}^3 \left\{ \frac{\partial \hat{I}_i}{\partial u} \frac{\partial \hat{I}_i}{\partial u} - (I_i - \hat{I}_i) \frac{\partial^2 \hat{I}_i}{\partial u^2} \right\}$$

$$\frac{\partial^2 J}{\partial u \partial I_{ak}} = 2 \sum_{i=1}^3 \left\{ \frac{\partial \hat{I}_i}{\partial I_{ak}} \frac{\partial \hat{I}_i}{\partial u} - (I_i - \hat{I}_i) \frac{\partial^2 \hat{I}_i}{\partial u \partial I_{ak}} \right\}$$

$$\frac{\partial^2 J}{\partial T_s \partial T_s} = 2 \sum_{i=1}^3 \left\{ \frac{\partial \hat{I}_i}{\partial T_s} \frac{\partial \hat{I}_i}{\partial T_s} - (I_i - \hat{I}_i) \frac{\partial^2 \hat{I}_i}{\partial T_s \partial T_s} \right\}$$

$$\frac{\partial^2 J}{\partial I_{ak} \partial u} = 2 \sum_{i=1}^3 \left\{ \frac{\partial \hat{I}_i}{\partial u} \frac{\partial \hat{I}_i}{\partial I_{ak}} - (I_i - \hat{I}_i) \frac{\partial^2 \hat{I}_i}{\partial I_{ak} \partial u} \right\}$$

$$\frac{\partial^2 J}{\partial I_{ak}^2} = 2 \sum_{i=1}^3 \left\{ \frac{\partial \hat{I}_i}{\partial I_{ak}} \frac{\partial \hat{I}_i}{\partial I_{ak}} - (I_i - \hat{I}_i) \frac{\partial^2 \hat{I}_i}{\partial I_{ak}^2} \right\} \quad (24)$$

The first derivatives of radiance are expressed as follows,

$$\frac{\partial I_i}{\partial T_s} = \frac{c_i c_{0i} c_{1i}}{T_s^2 \{ \exp(\frac{c_{0i}}{T_s}) - 1 \}^2} \exp \left\{ \frac{c_{0i}}{T_s} - \alpha_1 u^{\alpha_2} \right\}$$

$$\frac{\partial I_i}{\partial u} = c_{1i} \alpha_1 \alpha_2 \alpha_3 u^{\alpha_2 - 1} \left\{ (C_{1i} + C_{2i} I_{ak}) - \frac{c_i}{\exp(\frac{c_{0i}}{T_s}) - 1} \right\}$$

$$\frac{\partial I_i}{\partial I_{ak}} = C_{2i} \{ 1 - c_{1i} \exp(-\alpha_1 u^{\alpha_2}) \} \quad (25)$$

Also the second derivatives of radiance is represented as follows,

$$\frac{\partial^2 I_i}{\partial T_s^2} = \left[ c_i c_{0i} c_{1i} \exp \{ -\alpha_1 u^{\alpha_2} \} \right]$$

$$\left\{ \frac{-c_{0i} e^{\frac{c_{0i}}{T_s}} - 2T_s e^{\frac{c_{0i}}{T_s}}}{T^4 (e^{\frac{c_{0i}}{T_s}} - 1)^2} + \frac{2c_{0i} e^{\frac{c_{0i}}{T_s}}}{T^4 (e^{\frac{c_{0i}}{T_s}} - 1)^3} \right\}$$

$$\frac{\partial^2 I_i}{\partial T_s \partial u} = -\frac{c_i c_{0i} c_{1i}}{T_s^2 \{ \exp(\frac{c_{0i}}{T_s}) \}^2} \exp \left\{ \frac{c_{0i}}{T_s} - \alpha_1 u^{\alpha_2} \right\} \alpha_1 \alpha_2 u^{\alpha_2 - 1}$$

$$\frac{\partial I_i}{\partial T_s \partial I_{ak}} = 0$$

$$\frac{\partial^2 I_i}{\partial u \partial T_s} = -\frac{c_i c_{0i} c_{1i}}{T_s^2 \{ \exp(\frac{c_{0i}}{T_s}) - 1 \}^2} \alpha_1 \alpha_2$$

$$\exp \left\{ \frac{c_{0i}}{T_s} - \alpha_1 u^{\alpha_2} \right\} u^{\alpha_2 - 1}$$

$$\frac{\partial^2 I_i}{\partial u^2} = c_{1i} \alpha_1 \alpha_2 \left\{ (C_{1i} + C_{2i} I_{ak}) - \frac{c_i}{\exp(\frac{c_{0i}}{T_s}) - 1} \right\}$$

$$\frac{\partial^2 I_i}{\partial u \partial I_{ak}} = c_{1i} C_{2i} \alpha_1 \alpha_2 \alpha_3 u^{\alpha_2 - 1}$$

$$\frac{\partial^2 I_i}{\partial I_{ak} \partial T_s} = 0$$

$$\frac{\partial^2 I_i}{\partial I_{ak} \partial u} = c_{1i} C_{2i} \alpha_1 \alpha_2 \alpha_3 u^{\alpha_2 - 1}$$

$$\frac{\partial^2 I_i}{\partial I_{ak}^2} = 0 \quad (26)$$

where

$$\alpha_1 = c_{2i} + \frac{c_{3i}}{\cos \theta}$$

$$\alpha_2 = c_{4i} + \frac{c_{5i}}{\cos \theta}$$

$$\alpha_3 = \exp \{ -\alpha_1 u^{\alpha_2} \}$$

### G. Conventional Regression Based Method of Split Window

Split window method is based on regression with some training dataset which consists of truth data of SST and TIR spectral band data.

Namely, once regression analysis is made, then SST can be estimated with TIR spectral band data (TIR<sub>i</sub>). Regression analysis uses the following regressive equation,

$$T_s = \sum_i c_i TIR_i \quad (27)$$

Where  $c_i$  denotes regressive coefficients for spectral band  $i$ .

### H. Conventional MCSST

Multi Channel Sea Surface Temperature: MCSST is the method for SST estimation with NOAA/AVHRR (National Oceanic and Atmospheric Administration / Advanced Very High Resolution Radiometer) data. MCSST is based on split window method. AVHRR consist five channels, two channels in visible band, one channel in shortwave infrared band, and two channels in thermal infrared bands (Band 4 and 5). In general, MCSST is expressed in equation (28).

$$T_s = A \cdot TB_4 + B(TB_4 - TB_5) + C(TB_4 - TB_5)(\sec(\theta) - 1) + D(\sec(\theta) - 1) + E \quad (28)$$

where

- $T_s$  : Sea Surface Temperature
- $TB_i$  : Brightness Temperature of Band  $i$
- $\theta$  : Observation Zenith Angle
- $A, B, C, D, E$  : Regression Coefficients

In accordance with Kidwell, 1991, MCSST is expressed as follows,

$$T_s = 0.9731T_4 + 2.6353(T_4 - T_5) - 265.4789 \quad \text{for daytime,}$$

$$T_s = 0.9994T_4 + 2.7057(T_4 - T_5) - 0.27(T_4 - T_5)(\sec \theta_z - 1) + 0.73(\sec \theta_z - 1) - 273.0323 \quad \text{for nighttime,} \quad (29)$$

where  $T_s$  is given in °C and  $T_4$  and  $T_5$  are in Kelvin. The RMSE and the bias is 1.03°C and -0.51°C for daytime, and 0.73°C and 0.19°C for nighttime, respectively.

## III. EXPERIMENT

### A. Experimental Conditions

The following parameters are set for the experiments with MODTRAN obtaining at sensor radiance of spectral TIR band data.

Atmospheric Model: Tropic, Mid.Latitude Summer,  
Mid.Latitude Winter, SubArctic Summer, SubArctic  
Winter, 1976 US Standard Atmosphere

Constraint:  $\pm 2$  [K]

Meteorological Range:  $\pm 0\%$ ,  $\pm 10\%$ ,  $\pm 20\%$

Relative Humidity: Default x1.0, x1.1, x1.2, x0.9, x0.8

Air-Temperature: Default  $\pm 0$ ,  $\pm 3$  [K]

Sea surface temperature: Default  $\pm 0$ ,  $\pm 3$  [K]

Wind speed: 3.5, 7.0, 14.0 [m/s]

Aerosol Model: Navy Maritim, Maritim, Tropospheric, Desert

Observation Zenith Angle: 0, 30, 60 [deg]

Then SST is estimated with the proposed method and the conventional split window method using the calculated at sensor radiance.

**B. Example of Solution Behavior**

RMSE is estimated with a variety of precipitable water and representative radiance of TIR band. One of the examples of solution behavior is illustrated in Figure 1.

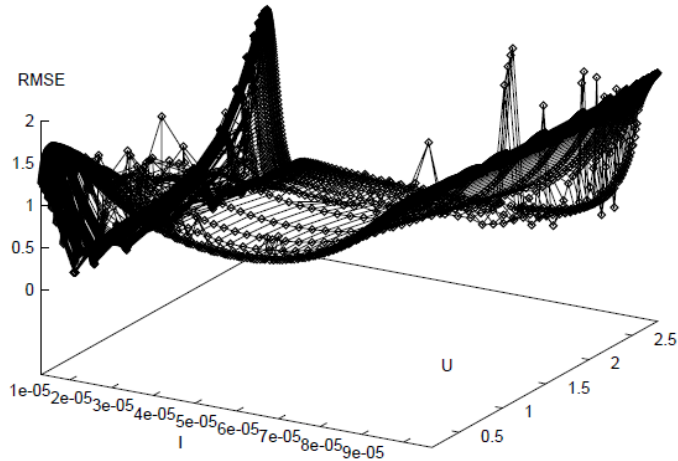
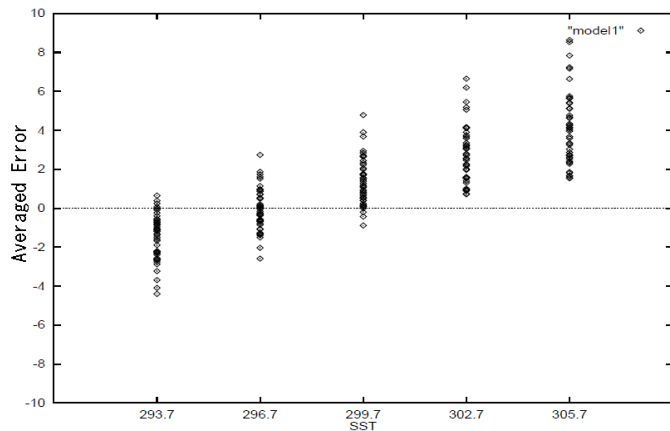
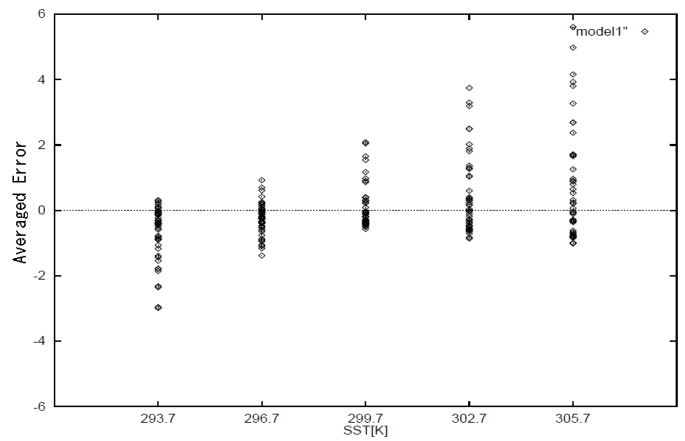


Fig.1. Example of solution behavior in solution space

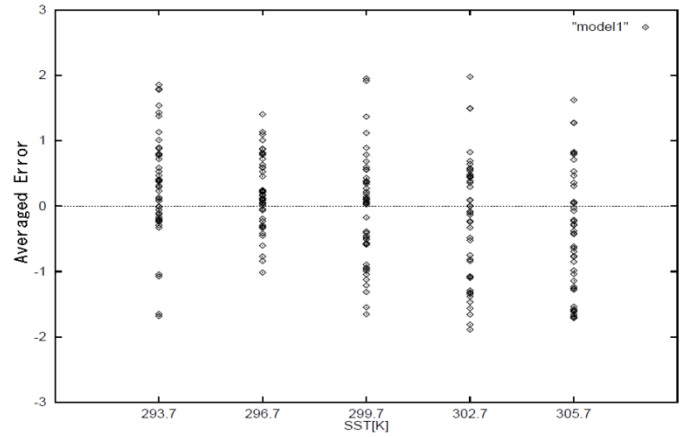
In general, RMSE (SST estimation error) is proportional to the precipitable water. On the other hands, the relation between representative radiance of TIR band and RMSE shows complicated characteristics, in particular for small representative radiance regions. This implies that it is not easy to find the global optimum in the solution space. In other words, it is easy to fall in one solution of local minima.



(a)MCSST

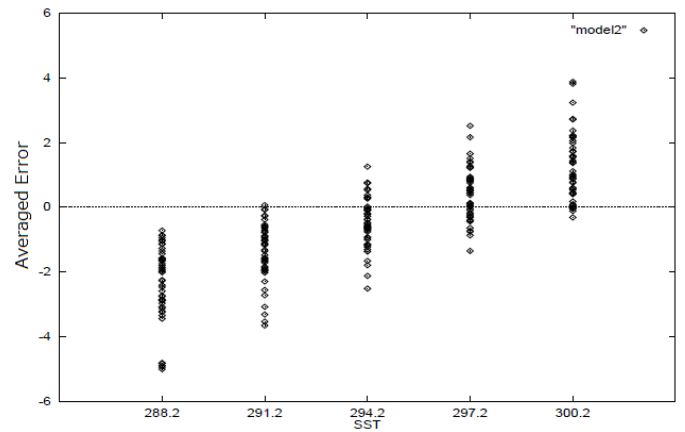


(b)Split Window

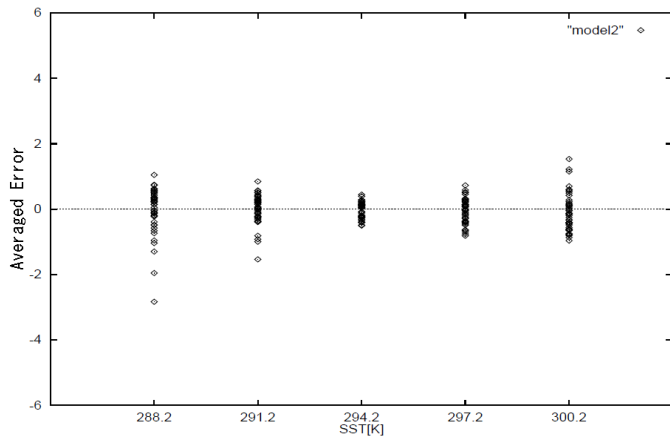


(c)Conjugate Gradient

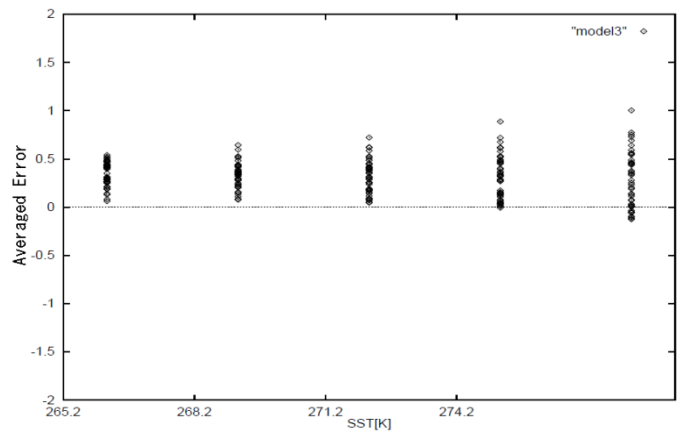
Fig.2. Averaged SST estimation error for Tropic atmosphere model



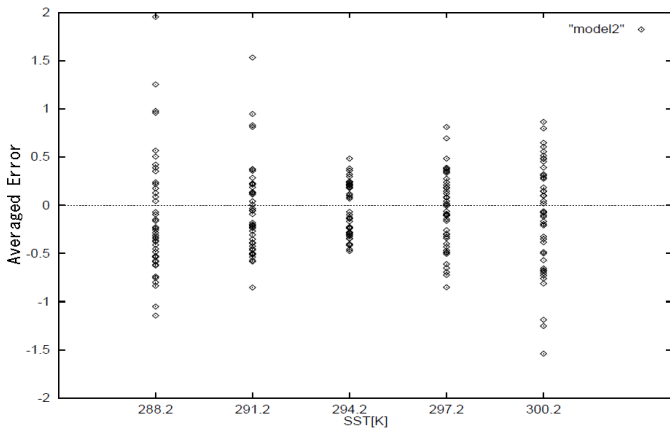
(a)MCSST



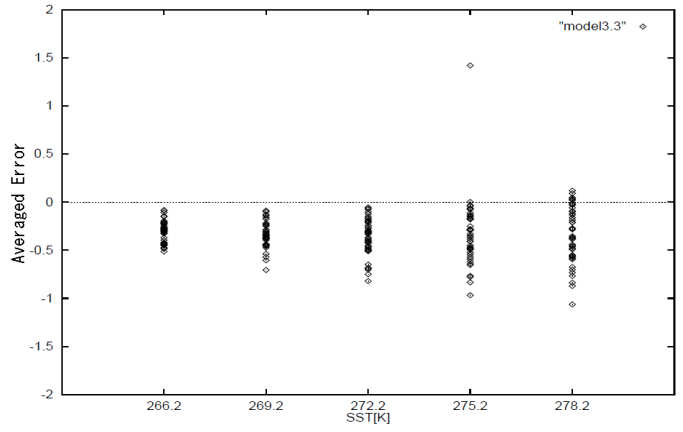
(b)Split Window



(b)Split Window



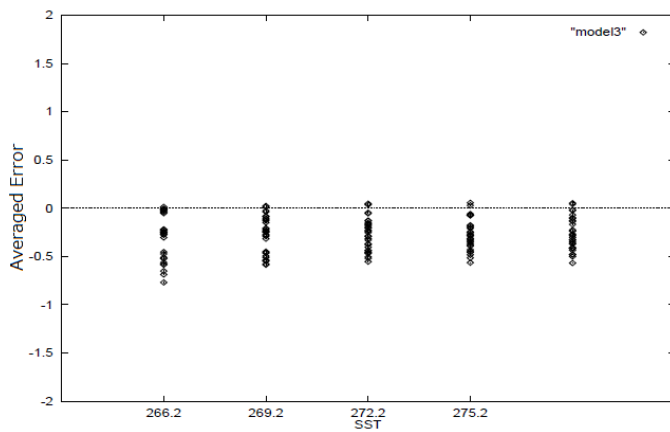
(c)Conjugate Gradient



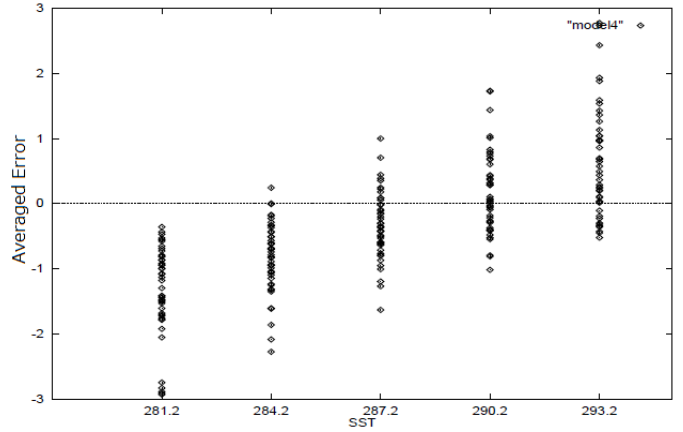
(c)Conjugate Gradient

Fig.3. Averaged SST estimation error for Mid. Latitude Summer atmosphere model

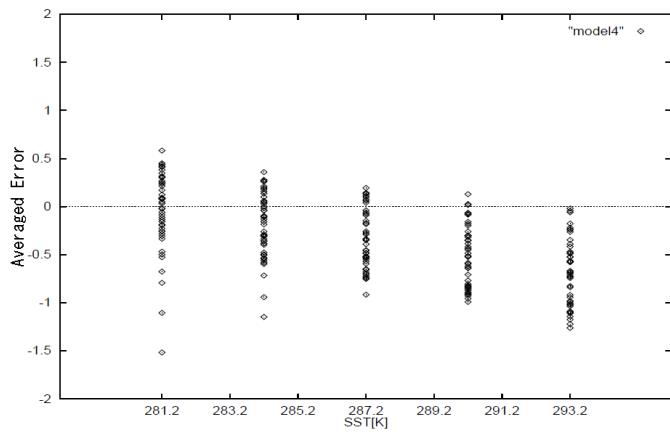
Fig.4. Averaged SST estimation error for Mid. Latitude Winter atmosphere model



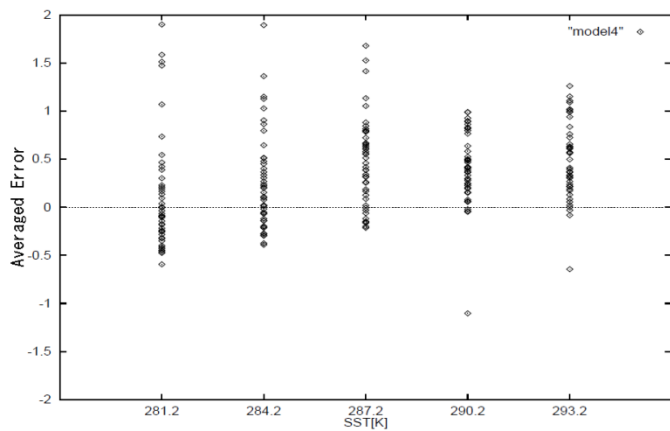
(a)MCSST



(a)MCSST

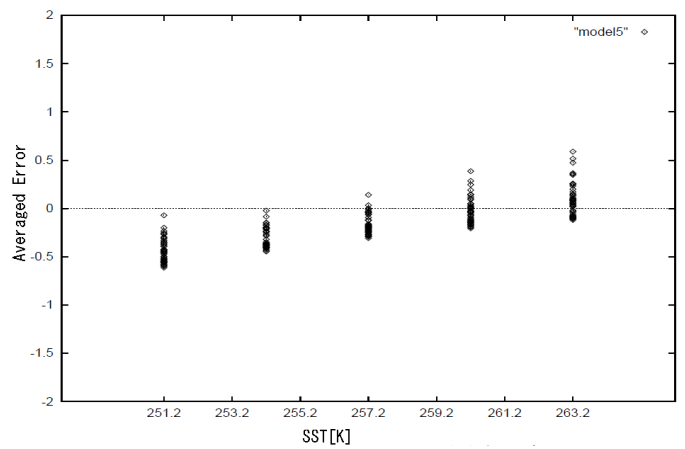


(b)Split Window

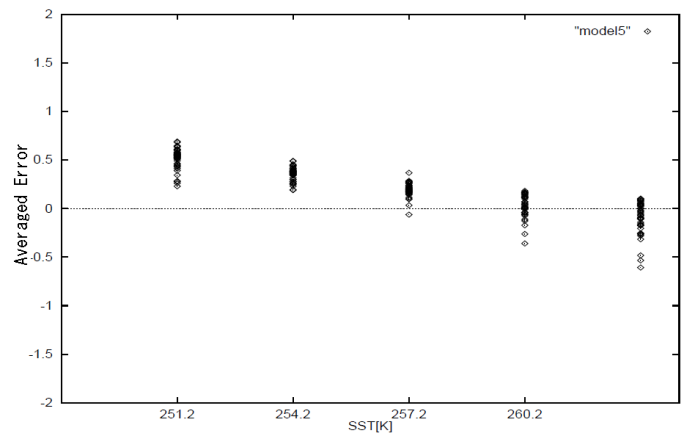


(c)Conjugate Gradient

Fig.5. Averaged SST estimation error for Sub Arctic Summer atmosphere model

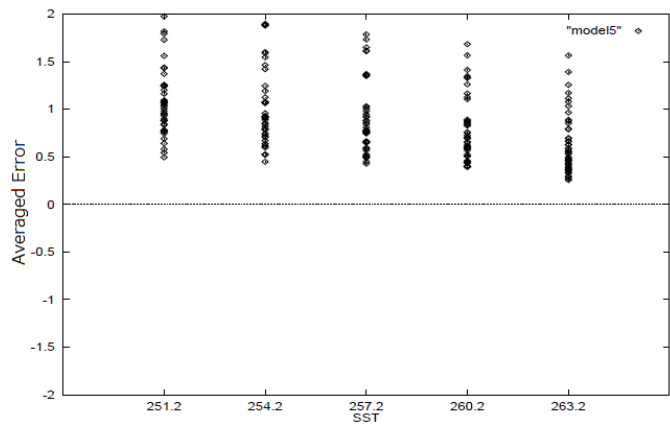


(b)Split Window

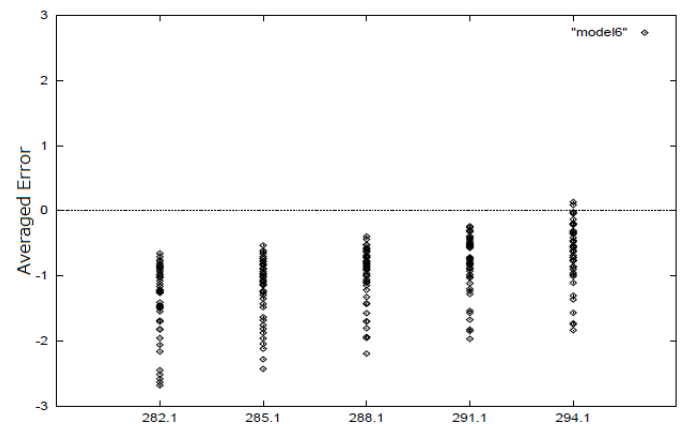


(c)Conjugate Gradient

Fig.6. Averaged SST estimation error for Sub Arctic Winter atmosphere model



(a)MCSST



(a)MCSST

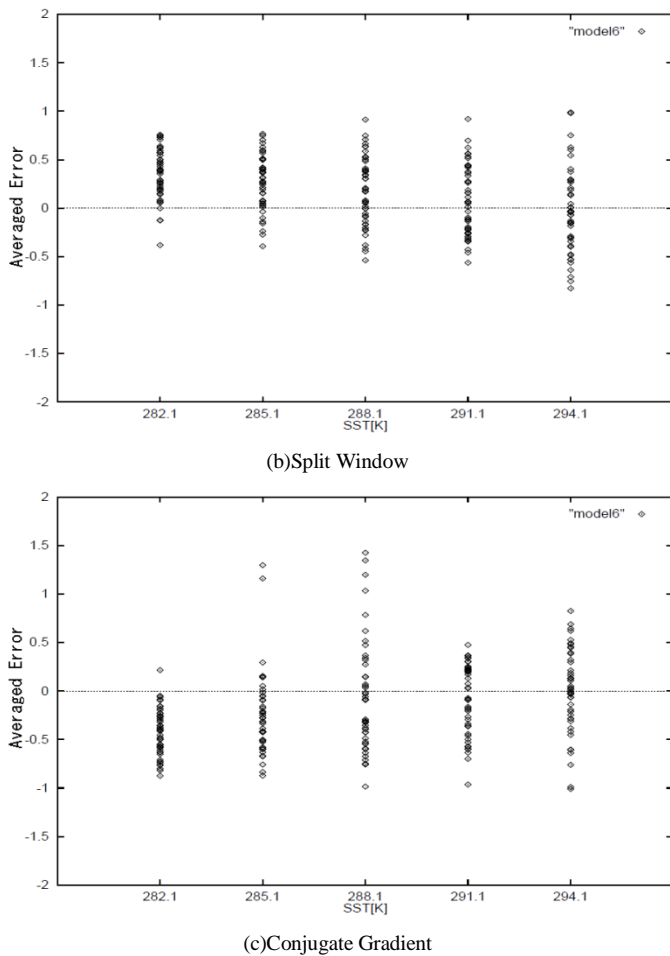


Fig.7. Averaged SST estimation error for 1976 US standard atmosphere model

TABLE III. RMSE OF SST ESTIMATION FOR THE CONVENTIONAL MCSST, SPLIT WINDOW AND CONJUGATE GRADIENT METHOD FOR THE DIFFERENT ATMOSPHERIC MODELS

Atmospheric Model	MCSST(K)	Split Window(K)	CGM Method(K)
Tropic	2.77	1.195	0.864
Mid. Latitude Summer	1.67	0.702	0.479
Mid. Latitude Winter	0.72	0.472	0.408
Sub Arctic Summer	1.01	0.641	0.596
Sub. Arctic Winter	0.99	0.483	0.317
1976 US Standard	1.15	0.505	0.478
Average	1.53	0.726	0.559

C. Evaluated Averaged SST Estimation Error

Averaged SST estimation error of MCSST method, Split Window method, and Conjugate Gradient method for the basic atmospheric models, Tropic (Figure 2), Mid. Latitude Summer (Figure 3) and Winter (Figure 4), Sub Arctic Summer (Figure 5) and Winter (Figure 6) as well as 1976 US standard atmosphere (Figure 7).

For all cases, the proposed conjugate gradient method is superior to the other conventional methods of MCSST and Split Window, in particular for thick atmosphere (precipitable water rich atmosphere). Furthermore, MCSST has systematic errors of which the SST estimation error increases in accordance with increasing of SST.

Although only the difference between MCSST and Split Window methods is the regression coefficients, Split Window method is superior to the MCSST method because the regression coefficients are different among the atmospheric models for Split Window method; MCSST method uses the same coefficients for all atmospheric models.

IV. CONCLUSION

Comparative study on Sea Surface Temperature: SST estimations among the conventional Multi-Channel Sea Surface Temperature: MCSST, split window method and the proposed Conjugate Gradient based method: CGM with Thermal Infrared Radiometer:

TIR data through simulations is conducted. Utilizing the proposed linearized inversion of radiative transfer equation, SST can be estimated. SST estimation accuracy of the proposed method is compared to the conventional regression based method (Split Window method and MCSST).

Through the experiments, it is found that the proposed conjugate gradient method is superior to the other conventional methods of MCSST and Split Window for all cases, in particular for thick atmosphere (precipitable water rich atmosphere).

Furthermore, MCSST has systematic errors of which the SST estimation error increases in accordance with increasing of SST. Although only the difference between MCSST and Split Window methods is the regression coefficients, Split Window method is superior to the MCSST method because the regression coefficients are different among the atmospheric models for Split Window method; MCSST method uses the same coefficients for all atmospheric models.

ACKNOWLEDGMENT

The author would like to thank Mr. Noriyuki Takamatsu for his effort to conduct the experiments.

REFERENCES

- [1] Anding, D. and R. Kauth (1970): Estimation of sea surface temperature from space. *Remote Sens. Environ.*, **1**, 217–220.
- [2] McMillin, L. M. (1975): Estimation of sea surface temperatures from two infrared window measurements with different absorption. *J. Geophys. Res.*, **80**, 5113–5117.
- [3] Prabhakara, C., G. Dalu and V. G. Kunde (1974): Estimation of sea surface temperature from remote sensing in the 11- to 13- $\mu$ m window region. *J. Geophys. Res.*, **79**, 5039–5044.
- [4] Kohei Arai, Preliminary Assessment of Radiometric Accuracy for MOS-1 Sensors, International Journal of Remote Sensing, Vol.9, No.1, pp.5-12, Apr.1988.
- [5] Kidwell, K. B. (1991): NOAA Polar Orbiter Data Users Guide. NOAA/NESDIS/NCDC/SDSD, Washington, D.C., 192 pp.
- [6] Barton, I. J. (1995): Satellite-derived sea surface temperatures: Current status. *J. Geophys. Res.*, **100**, 8777–8790.

AUTHORS PROFILE

- [7] Moriyama,M., K.Mima and K.Arai, Comparison of the sea surface temperature estimation methods, *Advances in Space Reserach*, Vol.16, NO.10, pp.121-124, A1-044, July 1994.
- [8] K.Arai, Hidemasa Kobayashi, Masao Moriyama, Sea surface temperature estimation method based on Inversion and Linearized Inversion, *Journal of Remote Sensing Society of Japan*, 18, 3, 43-50, 1998.
- [9] K.Arai, Optimum band selection for sea surface teperature estimation based on regressive analysis, *Journal of Japanese Remote Sensing and Photogrammetry*, 39, 2, 74-81, 2000.
- [10] K.Arai, Sea Surface Temperature estimation method for ocean areas and seasons using Geographic Information System as a neural network, *Sediment and Ecohydraulics, Proc.in Marine Science*, 9, Elsevier ISBN978-0-444 53184-1, 2007.

**Kohei Arai**, He received BS, MS and PhD degrees in 1972, 1974 and 1982, respectively. He was with The Institute for Industrial Science, and Technology of the University of Tokyo from 1974 to 1978 also was with National Space Development Agency of Japan (current JAXA) from 1979 to 1990. During from 1985 to 1987, he was with Canada Centre for Remote Sensing as a Post Doctoral Fellow of National Science and Engineering Research Council of Canada. He was appointed professor at Department of Information Science, Saga University in 1990. He was appointed councilor for the Aeronautics and Space related to the Technology Committee of the Ministry of Science and Technology during from 1998 to 2000. He was also appointed councilor of Saga University from 2002 and 2003 followed by an executive councilor of the Remote Sensing Society of Japan for 2003 to 2005. He is an adjunct professor of University of Arizona, USA since 1998. He also was appointed vice chairman of the Commission "A" of ICSU/COSPAR in 2008. He wrote 30 books and published 332 journal papers.

# Prediction Method of El Nino Southern Oscillation: ENSO by Means of Wavelet Based Data Compression with Appropriate Support Length of Base Function

Kohei Arai

Graduate School of Science and Engineering  
Saga University  
Saga City, Japan

**Abstract**— Method for El Nino/Southern Oscillation: ENSO by means of wavelet based data compression with appropriate support length of base function is proposed. Through the experiments with observed southern oscillation index, the proposed method is validated. Also a method for determination of appropriate support length is proposed and is validated.

**Keywords**- Prediction; Time series analysis; wavelet; ENSO; support length of mother wavelet function; base function

## I. INTRODUCTION

El Nino is worldwide meteorological phenomena [1]-[5]. There are not so small number of papers which deals with prediction and forecasting of the phenomena. Most of these papers proposes methods for prediction and forecasting methods which are mainly focusing on extrapolations with numerical models and system equations expressing the phenomena. One of the paper proposed by Japanese Meteorological Agency describes that more than 10 months of observed data are required for prediction and forecasting of El Nino phenomena.

This paper describes a method for prediction of El Nino phenomena based on data compression utilizing wavelet Multi Resolution Analysis: MRA based feature extraction. Detection of El Nino phenomena can be done with MRA based time series analysis with the Southern Oscillation Index: SOI data and the Sea Surface Temperature: SST data. Also the paper describes a method for determination of support length of the mother wavelet of base function for MRA.

In accordance with Japanese Meteorological Agency: JMA, El Nino is defined as the ocean area of Eastern Pacific of Equatorial region at the latitude ranges from 4 degree North to 4 degree South and at the longitude ranges from 90 West to 150 West at which is called El Nino ocean area. Also El Nino is defined as the phenomena of which the difference between moving averaged Sea Surface Temperature: SST for five months is greater than 0.5 degree Celsius for 6 months compared to the averaged SST for 30 years starting from 1961 to 1990 as a reference. Therefore, JMA needs at least  $2 + 6 + 2 = 10$  months for detection of El Nino phenomena.

In order to shorten the time required for detection of El

Nino phenomena, the prediction and forecasting method for detection of El Nino phenomena based on wavelet MRA is proposed. MRA is a kind of filter bank which allows extraction of wavelet frequency components. Therefore, there is a possibility to detect El Nino phenomena by using MRA in an efficient manner.

MRA is based on Discrete Wavelet Transformation: DWT with mother wavelet function. Mother wavelet function can be expressed with order and support length. In particular, support length is important parameter for time series analysis. Therefore, a method which allows determination of appropriate support length is proposed.

Through experiments with SOI and SST data, the proposed prediction and forecasting method for detection of El Nino phenomena as well as determination of appropriate support length of mother wavelet function are validated.

In the following section, the proposed method is described followed by some experimental results. Then conclusion is described together with some discussions.

## II. PROPOSED METHOD

### A. Discrete Wavelet Transformations

Discrete wavelet transformation for the given time series of scalar variables,  $\eta_i$  are defined in equation (1) with square matrix,  $C_n$  (wavelet transformation matrix) which consists of low wavelet frequency component coefficients,  $p_i$  and high wavelet frequency component coefficients,  $q_i$ .

$$C_n \begin{bmatrix} \eta_1 \\ \eta_2 \\ \vdots \\ \eta_n \end{bmatrix} \quad (1)$$

Then the given time series of scalar variables can be divided into two parts, low frequency and high frequency components. There is a variety of wavelet transformation matrix with the different parameters of the order and the support length of the base function. For instance, the wavelet transformation matrix for the 8<sup>th</sup> order and two of the support

length is shown in equation (2). In the case of the wavelet transformation matrix for the 8<sup>th</sup> order with two support length is expressed in equation (3).

In the case of Daubechies base function, the wavelet transformation matrix with two of the support length can be calculated with equation (4) while that with four of the support length can be calculated with equation (5). Meanwhile, the wavelet transformation matrix with the arbitrary support length, (sup) can be calculated with equation (6).

$$C_8^{[2]} = \begin{bmatrix} \eta_1 \\ \eta_2 \\ \eta_3 \\ \eta_4 \\ \eta_5 \\ \eta_6 \\ \eta_7 \\ \eta_8 \end{bmatrix} = \begin{bmatrix} p_0 & p_1 & & & & & & \\ q_0 & q_1 & & & & & & \\ & & p_0 & p_1 & & & & \\ & & q_0 & q_1 & & & & \\ & & & & p_0 & p_1 & & \\ & & & & q_0 & q_1 & & \\ & & & & & & p_0 & p_1 \\ & & & & & & q_0 & q_1 \end{bmatrix} \begin{bmatrix} \eta_1 \\ \eta_2 \\ \eta_3 \\ \eta_4 \\ \eta_5 \\ \eta_6 \\ \eta_7 \\ \eta_8 \end{bmatrix}$$

$$= \begin{bmatrix} p_0x_1 + p_1x_2 \\ q_0\eta_1 + q_1\eta_2 \\ p_0\eta_3 + p_1\eta_4 \\ q_0\eta_3 + q_1\eta_4 \\ p_0\eta_5 + p_1\eta_6 \\ q_0\eta_5 + q_1\eta_6 \\ p_0\eta_7 + p_1\eta_8 \\ q_0\eta_7 + q_1\eta_8 \end{bmatrix} \quad (2)$$

$$C_8^{[4]} = \begin{bmatrix} \eta_1 \\ \eta_2 \\ \eta_3 \\ \eta_4 \\ \eta_5 \\ \eta_6 \\ \eta_7 \\ \eta_8 \end{bmatrix} = \begin{bmatrix} p_0 & p_1 & p_2 & p_3 & & & & \\ q_0 & q_1 & q_2 & q_3 & & & & \\ & & p_0 & p_1 & p_2 & p_3 & & \\ & & q_0 & q_1 & q_2 & q_3 & & \\ & & & & p_0 & p_1 & p_2 & p_3 \\ & & & & q_0 & q_1 & q_2 & q_3 \\ p_2 & p_3 & & & & & p_0 & p_1 \\ q_2 & q_3 & & & & & q_0 & q_1 \end{bmatrix} \begin{bmatrix} \eta_1 \\ \eta_2 \\ \eta_3 \\ \eta_4 \\ \eta_5 \\ \eta_6 \\ \eta_7 \\ \eta_8 \end{bmatrix}$$

$$= \begin{bmatrix} p_0\eta_1 + p_1\eta_2 + p_2\eta_3 + p_3\eta_4 \\ q_0\eta_1 + q_1\eta_2 + q_2\eta_3 + q_3\eta_4 \\ p_0\eta_3 + p_1\eta_4 + p_2\eta_5 + p_3\eta_6 \\ q_0\eta_3 + q_1\eta_4 + q_2\eta_5 + q_3\eta_6 \\ p_0\eta_5 + p_1\eta_6 + p_2\eta_7 + p_3\eta_8 \\ q_0\eta_5 + q_1\eta_6 + q_2\eta_7 + q_3\eta_8 \\ p_0\eta_7 + p_1\eta_8 + p_2\eta_1 + p_3\eta_2 \\ q_0\eta_7 + q_1\eta_8 + q_2\eta_1 + q_3\eta_2 \end{bmatrix} \quad (3)$$

$$\begin{aligned} (C_n^{[2]})^T C_n^{[2]} &= I_n \\ p_0 + p_1 &= \sqrt{2} \\ q_0 &= p_1 \\ q_1 &= -p_0 \\ 0^0 q_0 + 1^0 q_1 &= 0 \end{aligned} \quad (4)$$

$$\begin{aligned} (C_n^{[4]})^T C_n^{[4]} &= I_n \\ p_0 + p_1 + p_2 + p_3 &= \sqrt{2} \\ q_0 &= p_3 \\ q_1 &= -p_2 \\ q_2 &= p_1 \\ q_3 &= -p_0 \\ 0^0 q_0 + 1^0 q_1 + 2^0 q_2 + 3^0 q_3 &= 0 \\ 0^1 q_0 + 1^1 q_1 + 2^1 q_2 + 3^1 q_3 &= 0 \end{aligned} \quad (5)$$

$$\begin{aligned} (C_n^{[sup]})^T C_n^{[sup]} &= I_n \\ \sum_{j=0}^{sup-1} p_j &= \sqrt{2} \\ q_j &= (-1)^j p_{(sup-1)-j} \quad (j=0,1,2,\dots,(sup-1)) \\ \sum_{j=0}^{sup-1} j^r q_j &= 0 \quad \left( r=0,1,2,\dots,\left(\frac{sup}{2}-1\right) \right) \end{aligned} \quad (6)$$

Where n denotes the number of observed data while sup denotes support length of mother wavelet which is determined by the analysts.

### B. Generalized Inversion Matrix

Cn is also described as follows,

$$C_n = \begin{bmatrix} P_n \\ Q_n \end{bmatrix} \quad (7)$$

Where Pn and Qn which are n/2 by n matrices can be expressed from the generalized inverse matrices as follows,

$$P_n^+ = P^T(P P^T)^{-1} \quad (8)$$

$$Q_n^+ = Q^T(Q Q^T)^{-1} \quad (9)$$

If the rank M of Pn and Qn is within a range from 0 to n/2, then both are decomposed with Singular Value Decomposition: SVD as follows,

$$P_n = \sum_{i=1}^M \kappa_i w_i v_i^T \quad (\kappa_1 \geq \kappa_2 \geq \dots \geq \kappa_M > 0) \quad (10)$$

$$Q_n = \sum_{i=1}^M \kappa_i w_i v_i^T \quad (\kappa_1 \geq \kappa_2 \geq \dots \geq \kappa_M > 0) \quad (11)$$

Then

$$P_n^+ = \sum_{i=1}^M \kappa_i^{-1} v_i w_i^T \quad (12)$$

$$Q_n^+ = \sum_{i=1}^M \kappa_i^{-1} v_i w_i^T \quad (13)$$

Where  $v$  and  $w$  denotes orthogonal matrix while  $k$  denotes singular matrix which consists of square root of eigen values.

### C. Multi Resolution Analysis: MRA

The input data of scalar variables can be transformed to high (H) and low (L) wavelet frequency components with the wavelet transformation matrix. This Discrete Wavelet Transformation: DWT is called as the first level of DWT. L component can be divided into H and L components. This DWT is called as the second level of DWT. Furthermore, these transformations can be repeatedly applied to the L components again. These DWT is called as decomposition. The level is corresponding to the frequency components. In other words, arbitrary frequency component can be extracted with the different level of wavelet frequency component.

Because of the  $C^T C = C^{-1} C$ , it is possible to reconstruct original input data of scalar variables with the all levels of H components and the highest level of L component. This process is called with reconstruction, or Inverse Discrete Wavelet Transformation: IDWT.

DWT and IDWT can also be defined to the two dimensional image data as well as three dimensional moving pictures. Furthermore, these can be applied to arbitrary dimensional data  $f$  as follows,

$$(fC^T)^T C^T \dots C^T \quad (7)$$

For instance, DWT divides two dimensional input data into LL, HL, LH, and HH. The first and the second characters denote horizontal and vertical directions, respectively.

### D. Process Flow of the Proposed Method

Process flow of the proposed method is as follows,

- 1) Determination of base function,
- 2) Determination of support length
- 3) Decompose the given time series of data by using DWT
- 4) Select the most nearest data compared to the most recent data from the low wavelet frequency components
- 5) Reconstruct the data by using the selected low frequency components based on Inverse DWT: IDWT.

## III. EXPERIMENTS

### A. The Data Used

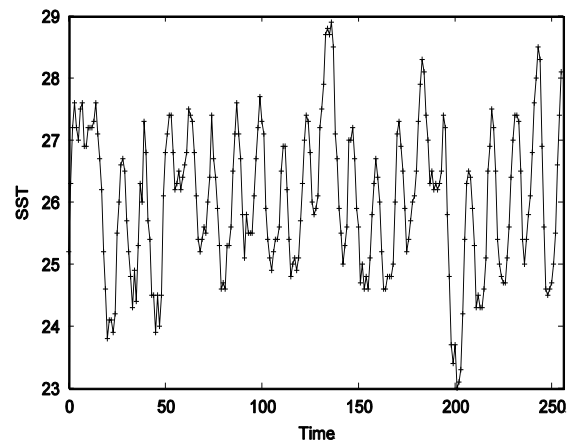
Monthly averages data of SOI and SST data are used for the experiments. 21.3 years starting from January, 1972 of data are used. SOI and SST are usually varied together and can be confirmed the changes of SOI and SST.

Time series of SST data are shown in Figure 1 (a) while those of SOI data are shown in Figure 1 (b), respectively. SST data is for the ocean area of Eastern Pacific of Equatorial region at the latitude ranges from 4 degree North to 4 degree South and at the longitude ranges from 90 West to 150 West at which is called El Nino ocean area. From Figure 1 (a), it is found that SST ranges from 23 to 29 degree Celsius.

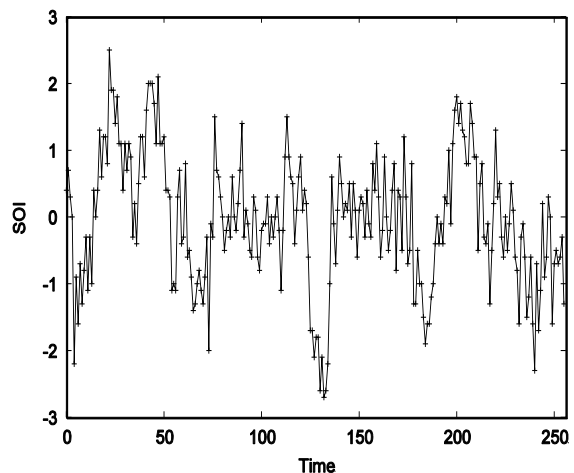
Meanwhile, SOI data is derived from the surface atmospheric pressure measured at the Tahiti and Darwin in Australia. SOI indicate jet stream changes. From Figure 1 (b), it is found that the SOI ranges from -3 to +3.

### B. Method for Evaluation of Effect of the Support Length

Effect of the support length of mother wavelet function of DWT and IDWT used for decomposition and reconstruction is confirmed with the data used. Applying DWT with the different support length of mother wavelet, then IDWT with the same support length of mother wavelet with only low frequency components is performed. Then Root Mean Square: RMS error between both the original and the reconstructed time series data is evaluated. Figure 2 (a) and (b) shows the RMS errors for SST and SOI data.



(a) Relatively calm changes of SST



(b) Relatively rapid changes of SOI

Fig.1. Two different types of time series of data

### C. Effect of the Support Length

In order to clarify the effect of the support length, relatively calmly changed Southern Oscillation Index: SOI is compared to relatively rapidly changed SOI which are shown in Figure 1 (a) and (b), respectively. DWT is applied at once (first level) to the data with the different support length. After that IDWT is applied to the transformed wavelet frequency

component with L component only. Root Mean Square Error: RMSE between the reconstructed data and the original data is evaluated. The results are shown in Figure 2.

**D. Evaluation of Effect of the Support Length**

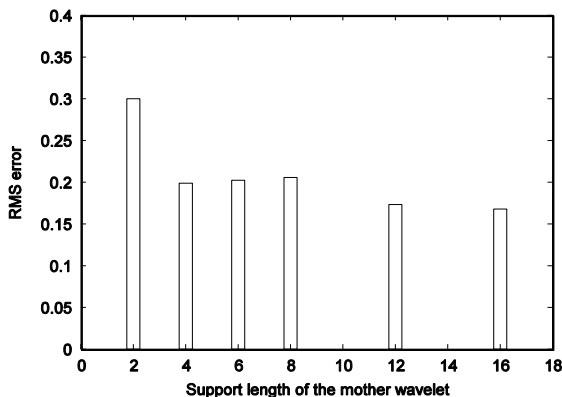
From Figure 2 (a) and (b), it is found that the appropriate support length for SST is 16 while that for SOI is 8.

In order to check the relation between appropriate support length and the changes of the time series of data, the following equation is proposed.

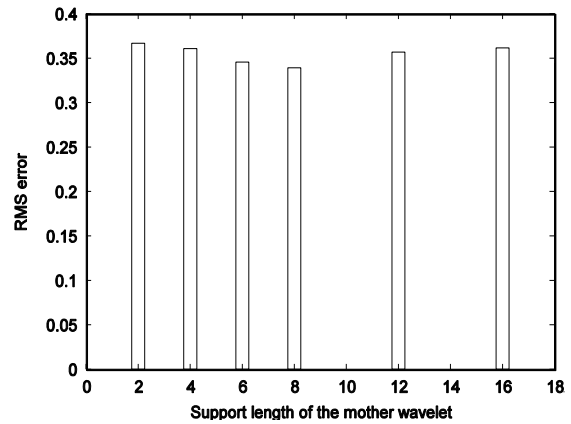
$$\begin{aligned}
 P(i, j) &= \frac{\overline{\Delta \epsilon(i, j)}}{\sqrt{\frac{U^2(i, j)}{N}}} \\
 U^2(i, j) &= \frac{1}{N-1} \sum_{k=1}^N (\alpha^{[k]}(i, j) - \overline{\Delta \epsilon(i, j)})^2 \\
 \alpha^{[k]}(i, j) &= \epsilon^{[k]}(j) - \epsilon^{[k]}(i) \\
 \overline{\Delta \epsilon(i, j)} &= \frac{\epsilon(j) - \epsilon(i)}{N}
 \end{aligned}
 \tag{14}$$

Where  $\epsilon^{[k]}(sup)$  denotes square error at the support length is “sup” and at the time “k” while  $\overline{\epsilon}(sup)$  denotes average of the  $\epsilon^{[k]}(sup)$ . Namely, if  $P(i, j)$  is large, then the effect of support length is also large. In the evaluation N is set at 256.

$P(16,8)$  for SST is 1.774 while  $P(8,16)$  for SOI is 1.624, respectively. It is found that  $P(i, j)$  for SST is confidential at 95% of confidence level while  $P(i, j)$  for SOI is confidential at the confidence level of 90% through Chi square test..If  $P(i, j)$  is greater than 1.65, then  $P(i, j)$  is 95 % confidential.



(a) Relatively calm changes of SST



(b) Relatively rapid changes of SOI

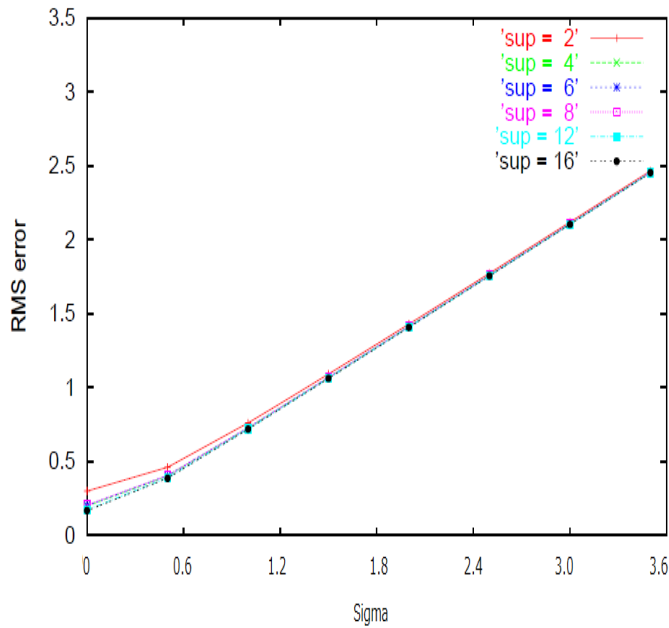
Fig.2. Root Mean Square error between original and reconstructed time series data through DWT with different support length (2-16) of mother wavelet.

**E. In Case When the Low Frequency Components of the Past Data Does not Match to That of Present Data**

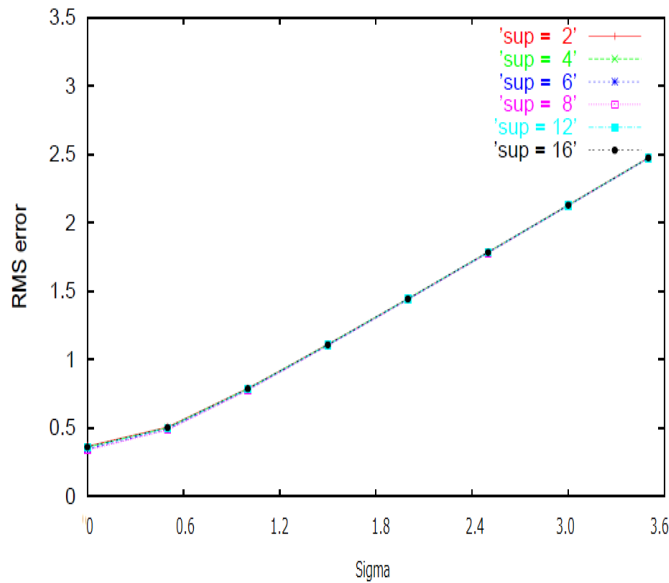
It is not always that the low frequency components of the past data are matched to those of the current data. In such case, normal distributed random number of noise (zero mean and  $\sigma$  of standard deviation) is added to the low frequency component derived from the past time series data through DWT of decomposition. Then the noise added low frequency component is used for reconstruction. It has to be matched to the low frequency component of the current data. After that, the reconstructed data is compared to the original time series of data before the decomposition. RMS difference between both shows a goodness of the restoration.

Figure 3 shows RMS error between the reconstructed data and the original time series of data before the decomposition as a function of sigma of standard deviation of added noise to the low frequency component derived from the past time series of data through DWT, decomposition. Figure 3 (a) shows RMS error for SST while Figure 3 (b) shows that for SOI.

In accordance with increasing of added noise, RMS error is increased for the SST and the SOI cases. It is also found that RMS error is increased in accordance with decreasing of support length in particular for the SST case, relatively calm changes of time series data. As is mentioned already, it is found that the appropriate support length for SST is 16 while that for SOI is 8.



(a)SST



(b)SOI

Fig.3. RMS error between the reconstructed data and the original time series of data before the decomposition as a function of sigma of standard deviation of added noise to the low frequency component derived from the past time series of data through DWT, decomposition.

#### IV. CONCLUSION

Method for El Nino/Southern Oscillation: ENSO by means of wavelet based data compression with appropriate support length of base function is proposed. Through the experiments with observed southern oscillation index, the proposed method is validated. Also a method for determination of appropriate support length is proposed and is validated.

In accordance with increasing of added noise, RMS error is increased for the SST and the SOI cases. It is also found that RMS error is increased in accordance with decreasing of support length in particular for the SST case, relatively calm changes of time series data. As is mentioned already, it is found that the appropriate support length for SST is 16 (relatively calm changes) while that for SOI is 8 (relatively rapid changes).

#### ACKNOWLEDGMENT

The authors would like to thank Arai's laboratory members for their valuable discussions and suggestions through this research.

#### REFERENCES

- [1] T.Yasanari, Global structure of the El Nin/ Southern Oscillation, Part-I, Meteorological Journal, 65, 1, 67-80, 1987.
- [2] T.Yasanari, Global structure of the El Nin/ Southern Oscillation, Part-II, Meteorological Journal, 65, 1,81-102, 1987.
- [3] T.Nita and T.Motoki, Abrupt enhancement of convective activity and low-level westerly first during the onset phase of the 1986-87 El Nino, Meteorological Journal, 65, 3, 497-506, 1987.
- [4] T.Maruyama and Y.Tsuneoka, Anomalous short duration of the easterly wind phase of QBO at 50 hPa in 1987 and its relationship, Meteorological Journal, 66, 4, 629-634, 1988.
- [5] T.Nitta, Development of a twin cyclone and westerly burst during the initial phase of the 1986-87 El Nino, Meteorological Journal, 67, 4, 677-681, 1989.

#### AUTHORS PROFILE

**Kohei Arai**, He received BS, MS and PhD degrees in 1972, 1974 and 1982, respectively. He was with The Institute for Industrial Science and Technology of the University of Tokyo from April 1974 to December 1978 also was with National Space Development Agency of Japan from January, 1979 to March, 1990. During from 1985 to 1987, he was with Canada Centre for Remote Sensing as a Post Doctoral Fellow of National Science and Engineering Research Council of Canada. He moved to Saga University as a Professor in Department of Information Science on April 1990. He was a councilor for the Aeronautics and Space related to the Technology Committee of the Ministry of Science and Technology during from 1998 to 2000. He was a councilor of Saga University for 2002 and 2003. He also was an executive councilor for the Remote Sensing Society of Japan for 2003 to 2005. He is an Adjunct Professor of University of Arizona, USA since 1998. He also is Vice Chairman of the Commission "A" of ICSU/COSPAR since 2008. He wrote 30 books and published 322 journal papers

# Multi Spectral Image Classification Method with Selection of Independent Spectral Features through Correlation Analysis

Kohei Arai

Graduate School of Science and Engineering  
Saga University  
Saga City, Japan

**Abstract**— Multi spectral image classification method with selection processes of independent spectral features through correlation analysis is proposed. The proposed method is validated by applying to the polarimetric Synthetic Aperture Radar: SAR data. Also Probability Distribution Function: PDF for of features are checked and confirmed the most independent PDF allows greatest classification performance.

**Keywords**- image classification; polarimetric SAR; correlation analysis;

## I. INTRODUCTION

Due to the fact that the Synthetic Aperture Radar image contains not so small noises, speckle noise in particular, classification is not so easy. There are so many methods for speckle noise removals. After the speckle noise is removed, it still difficult to get high classification performance.

From full polarimetric SAR images, not so small number of features can be derived in comparison to the single polarization of SAR images. It is possible to select independent feature among the not so small number of features. The classification method proposed here is to apply feature selection in accordance with the correlation among the features derived from full polarimetric SAR imagery data.

Radar polarimetry allows measurement the physical characteristics such as di-electric constant, slope of the ground cover targets as well as directionality of artificial objects by using scattering mechanism between electromagnetic (EM) wave and the targets [1], [2]. Polarimetric SAR image classification with the following three components of the polarimetric SAR data, (1) transmit Electro-magnetic wave with Horizontal Polarization(H-Pol) and receive the echo from the ground with H-Pol(HH), (2) transmit Electro-magnetic wave with H-Pol and receive the echo with Vertical Polarization(V-Pol)(HV) and (3) transmit Electro-magnetic wave with V-Pol and receive the echo with V-pol(VV) is widely available [3],[4]. On the other hand, the extraction of the scattering characteristics of the targets of interest by applying eigen value decomposition to the covariance matrix derived from the scattering matrix which is calculated from the three components are proposed [5]. Furthermore, the classification methods with the single / double /multiple, odd / even / diffuse, and odd / even / Bragg / multiple scattering components derived from the eigen value decomposition were

proposed [6] while the classification methods with the sphere / deplane / helix, and sphere / Bragg / double of scattering components which are based on the spherical polarization which are derived from the scattering matrix were also proposed [7],[8].

Aforementioned proposed methods were reviewed [9]. Moreover, the classification method with the entropy (H) which is defined with the sum of the first to third eigen values and the ratio of each eigen values, the anisotropy (A) which is defined as the ratio of sum and subtraction of the second and the third eigen values and cosine  $\alpha$  ( $\cos(\alpha)$ ) which is defined with the elements of the eigen vector corresponding to the first eigen value which is called coherency matrix(3 by 3) was proposed by E.Pottier [10].

The application of these methods to sea ice discrimination (such as thin ice (TI), smooth first year ice (SF), rough first year ice (RF) and open water (OW)) with the polarimetric SAR were attempted by using H, A, and  $\cos(\alpha)$  [11]. Classification performance, however, were not satisfactory (20-40% of classification errors were occurred for the classification of sea ice into four classes, ridged, compressed, new forming and smooth surface due to the fact that scattering mechanism based features were not used effectively. Meanwhile polarimetric SAR image classification with polarization signature which are derived from Stokes or Muller or scattering matrix is widely available [12]. Polarization signature represents the scattering mechanism, in particular, surface roughness of the targets in concern.

One of the problems on the classification with polarization signature is classification performance. The method for effective utilization of polarization signature is still unclear to improve classification performance. The method proposed here is for extraction of effective information from the polarization signature by transforming the polarization signature onto an eigen space (eigen value decomposition). As the results from the eigen value decomposition which corresponds to the largest eigen value, a trajectory can be drawn. The trajectory represents the scattering mechanism in concern so that the largest curvature of the trajectory represents the most effective representatives of the scattering mechanism of the target of interest [13]. This is the theoretical background to propose the utilization of maximum curvature of the trajectory in an eigen space which is derived from the

polarization signature to the sea ice classification.

The following section, the proposed method is described followed by the experiments. Then conclusion is described together with some discussions.

## II. PROPOSED METHOD

### A. Principle of Polarimetric SAR

Sending and receiving EM signals are expressed in Equation (1).

$$\begin{pmatrix} E_h \\ E_v \end{pmatrix}_{rec} = \frac{e^{-jkR}}{kR} \begin{pmatrix} S_{hh} & S_{hv} \\ S_{vh} & S_{vv} \end{pmatrix} \begin{pmatrix} E_h \\ E_v \end{pmatrix}_{ill} \quad (1)$$

where  $S_{hh}$ ,  $S_{hv}$ , and  $S_{vv}$  denotes sending and receiving polarizations of scattering components while  $E_h$ ,  $E_v$  denotes EM signals in horizontal and vertical polarizations.  $R$  and  $k$  denotes range between sending antenna to the ground and the wave number of EM signals.

Stokes vector,  $J$  is defined in equation (2).

$$J = \begin{pmatrix} J_0 \\ J_1 \\ J_2 \\ J_3 \end{pmatrix} = \begin{pmatrix} |E_h|^2 + |E_v|^2 \\ |E_h|^2 - |E_v|^2 \\ 2(Re(E_h E_v^*)) \\ -2(Im(E_h E_v^*)) \end{pmatrix} = \begin{pmatrix} J_0 \\ J_0 \cos(2\chi) \cos(2\phi) \\ J_0 \cos(2\chi) \sin(2\phi) \\ J_0 \sin(2\chi) \end{pmatrix} \quad (2)$$

Also Muller matrix is defined in equation (3).

$$M = RWR^{-1}$$

$$W = \begin{pmatrix} S_{hh}S_{hh}^* & S_{hh}S_{hv}^* & S_{hv}S_{hh}^* & S_{hv}S_{hv}^* \\ S_{hh}S_{vh}^* & S_{hh}S_{vv}^* & S_{hv}S_{vh}^* & S_{hv}S_{vv}^* \\ S_{vh}S_{hh}^* & S_{vh}S_{hv}^* & S_{vv}S_{hh}^* & S_{vv}S_{hv}^* \\ S_{vh}S_{vh}^* & S_{vh}S_{vv}^* & S_{vv}S_{vh}^* & S_{vv}S_{vv}^* \end{pmatrix}$$

$$R = \begin{pmatrix} 1 & 0 & 0 & 1 \\ 1 & 0 & 0 & -1 \\ 0 & 1 & 1 & 0 \\ 0 & j & -j & 0 \end{pmatrix} \quad U_4 = \begin{pmatrix} 1 & 0 & 0 & 0 \\ 0 & 1 & 0 & 0 \\ 0 & 0 & 1 & 0 \\ 0 & 0 & 0 & -1 \end{pmatrix}$$

$$2U_4 M_s = M \quad M_s = \frac{1}{2} U_4^{-1} M \quad (3)$$

Elements of the Muller matrix can be calculated with the equation (4),

$$\begin{aligned} M_{11} &= \frac{1}{4}(S_{hh}S_{hh}^* + S_{vv}S_{vv}^* + S_{hv}S_{hv}^* + S_{vh}S_{vh}^*) \\ M_{12} &= \frac{1}{4}(S_{hh}S_{hh}^* - S_{vv}S_{vv}^* - S_{hv}S_{hv}^* + S_{vh}S_{vh}^*) \\ M_{13} &= \frac{1}{2}Re(S_{hh}S_{hv}^* + S_{vv}S_{vh}^*) \\ M_{14} &= \frac{1}{2}Im(S_{hh}S_{hv}^* + S_{vv}S_{vh}^*) \\ M_{21} &= \frac{1}{4}(S_{hh}S_{hh}^* - S_{vv}S_{vv}^* + S_{hv}S_{hv}^* - S_{vh}S_{vh}^*) \\ M_{22} &= \frac{1}{4}(S_{hh}S_{hh}^* + S_{vv}S_{vv}^* - S_{hv}S_{hv}^* - S_{vh}S_{vh}^*) \\ M_{23} &= \frac{1}{2}Re(S_{hh}S_{hv}^* - S_{vh}S_{vh}^*) \\ M_{24} &= \frac{1}{2}Im(S_{hh}S_{hv}^* + S_{vh}S_{vh}^*) \\ M_{31} &= \frac{1}{2}Re(S_{hh}S_{vh}^* + S_{hv}S_{vv}^*) \\ M_{32} &= \frac{1}{2}Re(S_{hh}S_{vh}^* - S_{hv}S_{vv}^*) \\ M_{33} &= \frac{1}{2}Re(S_{hh}S_{vv}^*) + \frac{1}{4}(S_{vh}S_{hv}^* + S_{hv}S_{vh}^*) \\ M_{34} &= \frac{1}{2}Im(S_{hh}S_{vv}^* + S_{hv}S_{vh}^*) \\ M_{41} &= \frac{1}{2}Im(S_{hh}S_{vh}^* + S_{hv}S_{vv}^*) \\ M_{42} &= \frac{1}{2}Im(S_{hh}S_{vh}^* - S_{hv}S_{vv}^*) \\ M_{43} &= \frac{1}{2}Im(S_{hh}S_{vv}^* - S_{hv}S_{vh}^*) \\ M_{44} &= -\frac{1}{2}Re(S_{hh}S_{vv}^*) + \frac{1}{4}(S_{vh}S_{hv}^* + S_{hv}S_{vh}^*) \end{aligned} \quad (4)$$

Meanwhile polarization signature can be defined as follows,

$$\sigma_0 = C J_r^T \langle M_s \rangle J_t = \sigma_0(\chi_r, \psi_r, \chi_t, \psi_t) \quad C : const.$$

Thus polarization signature can be characterized with  $\chi, \psi$  as shown in Figure 1.

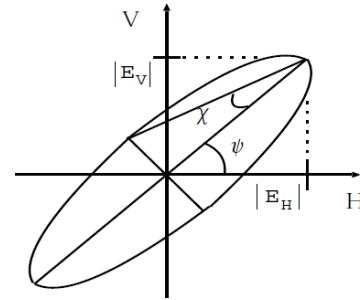


Fig.1. Characterization of polarization signature

### B. Full Polarimetric SAR Imagery Data Decompositions

Full polarimetric SAR is defined as the SAR which allows acquisition the scattering components of which polarimetric SAR sends Electric Magnetic: EM signals to the ground cover targets in horizontal and vertical polarizations and also that receives EM signals from the ground cover targets in horizontal and vertical polarizations. Therefore, scattering matrix of equation (5) can be obtained.

$$X = [S_{hh}S_{hv}S_{vv}]^T \quad (5)$$

Where  $S_{ij}$  denotes scattering coefficients while the first and the second suffix of  $S_{hh}$ ,  $S_{hv}$ , and  $S_{vv}$  denotes sending and receiving polarizations.

$$C = \langle XX^{*T} \rangle \quad (6)$$

$$C = \lambda_1 K_1 (K_1)^{*T} + \lambda_2 K_2 (K_2)^{*T} + \lambda_3 K_3 (K_3)^{*T} \quad (7)$$

$K_1$ ,  $K_2$ ,  $K_3$  denotes Single scattering coefficient (Odd), Double scattering coefficient (Even), and Defuse scattering coefficient (Defuse) while  $\lambda_1, \lambda_2, \lambda_3$  denotes eigen values for  $K_1, K_2, K_3$ . Ratio of these three variables can be determined by the following contribution factors

$$\lambda_i / (\lambda_1 + \lambda_2 + \lambda_3), (i = 1, 2, 3) \quad (8)$$

Not only these three features but also the other features can be decomposed. Circular polarization of EM wave,  $S_{LR}$ ,  $S_{LL}$ ,  $S_{RR}$ ,  $S_{RL}$  can be derived from  $S_{ij}$  as follows,

$$\begin{aligned} S_{RR} &= \frac{1}{2}(S_{hh} - S_{vv} + j2S_{hv}) \\ S_{LL} &= \frac{1}{2}(S_{hh} - S_{vv} - j2S_{hv}) \\ S_{LR} &= \frac{1}{2}(S_{hh} + S_{vv}) \end{aligned} \quad (9)$$

Linear and circular polarization is illustrated in Figure 2.

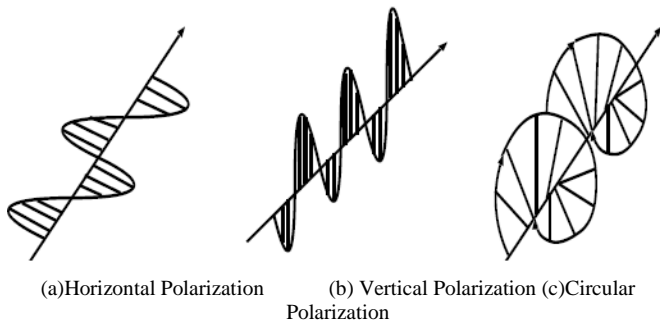


Fig.2. Polarization features

Then Sphere, Di-plane and Helix components are defined as follows,

$$\begin{aligned} K_s &= |S_{LR}| \quad K_d = |S_{LL}| \quad K_h = |S_{RR}| - |S_{LL}| \quad \text{for } |S_{RR}| > |S_{LL}| \\ K_s &= |S_{LR}| \quad K_d = |S_{RR}| \quad K_h = |S_{RR}| - |S_{LL}| \quad \text{for } |S_{RR}| < |S_{LL}| \end{aligned}$$

Contribution factors for each component can be calculated as follows,

$$K_i / (K_s + K_d + K_h), (i = s, d, h) \quad (10)$$

Namely, this decomposition can be done with eigen value decomposition of covariance matrix of scattering matrix.

Other than these, there is another decomposition method

which allows extract odd number scattering component, even number scattering component, Bragg scattering component, orthogonal polarization scattering component, etc. can be extracted from  $S_{ij}$ . Furthermore, there are some other decomposition methods for not only covariance matrix but also coherence matrix as well.

### C. Classification Method Used

There are many image classification methods with features. Probability Density Function: PDF of the extracted features are followed by normal distribution, usually. Therefore, widely used Maximum Likelihood Classification: MLH method assuming normal distribution is used.

### D. Correlation Matrix

Through correlation analysis, correlation coefficients among the extracted features are calculated and create correlation matrix. Then summation of correlation matrix elements is calculated. This variable is referred to SUM hereafter. After that, sorting of the summation of correlation matrix elements is performed. Small summation of correlation matrix elements implies independent feature or effective feature for classification.

### E. Overlapped Portion of Probability Density Function between Features

Another measure for effectiveness features, or features can be assessed with overlapped portion of PDFs between two features. If the overlapped portion is small, then it is effective to image classification.

## III. EXPERIMENTS

### A. Polarimetric SAR Image Data Used

The PI-SAR (Polarimetric and Interferometric SAR) data of Tsukuba in Japan which was acquired by CRL (Communication Research Laboratory, current NICT: National Institute of Communication Technology) and NASDA (National Space Development Agency of Japan, current JAXA: Japan Aeronautics Exploration Agency) on 23 February 1999 was used. The major characteristics of the PI-SAR are in Table 1.

TABLE I. MAJOR CHARACTERISTICS OF PI-SAR

Instrument	NASDA/L-band SAR
Center frequency	1.27GHz
Peak power	3.5kW
Band width	50MHz
Antenna size	1.6m x 0.7m
Polarization	HH/HV/VH/VV(Full Pol.)
Incident angle	20-60degrees(Fixed)
Swath width	42.5km
Spatial resolution	3m
Quantization bit	8bits(I and Q)

From the data of SSC (Single-look Slant-range Complex) of the data, the imagery data of PISAR used for experiments is created. Figure 3 shows the imagery data used for the experiments of Okhotsk Sea.

Intensive Study Area is situated in the Sea of Okhotsk. The data is acquired on 23 February 1999. The imagery data is created with Single Look Slant Range of Complex Data. The data is reprocessed with 8 look processing and is composed with  $1000 \times 987$  pixels. It is acquired with PISAR instrument with the parameters of L band of HH polarization which is onboard the aircraft. In Figure 3, Green colored areas show Open Water while Black colored areas show Rough Surface Ice. On the other hand, Blue colored areas show Thin Ice while White colored areas show Smooth Surface Ice.

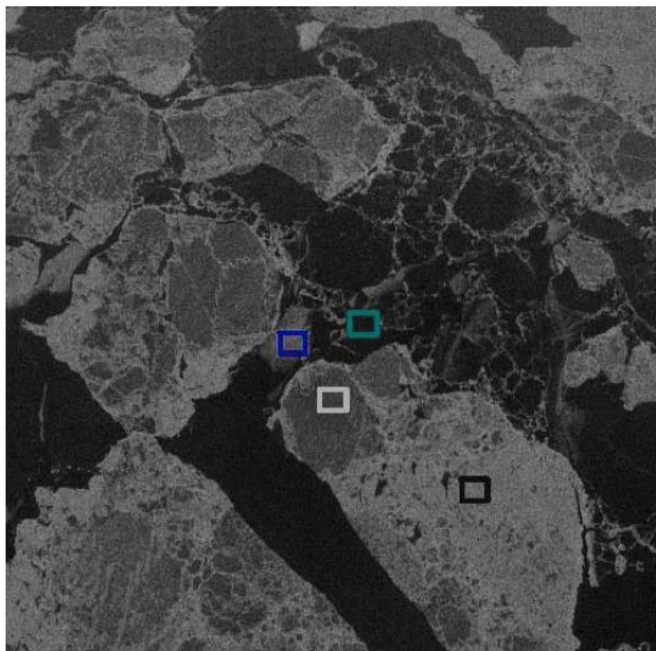


Fig.3. Intensive Study Area in the sea of Okhotsk 23 Feb.1999(Single look Slant range Complex Data,8look  $1000 \times 987$  pixels,L band HH polarization)

Green: Open water, Black: Rough surface ice, Blue Thin ice White: Smooth surface ice.

### B. Correlation Matrix

Correlation matrix for open water is shown in Table 2 while that of rough first year ice is shown in Table 3, respectively.. Meanwhile, correlation matrix for smooth first year ice is shown in Table 4 while that for thin ice is shown in Table 5, respectively. Two rows from the bottom shows SUM and |SUM|, respectively.

It is found that the smallest SUM for open water is Sphere followed by Diffuse and Helix while that for rough surface of first year ice is Odd number of scattering followed by Even number of scattering and Sphere. It is also found that the smallest SUM for smooth surface of first year ice is Sphere followed by Odd number scattering and Helix as well as Diffuse while that of thin ice is Odd number of scattering followed by Sphere and Even number of scattering. It totally depends on the scattering mechanism for the ground cover targets.

TABLE II. CORRELATION MATRIX FOR OPEN WATER

open water	Odd	Even	Diffuse	Sphere	Diplane	Helix	HH	HV	VV
Od	1	-0.99	-0.49	0.399	-0.22	-0.3	0.527	0.13	0.608
Ev	-0.99	1	0.402	-0.37	0.233	0.233	-0.49	-0.18	-0.57
Df	-0.49	0.402	1	-0.41	-0.05	0.66	-0.56	0.39	-0.58
Sp	0.399	-0.37	-0.41	1	-0.74	-0.48	0.504	-0.06	0.377
Dp	-0.22	0.233	-0.05	-0.74	1	-0.23	-0.22	-0.19	-0.09
Hx	-0.3	0.233	0.66	-0.48	-0.23	1	-0.44	0.32	-0.43
HH	0.527	-0.49	-0.56	0.504	-0.22	-0.44	1	0.38	0.93
HV	0.13	-0.18	0.385	-0.06	-0.19	0.322	0.38	1	0.403
VV	0.608	-0.57	-0.58	0.377	-0.09	-0.43	0.93	0.4	1
	0.07	-0.1	0.04	0.02	-0.1	0.04	0.18	0.24	0.18
	0.07	0.08	0.04	0.02	0.06	0.04	0.18	0.24	0.18

TABLE III. CORRELATION MATRIX FOR ROUGH FIRST YEAR ICE

rough FYI	Odd	Even	Diffuse	Sphere	Diplane	Helix	HH	HV	VV
Od	1	-0.99	-0.32	0.621	-0.51	-0.29	0.286	-0.04	0.349
Ev	-0.99	1	0.174	-0.56	0.502	0.215	-0.26	-0.05	-0.32
Df	-0.32	0.174	1	-0.53	0.193	0.545	-0.2	0.59	-0.29
Sp	0.621	-0.56	-0.53	1	-0.74	-0.57	0.332	-0.24	0.402
Dp	-0.51	0.502	0.193	-0.74	1	-0.13	-0.3	-0.07	-0.32
Hx	-0.29	0.215	0.545	-0.57	-0.13	1	-0.13	0.44	-0.2
HH	0.286	-0.26	-0.2	0.332	-0.3	-0.13	1	0.52	0.789
HV	-0.04	-0.05	0.586	-0.24	-0.07	0.437	0.519	1	0.44
VV	0.349	-0.32	-0.29	0.402	-0.32	-0.2	0.789	0.44	1
	0.01	-0	0.13	-0	-0	0.1	0.23	0.29	0.21
	0.01	0.03	0.13	0.03	0.04	0.1	0.23	0.29	0.21

TABLE IV. CORRELATION MATRIX FOR SMOOTH FIRST YEAR ICE

smooth FYI	Odd	Even	Diffuse	Sphere	Diplane	Helix	HH	HV	VV
Od	1	-0.99	-0.55	0.693	-0.53	-0.35	0.537	-0.04	0.629
Ev	-0.99	1	0.414	-0.65	0.546	0.271	-0.48	-0.06	-0.58
Df	-0.55	0.414	1	-0.55	0.179	0.589	-0.57	0.53	-0.59
Sp	0.693	-0.65	-0.55	1	-0.75	-0.53	0.638	-0.14	0.597
Dp	-0.53	0.546	0.179	-0.75	1	-0.16	-0.43	-0.18	-0.37
Hx	-0.35	0.271	0.589	-0.53	-0.16	1	-0.39	0.43	-0.42
HH	0.537	-0.48	-0.57	0.638	-0.43	-0.39	1	0.15	0.834
HV	-0.04	-0.06	0.535	-0.14	-0.18	0.433	0.146	1	0.14
VV	0.629	-0.58	-0.59	0.597	-0.37	-0.42	0.834	0.14	1
	0.04	-0.1	0.05	0.03	-0.1	0.05	0.14	0.2	0.14
	0.04	0.06	0.05	0.03	0.08	0.05	0.14	0.2	0.14

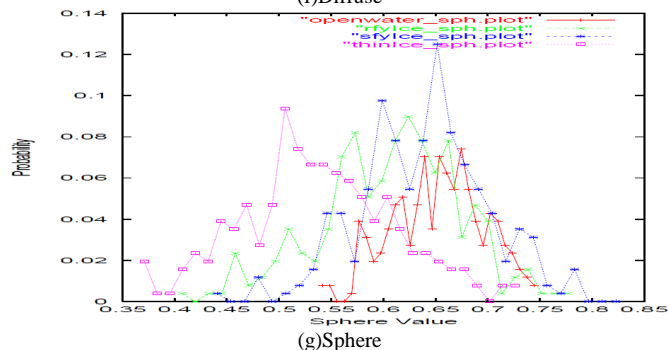
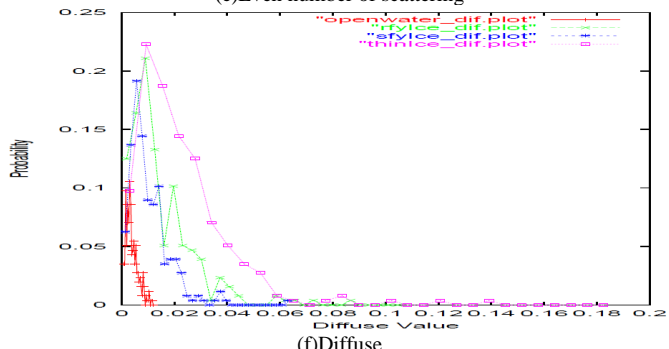
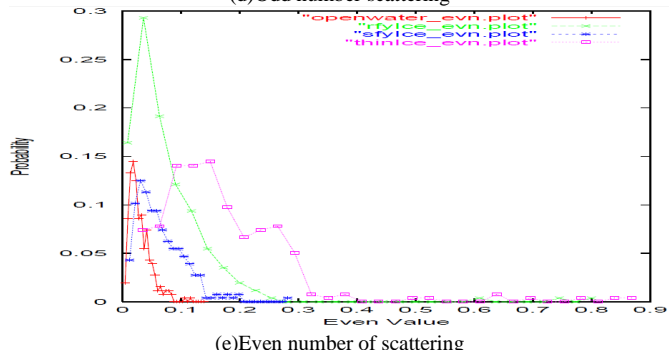
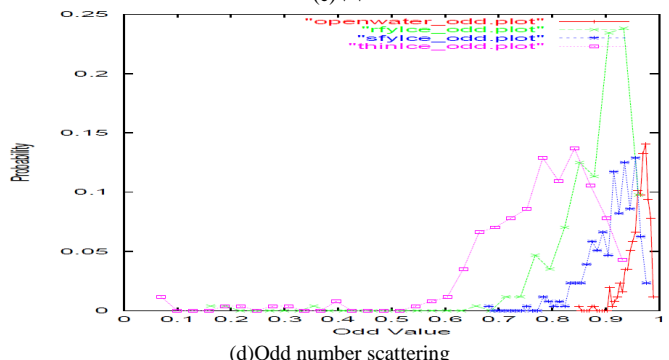
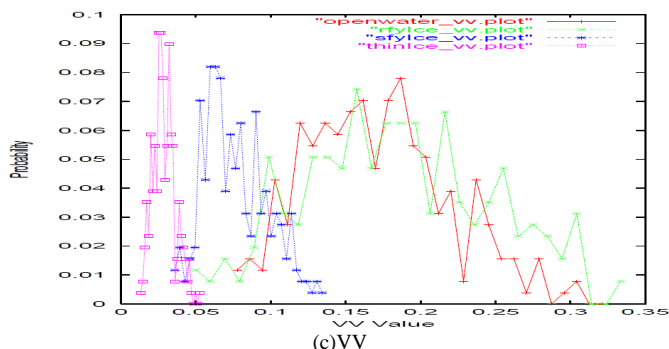
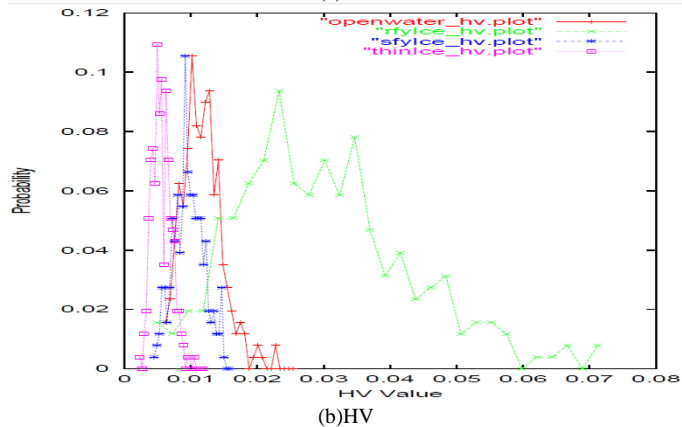
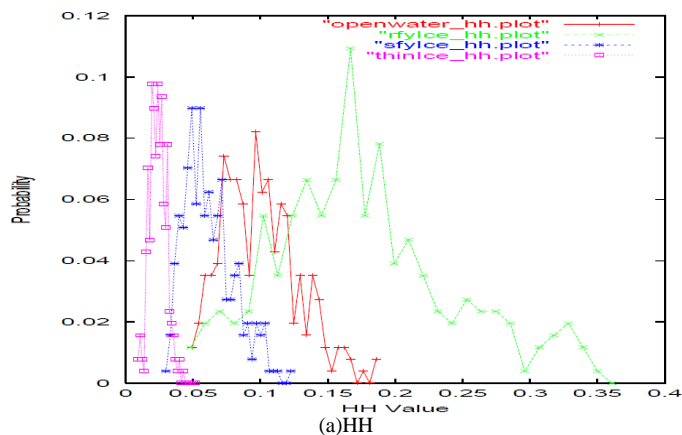
TABLE V. CORRELATION MATRIX FOR THIN ICE

thin ice	Odd	Even	Diffuse	Sphere	Diplane	Helix	HH	HV	VV
Od	1	-0.99	-0.34	0.656	-0.48	-0.31	0.331	-0.15	0.44
Ev	-0.99	1	0.193	-0.61	0.493	0.235	-0.28	0.04	-0.38
Df	-0.34	0.193	1	-0.47	0.074	0.533	-0.42	0.73	-0.51
Sp	0.656	-0.61	-0.47	1	-0.68	-0.54	0.533	-0.27	0.537
Dp	-0.48	0.493	0.074	-0.68	1	-0.26	-0.28	-0.13	-0.25
Hx	-0.31	0.235	0.533	-0.54	-0.26	1	-0.38	0.51	-0.42
HH	0.331	-0.28	-0.42	0.533	-0.28	-0.38	1	-0.06	0.425
HV	-0.15	0.044	0.73	-0.27	-0.13	0.513	-0.06	1	-0.11
VV	0.44	-0.38	-0.51	0.537	-0.25	-0.42	0.425	-0.11	1

0.02 -0 0.09 0.02 -0.1 0.04 0.1 0.17 0.08  
 0.02 0.03 0.09 0.02 0.06 0.04 0.1 0.17 0.08

C. Overlapped Portion of Probability Density Function between Features

Figure 4 shows PDF of each class for each feature extracted from the full polarization SAR and decomposed components from the full polarization of SAR. Some of the features, in particular, odd and even number of scattering as well as diffuse component shows not normal distribution at all. Therefore, it would better to check not only correlation coefficients but also PDF of the features.



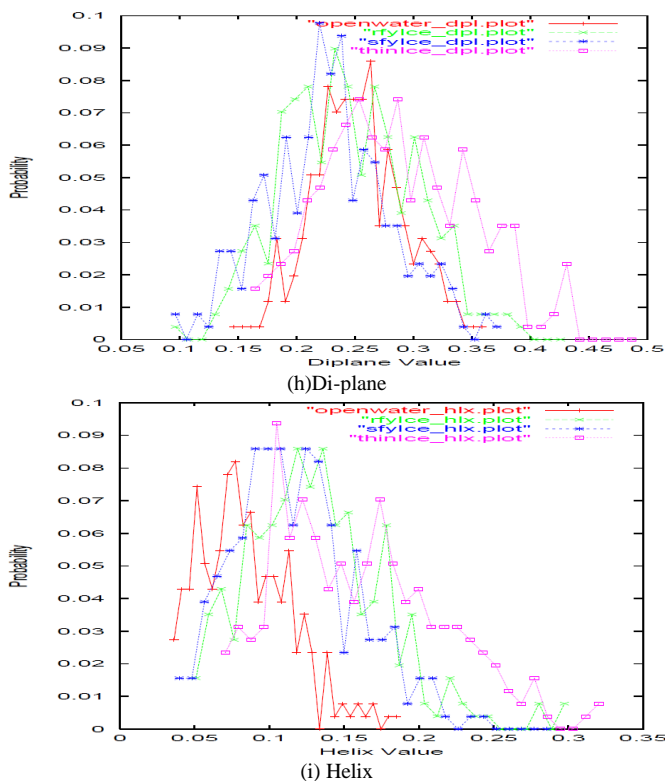


Fig.4. PDF of each class for each feature

D. Confusion Matrix

Nevertheless correlation among the received power signals of HH, HV, and VV, classification result shows highest Percent Correct Classification: PCC of 94.6 % among the all possible combination of receiving power signals and the decomposed components. Figure 5 shows the classified resultant image.

TABLE VI. CONFUSION MATRIX FOR UTILIZING THREE RECEIVED POSERS ONLY (PCC=94.6%)

	OpenWater	RoughIce	SmoothIce	ThinIce
OpenWater	92.2	0.8	7.0	0.0
RoughIce	2.0	92.2	5.8	0.0
SmoothIce	3.1	0.4	95.3	1.2
ThinIce	0.0	0.0	1.2	98.8

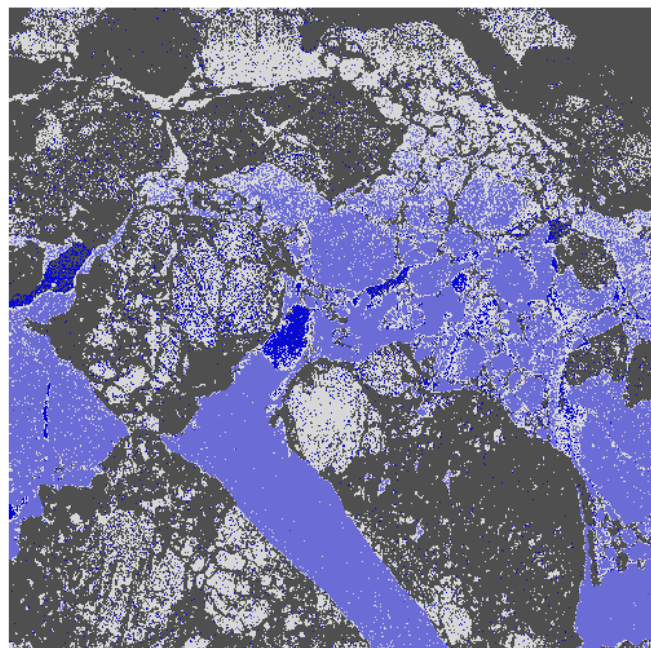


Fig.5. Classification resultant image for utilizing three received power singles only (Black: Rough surface ice, White: Smooth surface ice, Light blue: Open water, Dark blue: Thin ice)

The next highest PCC is achieved by the combination of three receiving power signals and Diffuse as well as Odd number of scattering components. Figure 6 shows classified resultant image.

TABLE VII. CONFUSION MATRIX FOR UTILIZING THREE RECEIVED POWERS AND ODD NUMBER OF SCATTERING AS WELL AS DIFFUSE COMPONENT (PCC=93.6%)

	OpenWater	RoughIce	SmoothIce	ThinIce
OpenWater	93.4	0.8	5.8	0.0
RoughIce	3.1	92.2	4.7	0.0
SmoothIce	6.6	0.8	92.2	0.4
ThinIce	0.8	0.0	3.5	95.7

Although PCC of the classification with three received power signals and Diffuse and Odd number of scattering components is lower than that with just three received power signals only, there are some thin ice pixels are observed in the open water and smooth surface of first year ice areas.

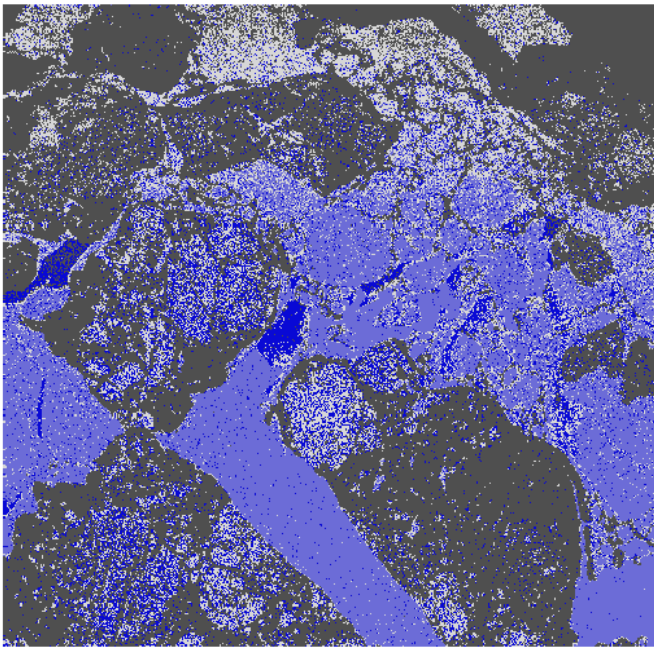


Fig.6. Classification resultant image for utilizing three received power singles and Diffuse, Odd number scattering components. (Black: Rough surface ice, White: Smooth surface ice, Light blue: Open water, Dark blue: Thin ice)

This is natural. Therefore, classified results from the classification with three received power signals and Diffuse and Odd number of scattering components shows much reliable classified results.

As the results, it is found that three receiving power signals plus Diffuse and Odd number of scattering component is effective to the sea ice classifications. The reasons for this are

1) *surface scattering is dominant for the smooth and rough surface first year ice.*

2) *Diffuse component of smooth surface first year ice is smaller than that of rough surface first year ice.*

On the other hand, thin ice consists of a kind of layered material with open water which is covered with ice so that it is hard to discriminate thin ice from smooth surface first year ice as well as open water.

#### IV. CONCLUSION

Multi spectral image classification method with selection processes of independent spectral features through correlation analysis is proposed. The proposed method is validated by applying to the polarimetric Synthetic Aperture Radar: SAR data. Also Probability Distribution Function: PDF for of features are checked and confirmed the most independent PDF allows greatest classification performance.

It is found that three receiving power signals plus Diffuse and Odd number of scattering component is effective to the sea ice classifications. The reasons for this are (1) surface scattering is dominant for the smooth and rough surface first

year ice. (2) Diffuse component of smooth surface first year ice is smaller than that of rough surface first year ice.

On the other hand, thin ice consists of a kind of layered material with open water which is covered with ice so that it is hard to discriminate thin ice from smooth surface first year ice as well as open water.

#### ACKNOWLEDGMENT

The author would like to thank Mr. Saeki for his efforts through experiments and simulations.

#### REFERENCES

- [1] Zebker, H.A., vanZyl, J.J. Imaging radar polarimetry: A review. Proc. IEEE 79, 1583–1606, 1991.
- [2] Ulaby, F.T., Elachi, C. Radar Polarimetry for Geoscience Applications. Artech House Inc., Dedham, 1990.
- [3] Mott, M. Antennas for Radar Communications – A Polarimetric Approach. John Wiley, New York, 1992.
- [4] Henderson, F.M., Lewis, A.J. Principles and applications of imaging radar, in: Manual of Remote Sensing, third ed. John Wiley, New York, 1998.
- [5] Krogager, E. Analysis of the absolute and relative phase conditions of transforming matrices for the Sinclair and covariance matrices in radar polarimetry. J. Opt. Soc. Am. E72B, 1A, 1993.
- [6] Dong, Y. Imaging radar polarimeter from wave synthesis. J. Geophys. Res. 92 (81), 638–701, 1987.
- [7] Zebker, H.A., et al., Imaging radar polarimeter from wave synthesis, J. Geophysical Research, Vol.92, No.81, pp.638-701, 1987.
- [8] Krogager, E., Czyz, Z.H. Properties of the sphere, di-plane, helix decomposition, in: Proceedings, Third International Workshop on Radar Polarimetry, vol. 1, pp. 106–114, 1995.
- [9] Cloude, S.R., Pottier, E. A review of target decomposition theorems in radar polarimetry. IEEE Trans. Geosci. Remote Sensing 34 (2), 498–518, 1995.
- [10] Pottier, E., Lee, J.S. Unsupervised classification scheme of PolSAR images based on the complex Wishart distribution and H/A/a polarimetric decomposition theorems, Proceedings of the Third European Conference on Synthetic Aperture Radar: EUSAR, 2000.
- [11] Scheuchl, B., Hajinsek, I., Cumming, I.G., et al. Sea ice classification using multi-frequency polarimetric SAR data, in: Proceedings of the IGARSS'02, 2002.
- [12] vanZyl, J.J., Zebker, H.A., Elachi, C. Imaging radar polarization signatures, theory and observation. Radio Sci. 22 (4), 529–543, 1987.
- [13] Kohei Arai and J.Wang, Polarimetric SAR image classification with maximum curvature of the trajectory in eigen space domain on the polarization signature, Advances in Space Research, 39, 1, 149-154, 2007.

#### AUTHORS PROFILE

**Kohei Arai**, He received BS, MS and PhD degrees in 1972, 1974 and 1982, respectively. He was with The Institute for Industrial Science and Technology of the University of Tokyo from April 1974 to December 1978 also was with National Space Development Agency of Japan from January, 1979 to March, 1990. During from 1985 to 1987, he was with Canada Centre for Remote Sensing as a Post Doctoral Fellow of National Science and Engineering Research Council of Canada. He moved to Saga University as a Professor in Department of Information Science on April 1990. He was a councilor for the Aeronautics and Space related to the Technology Committee of the Ministry of Science and Technology during from 1998 to 2000. He was a councilor of Saga University for 2002 and 2003. He also was an executive councilor for the Remote Sensing Society of Japan for 2003 to 2005. He is an Adjunct Professor of University of Arizona, USA since 1998. He also is Vice Chairman of the Commission "A" of ICSU/COSPAR since 2008. He wrote 30 books and published 322 journal papers

# Access Fee Charging System for Information Contents Sharing Through P2P Communications

Kohei Arai

Graduate School of Science and Engineering  
Saga University  
Saga City, Japan

**Abstract**—Charge system for information contents exchange through P2P communications is proposed. Security is the most important for this charge system and is kept with data hiding method with steganography and watermarking. Security level for this charge system is evaluated with image contents.

**Keywords**—P2P communication; steganography; data hiding; watermarking; charge system; content security

## I. INTRODUCTION

Although there are so many charge systems for client-server model of communications, a small number of charge system for P2P communications. From the begging of the information contents exchange and or selling and buying, information content provider is server and the customers are clients. Users' demands, however, are getting large for information contents exchange and or selling and buying through P2P communications. In particular, charge system for information contents exchange through P2P communications is getting more necessary.

When users share their files, Instant Messaging: IM, information including voice communications on Internet Protocol: IP networks (VoIP), charge system is highly required. The well known package based digital content business models are no longer work. In order to realize charging system for information sharing, the followings are proposed,

- 1) gather a fixed amount for information content access fees by the provider side,
- 2) charge access fees through authentication server.

Users have to have a right for accessing information contents from information providers in the case of (1) while users are charged when they get an authentication from the authentication server (information content access fees may change by amount of information contents) in the case of (2). Internet (or digital) stock company used to use the case of (2).

In the case of (1), there are two major problems, access fees do not depend on accessing information contents, and it require time consumable contraction processes on information sharing services. On the other hands, there is serious problem on information content accessing procedure of which users have to get authentication before accessing information contents. Furthermore, it is desired to access information contents directly from users. Moreover, there is no authentication server in the P2P communications.

The following section describes the proposed charge system for information sharing among users through P2P

communications followed by some experiments for the key components of the proposed charge system. Finally, conclusion is followed together with some discussions.

## II. PROPOSED CHAGE SYSTEM

### A. Blockdiagram, Configuration, and Process Flow of the Proposed Charge System for Informtion Content Sharing Through P2P Communications

Process flow of the proposed charge system for information content sharing through P2P communications is shown in Figure 1.

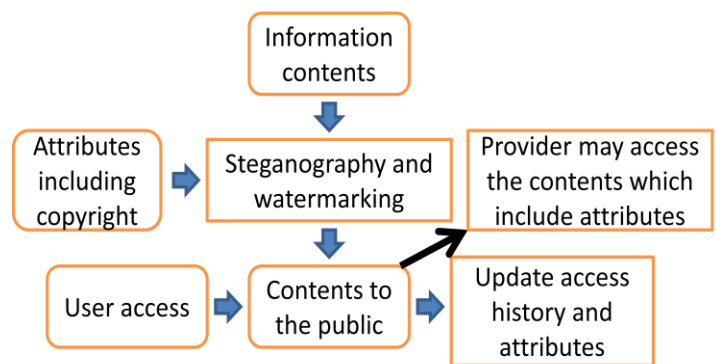


Fig.1. Process flow of the proposed charge system for information content sharing through P2P communications

Attributes include copyright information as well as the other information which are required for charging of access fees and for protect the copyright of the information contents. All the aforementioned attribute information are coded and embedded into the original information contents based on data hiding, steganography and watermarking. Then the attribute information hidden information contents are ready to provide. Data hiding method based on wavelet Multi Resolution Analysis: MRA has been proposed already [1]-[3]. Also the method for keyword extraction from the original documents based on Analytic Hierarchical Process: AHP<sup>1</sup> has been proposed already [4]. Invisibility of hidden documents has also been improved by means of random scanning [5].

Information providers will make web search catalog. When users would like to access the information content in concern through looking at the catalog, the attribute information

<sup>1</sup> <http://ja.wikipedia.org/wiki/%E9%9A%8E%E5%B1%A4%E5%88%86%E6%9E%90%E6%B3%95>

containing information content in concern is accessed. In the catalog information, there is access fee ("Point" in the proposed system). At that time, attribute information which includes access history is updated automatically. Also the information content provider may look at the attribute information because the information provider, owner of the information content, and copyright holder knows how to reconstruct the attribute information. Thus, the information content provider can protect information contents, copyright, and also can get the information of access history, etc.

The "Point" is updated after the information contents are accessed. Therefore, the "Point" of the information contents providers is increased after the access. The "Point" may be used for accessing the other information contents in the public domain.

Therefore, the "Point" is increased when users' information contents are accessed while users may lose their "Point" when they access the other information content from the other users.

**B. Specific Features of the Proposed Charge System**

The proposed charge system has the following specific features,

- 1) Information content providers may confirm the facts that receivers (users) access the information contents in concern,
- 2) Information content providers may protect their copyright because the provided contents include copyright signatures (or forms) based on steganography and watermarking,
- 3) Information content provider may look at access history parameters such as the number of access, access user ID, the access date, IP address, etc.
- 4) No real money is required for information contents sharing. Only thing users have to have for information content sharing is the "Point". Therefore, there is no need to provide any personal information at all.

**C. Key Components of the Proposed Charge System**

Key component of the proposed charge system is steganography and watermarking. Wavelet Multi Resolution Analysis: MRA based watermarking method is used. The principle of the method is Laplacian pyramid which is shown in Figure 2.

Even if the general users who do not authenticated at all access to the information contents database server and acquire the information contents, such users could not decryption the original information contents at all because such users do not know the way for decryption of the information contents which are protected by steganography and watermarking.

Original image can be decomposed with horizontally and vertically low as well as high wavelet frequency components based on wavelet MRA which is expressed in equation (1).

$$F=C_n\eta \tag{1}$$

Where  $F$ ,  $C_n$ , and  $\eta$  is wavelet frequency component, wavelet transformation matrix, and input data in time and/or

space domain. Because  $C_n^t=C_n^{-1}$ ,  $\eta$  can be easily reconstructed with wavelet frequency component,  $F$ .

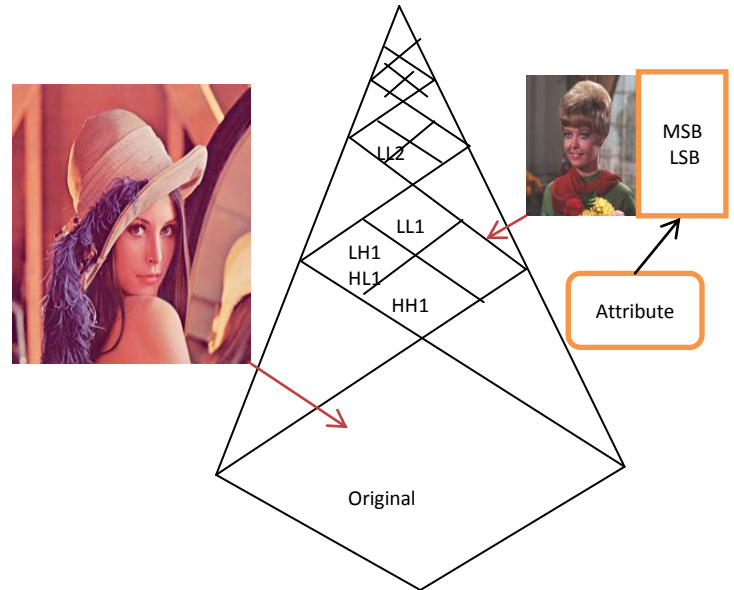


Fig.2. Schematic views of the proposed steganography and watermarking

Equation (1) is one dimensional wavelet transformation and is easily expanded to multi dimensional wavelet transformation.

$$F=(C_n (C_m (C_l \eta)^t)^t)^t \dots \tag{2}$$

In the case of wavelet transformation of images, two dimensional wavelet transformation is defined as follows. Horizontally low wavelet frequency component and vertically low frequency component is called  $LL_1$  component at the first stage. Horizontally low wavelet frequency component and vertically high frequency component is called  $LH_1$  component at the first stage. Horizontally high wavelet frequency component and vertically low frequency component is called  $HL_1$  component at the first stage. Horizontally high wavelet frequency component and vertically high frequency component is called  $HH_1$  component at the first stage. Then  $LL_1$  component can be decomposed with  $LL_2$ ,  $LH_2$ ,  $HL_2$ , and  $HH_2$  components at the second stage. Also  $LL_2$  component is decomposed with  $LL_3$ ,  $LH_3$ ,  $HL_3$ , and  $HH_3$  components at the third stage as shown in Figure 3.

Thus Laplacian pyramid<sup>2</sup> which is shown in Figure 2 is created. If these four decomposed components,  $LL_n$ ,  $LH_n$ ,  $HL_n$ , and  $HH_n$  are given, then  $LL_{n-1}$  is reconstructed. Therefore, the original image can be reconstructed with all the wavelet frequency components perfectly.

The copied information contents can be replaced into the designated portion of wavelet frequency component. Furthermore, the Least Significant Bit: LSB is also replaced to the encrypted location of wavelet frequency component in which the copied information contents are replaced. Furthermore, attribute information are also can be embedded to the LSB. LSB data does not affect information contents, in particular for imagery data because imagery data is redundant

<sup>2</sup> [http://en.wikipedia.org/wiki/Laplacian\\_pyramid](http://en.wikipedia.org/wiki/Laplacian_pyramid)

enough. Therefore, LSB data is not visible in the information content in the public domain. If the information content in concern is not imagery data, then MSB to LSB-1 bits of data can be used for information contents. Moreover, the encrypted location is randomly scanned with Mersenne Twister<sup>3</sup> of random number generator. Therefore, only the authenticated users who know the parameters of the random number generator can decode the location of the wavelet frequency component.

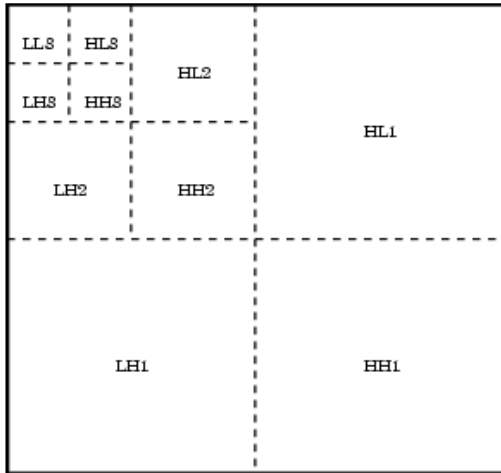


Fig.3. Two dimensional wavelet transformation

### III. EXPERIMENTS

#### A. Data Used

Figure 4 shows example images of information content in concern. Figure 4 (a) shows "Lena" image which is opened to the public while Figure 4 (b) shows "Zelda" image of one of the information contents in concern. Both images are derived from the well known standard image database, SIDBA. As shown in Figure 2, all the required information for reconstruction of "Zelda" image is included in the LSB of "Zelda" image together with copyright information. Then the designated wavelet frequency component image is replaced to this "Zelda" image. The authenticated user who knows the parameters for random number derived from Messene Twister access to the image (information content) in concern can reconstruct "Zelda" image. Otherwise, required information, attribute information cannot be decoded results in no reconstructed image can be obtained.

#### B. Experiemntal Results

Image quality of the "Lena" depends on the process parameters of the location of wavelet frequency component in which the information content in concern is replaced to it.

Figure 5 (a) shows the reconstructed image of "Lena" in which HH1 component is replaced to "Zelda" image while Figure 5 (b) shows the reconstructed "Lena" image in which HH1 frequency component is replaced to "Zelda" image together with all the required information of reconstruction of the "Zelda" image is embedded into LSB component based on

steganography. Through a comparison between Figure 5 (a) and (b), image defect due to steganography is almost invisible.



(a)Original image of "Lena"



(b)Information content in concern of "Zelda"

Fig.4. Examples of images which is opened to the public and information content in concern

Figure 6 (a) shows the reconstructed image of "Lena" in which HH1 component is replaced to "Zelda" image while Figure 6 (b) shows the reconstructed "Lena" image in which HH2 frequency component is replaced to "Zelda" image together with all the required information of reconstruction of the "Zelda" image is embedded into LSB component based on steganography. Through a comparison between Figure 6 (a) and (b), image defect due to steganography is almost invisible.

Figure 7 (a) shows the reconstructed image of "Lena" in which HH1 component is replaced to "Zelda" image while Figure 7 (b) shows the reconstructed "Lena" image in which HH3 frequency component is replaced to "Zelda" image together with all the required information of reconstruction of the "Zelda" image is embedded into LSB component based on steganography. Through a comparison between Figure 7 (a) and (b), image defect due to steganography is almost invisible.

<sup>3</sup> <http://www.math.sci.hiroshima-u.ac.jp/~m-mat/MT/mt.html>



(a)HH1 component is replaced to the "Zelda" image



(a)HH2 frequency component is replaced to "Zelda" image



(b)HH1 frequency component is replaced to the "Zelda" image together with all the required information of reconstruction of the "Zerlda" image is embedded into LSB component based on steganography

Fig.5. Reconstructed "Lena" images which containing "Zelda" image and "Zelda" and all the required information for reconstruction of "Zelda" image in concern



(b) HH2 frequency component is replaced to "Zelda" image together with all the required information of reconstruction of the "Zerlda" image is embedded into LSB component based on steganography

Fig.6. Reconstructed image from the image of which HH2 frequency component is replaced to "Zelda" image



(a)HH3 frequency component is replaced to "Zelda" image



(a)HH4 frequency component is replaced to "Zelda" image



(b) HH3 frequency component is replaced to "Zelda" image together with all the required information of reconstruction of the "Zerlda" image is embedded into LSB component based on steganography

Fig.7. Reconstructed image from the image of which HH2 frequency component is replaced to "Zelda" image



(b) HH4 frequency component is replaced to "Zelda" image together with all the required information of reconstruction of the "Zerlda" image is embedded into LSB component based on steganography

Fig.8. Reconstructed image from the image of which HH2 frequency component is replaced to "Zelda" image

Figure 8 (a) shows the reconstructed image of "Lena" in which HH4 component is replaced to "Zelda" image while Figure 8 (b) shows the reconstructed "Lena" image in which HH4 frequency component is replaced to "Zelda" image together with all the required information of reconstruction of the "Zelda" image is embedded into LSB component based on steganography. Through a comparison between Figure 8 (a) and (b), image defect due to steganography is almost invisible.

Image quality is decreases in accordance with the number of level or stage of MRA obviously. Also it is found that image defect due to steganography is not visible. Therefore, general users do not aware of the information content in concern (in this case, "Zelda" image). Root Mean Square: RMS difference between the reconstructed and the original "Lena" image is evaluated. The RMS difference between both images without steganography is shown in Table 1 while that with setganography is also shown in Table 2, respectively. For cases, HH1, HH2, HH3, and HH4 component is replaced to "Zelda" image. RMS difference for all these cases shows quite small.

Therefore, it is not easy to distinguish which is original or reconstructed image. It is also found that the RMS difference is getting large in accordance with the level, stage. Furthermore, image defect due to the steganography is small enough, negligible.

TABLE I. RMS DIFFERENCE BETWEEN BOTH IMAGES WITHOUT STEGANOGRAPHY

Stage, level	RMS diff.
1	0.01372
2	0.01435
3	0.01526
4	0.01691

TABLE II. RMS DIFFERENCE BETWEEN BOTH IMAGES WITH STEGANOGRAPHY

Stage, level	RMS diff.
1	0.01380
2	0.01443
3	0.01532
4	0.01688

On the other hands, authenticated users can reconstruct "Zelda" image because they know the location of frequency component which is derived from the LSB of the frequency

component. Only thing they have to know is initial condition of random number which is generated by Messene Twister.

Also the information content providers may access to their contents. Then they can decode attribute information which includes copyright information the number of access, user ID of the user who accesses the contents. Thus "Point" can be updated after the information contents are serviced.

#### IV. CONCLUSION

Access fee charge system for information contents sharing through P2P communications is proposed. Security is the most important for this charge system and is kept with data hiding method with steganography and watermarking. Security level for this charge system is evaluated with image contents.

#### ACKNOWLEDGMENT

The author would like to thank Dr. KanameSeto for his effort to conduct the experiments on data hiding.

#### REFERENCES

- [1] K.Arai and K.Seto, Data hiding method based on wavelet Multi Resolution Analysis: MRA, Journal of Visualization Society of Japan, Vol.22, Suppl.No.1, 229-232, 2002.
- [2] K.Arai and K.Seto, Data hiding method based on wavelet Multi Resolution Analysis: MRA utilizing eigen value decomposition, Journal of Visualization Society of Japan, Vol.23, No.8, pp.72-79,2003.
- [3] K.Arai and K.Seto, Data hiding method based on wavelet Multi Resolution Analysis: MRA utilizing image space coordinate conversion, Journal of Visualization Society of Japan, 25, Suppl.No.1, 55-58,(2005)
- [4] K.Arai, Keyword extraction method from paper based documents, drawings, based on knowledge importance evaluation with Analytic Hierarchical Process: AHP method, Journal of Image and Electronic Engineering Society of Japan, 34, 5, 636-644, (2005)
- [5] K.Arai and K.Seto, Data hiding method based on wavelet Multi Resolution Analysis: MRA utilizing random scanning for improving invisibility of the secret image, Journal of Visualization Society of Japan, 29, Suppl.1, 167-170, 2009.

#### AUTHORS PROFILE

**KoheiArai**, He received BS, MS and PhD degrees in 1972, 1974 and 1982, respectively. He was with The Institute for Industrial Science, and Technology of the University of Tokyo from 1974 to 1978 also was with National Space Development Agency of Japan (current JAXA) from 1979 to 1990. During from 1985 to 1987, he was with Canada Centre for Remote Sensing as a Post Doctoral Fellow of National Science and Engineering Research Council of Canada. He was appointed professor at Department of Information Science, Saga University in 1990. He was appointed councilor for the Aeronautics and Space related to the Technology Committee of the Ministry of Science and Technology during from 1998 to 2000. He was also appointedcouncilor of Saga University from 2002 and 2003 followed by an executive councilor of the Remote Sensing Society of Japan for 2003 to 2005. He is an adjunct professor of University of Arizona, USA since 1998. He also was appointedvice chairman of the Commission "A" of ICSU/COSPARin 2008. He wrote 30 books and published 332 journal papers.

# Wearable Computing System with Input-Output Devices Based on Eye-Based Human Computer Interaction Allowing Location Based Web Services

Kohei Arai

Graduate School of Science and Engineering  
Saga University  
Saga City, Japan

**Abstract**—Wearable computing with Input-Output devices Base on Eye-Based Human Computer Interaction: EBHCI which allows location based web services including navigation, location/attitude/health condition monitoring is proposed. Through implementation of the proposed wearable computing system, all the functionality is confirmed. It is also found that the system does work well. It can be used easily and also is not expensive. Experimental results for EBHCI show excellent performance in terms of key-in accuracy as well as input speed. It is accessible to internet, obviously, and has search engine capability.

**Keywords**—eye based human computer interaction; wearable computing; location based web services

## I. INTRODUCTION

For many years, wearable computing system has been studied. Not so small number of wearable computing systems has been proposed so far. One of the difficult problems on wearable computing systems is input and output devices in particular input device. There are some proposed input devices for wearable computing systems such as “Project Glass”<sup>1</sup> and “Contact Lens”<sup>2</sup>. These require relatively expensive devices such as projector which allows display a keyboard on hand or arm, and contact lens which has keyboard layout in the lens. On the other hand, Eye-Based Human Computer Interaction: EBHCI is proposed together with camera mouse [1]-[27]. EBHCI can be used as computer input device with human eyes only. Also camera mouse allows the entire mouse operations (click right and left button and drag and drop operations) with human eyes only. Computer input can be done with just by sight. EBHCI requires just web cameras, and display with Bluetooth capability. Furthermore, only thing users have to do is just looking at the desired key which is displayed onto Head mount Display: HMD. Also users can easily manipulate mouse with their eyes by looking at the icons. Therefore, EBHCI based wearable computing system can be created with not so expensive cost. Furthermore, it is easy to use.

In this paper, EBHCI based computer input device is proposed together with wearable computing system utilizing

EBHCI based device. Users may use web services including search engine during making actions. For instance, users may use search engine when they are walking. A variety of applications is available with the proposed wearable computing system. For example, users are navigated with the proposed system. One of key issues here is computer key-in devices, camera mouse, and indoor location estimation. Key-in accuracy of the proposed system, therefore, has to be clarified together with indoor location estimation accuracy.

The following section describes the proposed wearable computing system and examples of the applications of the proposed system. Then key-in accuracy assessment results is followed by through some experiments together with the indoor location estimation accuracy evaluation results. Then conclusion is described together with some discussions.

## II. PROPOSED METHOD

### A. Configuration of the Proposed Wearable Computing System

Configuration of the proposed wearable computing system is shown in Figure 1.

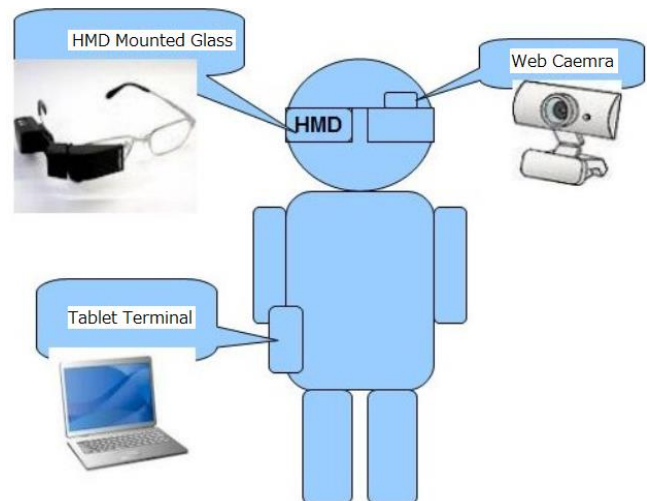


Fig.1. Configuration of the proposed wearable computing system

Users wear the Head Mount Display: HMD mounted glass. The glass also carries backward looking camera. The backward

<sup>1</sup> <http://arkouji.cocolog-nifty.com/blog/2013/01/googleproject-g.html>

<sup>2</sup> <http://commonpost.boo.jp/?p=19724>

<http://japanese.engadget.com/2008/01/17/researchers-put-circuits-on-contact-lenses-freak-out-rabbits/>

looking camera looks users' eye. Users' line of sight can be estimated with the acquired images of the backward looking camera. The HMD and the backward looking camera are connected to tablet terminals through wire and / or Bluetooth communication as shown in Figure 2.

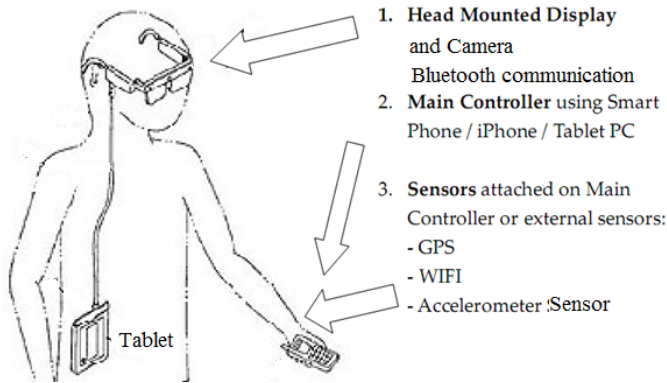


Fig.2. Connections HMD and the backward looking camera to tablet PC and / or mobile phones

The required processes for estimation of the position at which users is looking on the display screen of the HMD through line of sight estimation are done in the Tablet PC. Also gathered data of the user's location and accelerometer data are handled in the mobile terminals or Tablet PC. Therefore, user's location can be known with the GPS receiver data. Even if the user is situated indoors, WiFi capability allows estimation of the user's location by using signal lengths from the nearest three WiFi access points



Fig.3. Single HMD and backward looking camera mounted glass

**B. Computer Key-in with Eye Based Human-Computer Interaction: EBHCI**

One of the key issues here is computer key-in with Eye-Based Human-Computer Interaction EBHCI and Eye-Based mouse as well as location estimation based on the received signal lengths from WiFi access points.

EBHCI uses moving keyboard which is shown in Figure 4. On the typical key layout, there is five enlarged keys. The key at which user is looking is shown at the center key of the enlarged five keys. The character of the center key, therefore, may change depending on the gaze location where user is looking at. When user looks one of the four surrounding keys, left, right, top and bottom, then characters for the five enlarged keys are changed in accordance with user's gaze location. For instance, if user is looking at the right key, then the keyboard moves to the right direction with one key step and the

characters of the five surrounding keys are changes simultaneously as shown in Figure 5.

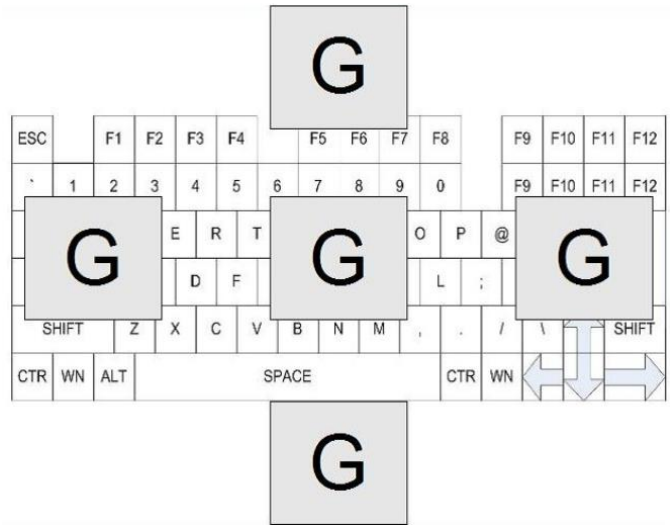


Fig.4. Key layout of the moving keyboard

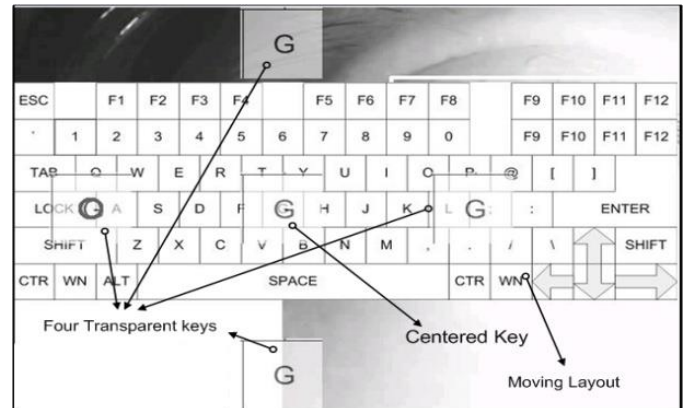


Fig.5. Key layout for the proposed moving keyboard (Circle denotes gaze location)

If the keyboard does not move, then the gaze location has to be determined precisely because key size is too small in comparison to the proposed moving keyboard. User has to retry key-in when the selected key is not intended key due to mis-identification of key location results in it takes much longer time in comparison to the required key-in time for the proposed moving keyboard. Therefore, the proposed moving keyboard does not require precise gaze estimation accuracy and makes high success rate of key-in performance with relatively short time period.

**C. Camera Mouse**

All mouse event and key-in can be done with human eyes only [1]-[15]. In the camera mouse, comparatively high gaze estimation accuracy is needed for identifying icons which are displayed onto HMD screen. Icon hold is available to keep the previous click event by using one additional key for hold. Thus right or left button clicks and multiple key selections are available. For instance, Ctl+Alt+Del for task manager activation can be selected by using the hold key operation. Thus all the icons for application software including search

engine can be activated. Therefore, user can use web services with the proposed wearable computing system.

D. Indoor Location Estimation

Some of the web services need the location information. When user is situated outdoor, GPS receiver included in smart phone, iPhone, or some other mobile devices is used. Location estimation accuracy of GPS receiver, however, is not good enough. It is not always that user is situated outdoor. Therefore, indoor location estimation is needed.

The authors proposed the indoor location estimation method and system. It achieved 2.5m of location accuracy [16]. It would be enough for web services. The first step is to draw a two-dimensional map of the building for data collection and tracking.

Based on the map, we create the grid in a rectangle shape and data gathering route is determined. Each route is stored as one path, and the collected signal data can be stored for each Access Point (AP) on each grid.

The signal strength information collected in the operation outlined above, needs to be processed for noise reduction as well as for the purposes of building a signal strength distribution model. The signal strength data collected from the APs is processed using an adaptive Kalman filtering algorithm to eliminate the noise and interference effects. In building the signal distribution model, interpolation is applied. The signal distribution at each point on the data gathering route is stored in the Radiomap database of the server computer.

In the tracking phase, signal data are processed in real-time by the filtering algorithm of the RSSI is compared with that stored in Radiomap. Based on this comparison, the optimal location is determined and marked on the map efficiently using color representative visualization approach. Thus geolocation utilizing web services are available with the proposed wearable computing system.

III. IMPLEMENTATION AND EXPERIMENTS

A. Hardware

Table 1 shows the major specifications for HMD while Table 2 shows the specification of the backward looking camera. These are attached to a glass. User wears the glass together with tablet PC and / or mobile device as wearable computing system.

TABLE I. SPECIFICATION OF SINGLE EYE OF HMD

Resolution	SVGA(800×600pixels)
Supposed distance	2m
Supposed size	60inch
Field of view	42degree
Input type	RGB
Operable temp.	0~40°C
Size	28mm(W)×35.24mm(H)×56mm(D)
Weight	20g

TABLE II. SPECIFICATION OF NEAR INFRARED CAMERA

Resolution	1,300,000pixels
Minimum distance	20cm
Frame rate	30fps
Minimum illumination	30lux
Size	52mm(W)×70mm(H)×65mm(D)
Weight	105g

B. Software

Figure 6 shows an example of the screen shot of displayed image onto the HMD display. Just behind the moving keyboard, there is an acquired face image. At the bottom right corner, there is an extracted eye image. White circle denotes the detected pupil. The extracted pupil image is situated just beside the bottom enlarged key “F” on the left. Also black circle which indicated the estimated gaze location is situated just bottom right corner of the left enlarged key “F”. In this case, moving keyboard moves to the left key “D” just 0.5 second after user looks at the left enlarged key “F”.

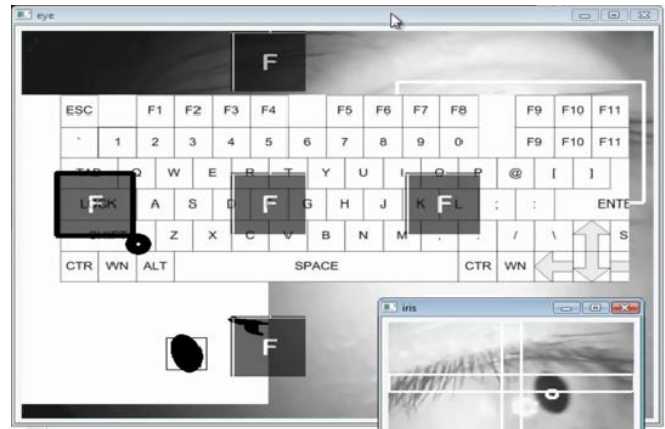


Fig.6. Example of the screen shot of displayed image onto the HMD display

C. Time Required for Key-in

If user looks at the center of enlarged key “F” for more than 0.5 second, then the key “F” is to be selected and determined. Therefore, it takes 0.5 to 5 seconds for one key-in results in approximately 2.5 seconds in average because key array consist five times ten keys typically. Figure 7 shows the time required for eye detection.

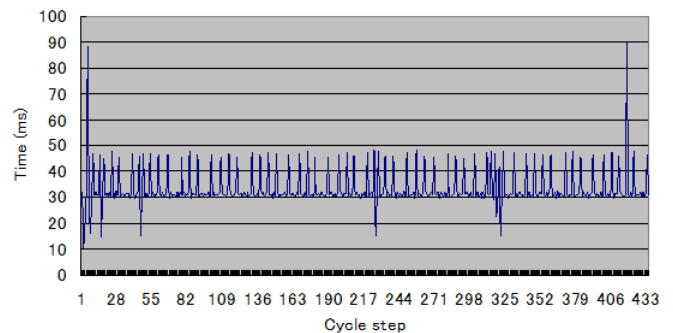


Fig.7. Processing time of eye detection and tracking on steady state condition, it looks faster than transient condition.

Meanwhile, Figure 8 shows the time required for key-in.

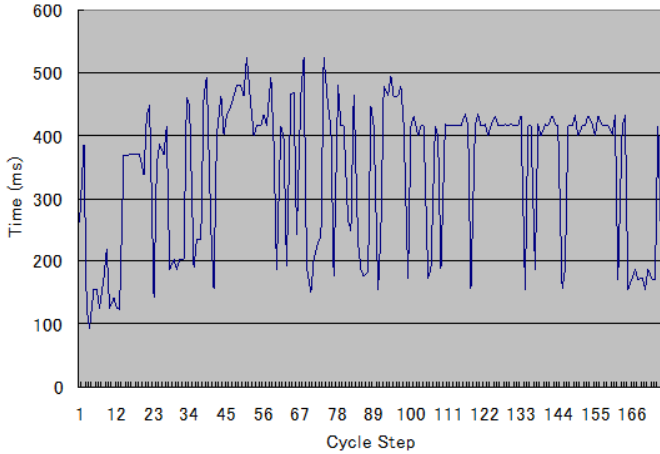


Fig.8. processing time of Eye gaze method

#### D. Mouse Operation

Mouse events are available for the proposed wearable computer. Therefore, application software can be activated by eye based mouse. At the bottom of Figure 9, there is the window for the word processing software is situated. User may confirm the character of which user selected and determined in the opened window.

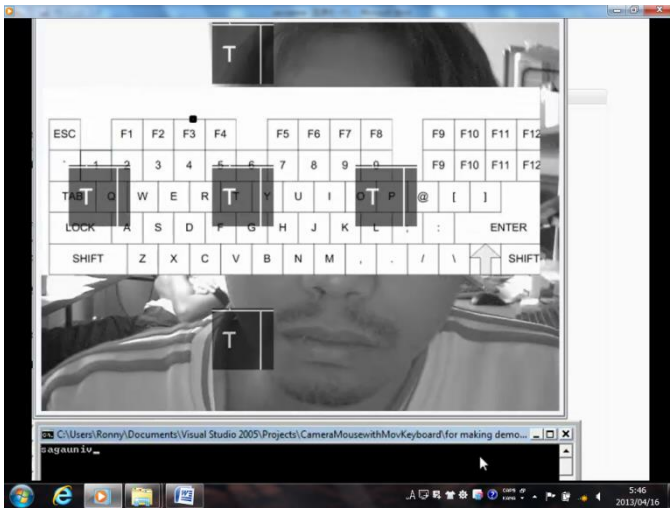


Fig.9. Another window can be opened by using the eye based mouse

#### E. Key-in Success Rate

Key-in success rate depends on the gaze location. Success rate for four corners are much worth than those for center and top, bottom right and left. Due to the fact that enlarged five keys are situated at center and top, bottom right and left of the screen display. Therefore, key-in success rate is almost 100 % for the key location of plus minus 15 degree in pitch direction and for the key locations of plus minus 30 degree in roll direction. The success rate in the horizontal direction is better than those in vertical direction. Meanwhile, success rate for the case that pitch angle is more than 20 degree gets worth as shown in Table 3.

TABLE III. KEY-IN SUCCESS RATE

		Yaw Angle (degree)						
		-30	-20	-10	0	10	20	30
Pitch Angle (degree)	Success Rate (%)							
	0	100	100	100	100	100	100	100
	5	100	100	100	100	100	100	100
	10	100	100	100	100	100	100	100
	15	100	100	100	100	100	100	100
	20	95	99	99	99	85.5	39	25
	25	6	15	63	72	36	5	2
30	4	15	26	54	18	3	2	

#### F. One of Applications of the Proposed Wearable Computing System

One of the applications of the proposed wearable computer is Google search. By using the proposed eye based mouse, Google search engine can be activated. Then keywords also be typed in the dialog box as keywords for Google search as shown in Figure 10..



Fig.10. Google search as an example of applications of the proposed wearable computing system

#### G. Location Based Web Services

Another example of applications of the proposed system is location based web services. Even if user is situated in house at where GPS signal cannot be reached, indoor location estimation can be done by using the signals from the near WiFi access points. The experiments are conducted for the building situation as shown in Figure 11. There are three access points in the building. User has mobile devices with WiFi receivers and walks in the buildings. Six locations are tested for evaluation of location estimation accuracy. User may recognize the WiFi access point ID. Therefore, discrimination of the signals from each access point can be easily done. Figure 12 shows an example of the received signal from each access point. By using signal strength differences from the different three WiFi access points, user may estimate own location as shown in Figure 13. Evaluation results of location estimation accuracy are shown in Table 4.

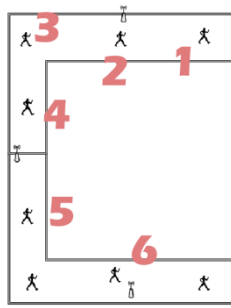


Fig.11. Experimental situation of user location and WiFi access point locations (Position #1: 3 meters, #2: 15 meters, #3:46 meters, #4:72 meters, #5:92 meters, and #6:132 meters)

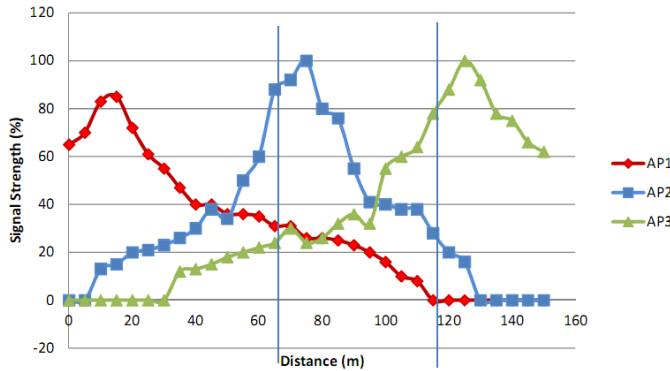


Fig.12. Received signals from each WiFi access point

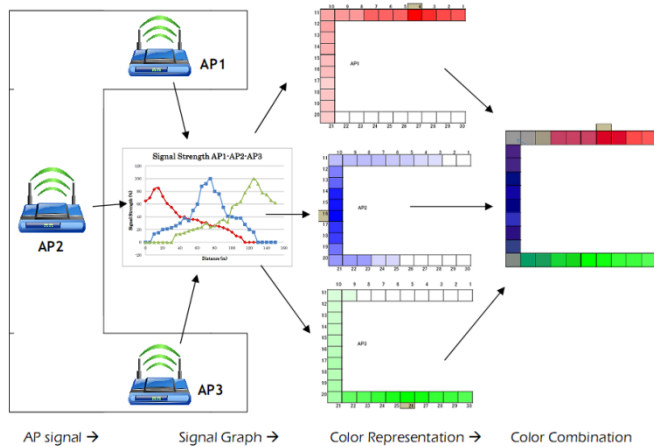


Fig.13. Three color coded received signals make estimation of user location

TABLE IV. GRID ESTIMATION RESULTS FOR 6 SAMPLES WITH ERROR

No	Online Position (meters)	Estimated Grid	Min Error (meters)	Max Error (meters)
1.	3	Grid 1 [0m-5m]	2	3
2.	15	Grid 2 [15m-20m]	0	5
3.	46	Grid 10 [45m-50m]	1	4
4.	72	Grid 15 [70m-75m]	2	3
5.	92	Grid 19 [90m-95m]	2	3
6	132	Grid 27 [130m-135m]	3	3

#### IV. CONCLUSION

Wearable computing with Input-Output devices Base on Eye-Based Human Computer Interaction: EBHCI which allows web services, location/attitude/health condition monitoring is proposed. Through implementation of the proposed wearable computing system, all the functionality is confirmed. It is also found that the system does work well. It can be used easily and also is not expensive. Experimental results for EBHCI show excellent performance in terms of key-in accuracy as well as input speed. It is accessible to internet, obviously, and has search engine capability.

It is also found that location based web services are available with the proposed wearable computing system because the location estimation accuracy of 2.5 m is a good enough for the services.

#### ACKNOWLEDGMENT

The author would like to thank Dr. Ronny Mardiyanto of the Institute Technology Surabaya and Dr. Herman Tolle of Brawijaya University for their great effort to conduct experiments of eye based human computer interaction and indoor location estimation. The author also would like to thank Mr. Fujise for his effort to conduct experiment of wearable computing system.

#### REFERENCES

- [1] Hailing Zhou, Lijun Xie, Xuliang Fang, "Visual Mouse: SIFT Detection and PCA Recognition," Proceedings of the International Conference on Computational Intelligence and Security Workshops (CISW 2007), 263-266, 2007
- [2] M.E. Erdem, I.A. Erdem, V. Atalay, A.E. Cetin, "Computer vision based unistroke keyboard system and mouse for the handicapped," Proceedings of the International Conference on Multimedia and Expo - Volume 2 (ICME '03), 765-768, 2003
- [3] Luca Lombardi, Marco Porta, "Adding Gestures to Ordinary Mouse Use: a New Input Modality for Improved Human-Computer Interaction," Proceedings of the 14th International Conference on Image Analysis and Processing (ICIAP 2007), 461-466, 2007
- [4] Jilin Tu, Thomas Huang, Hai Tao, "Face as Mouse Through Visual Face Tracking," Proceedings of the 2nd Canadian Conference on Computer and Robot Vision (CRV'05), 339-346, 2005
- [5] Nikolay Stefanov, Aphrodite Galata, Roger Hubbard, "Real-time Hand Tracking With Variable-Length Markov Models of Behavior," Proceedings of the IEEE Computer Society Conference on Computer Vision and Pattern Recognition (CVPRW'05) - Workshops, 73, 2005
- [6] Yun Fu, Thomas S. Huang, "hMouse: Head Tracking Driven Virtual Computer Mouse," Proceedings of the 8th IEEE Workshop on Applications of Computer Vision (WACV'07), 30, 2007
- [7] Takeshi Kurata, Takashi Okuma, Masakatsu Kourogi, Katsuhiko Sakaue, "The Hand Mouse: GMM Hand-Color Classification and Mean Shift Tracking," Proceedings of the IEEE ICCV Workshop on Recognition, Analysis, and Tracking of Faces and Gestures in Real-Time Systems (RATFG-RTS'01), 119, 2001
- [8] T. Ohno, "Features of Eye Gaze Interface for Selection Tasks," Proceedings of the 3rd Asian Pacific Computer and Human Interaction, 176, 1998
- [9] Zhu Hao, Qianwei Lei, "Vision-Based Interface: Using Face and Eye Blinking Tracking with Camera," Proceedings of the 2nd International Symposium on Intelligent Information Technology Application, 1, 306-310, 2008J. Clerk Maxwell, A Treatise on Electricity and Magnetism, 3rd ed., vol. 2. Oxford: Clarendon, 1892, pp.68-73.
- [10] Arai K. and H. Uwataki, Computer key-in based on gaze estimation with cornea center determination which allows students' movement, Journal of Electrical Engineering Society of Japan (C), 127, 7, 1107-1114, 2007

- [11] Arai K. and H. Uwataki, Computer input system based on viewing vector estimation with iris center detection from face image acquired with web camera allowing students' movement, *Electronics and Communication in Japan*, 92, 5, 31-40, John Wiley and Sons Inc., 2009.
- [12] Arai K., and M. Yamaura, Blink detection accuracy improvements for computer key-in by human eyes only based on molforgic filter, *Journal of Image Electronics Engineering Society of Japan*, 37, 5, 601-609, 2008.
- [13] Arai K. and R. Mardiyanto, Real time blinking detection based on Gabor filter, *International Journal of Human Computer Interaction*, 1, 3, 33-45, 2010.
- [14] Arai K. and R. Mardiyanto, Camera mouse and keyboard for handicap person with trouble shooting capability, recovery and complete mouse events, *International Journal of Human Computer Interaction*, 1, 3, 46-56, 2010.
- [15] Arai K. and M. Yamaura, Computer input with human eyes only use two Purkinje images which work in a real time basis without calibration, *International Journal of Human Computer Interaction*, 1, 3, 71-82, 2010.
- [16] Arai K., and K. Yajima, Communication aid based on computer key-in with human eyes only, *Journal of Electric Engineering Society of Japan*, (C), 128 -C, 11, 1679-1686, 2008.
- [17] Djoko P., R. Mardiyanto and K. Arai, Electric wheel chair control with gaze detection and eye blinking, *Artificial Life and Robotics*, AROB Journal, 14, 694,397-400, 2009.
- [18] Arai K. and K. Yajima, Communication Aid and Computer Input System with Human Eyes Only, *Electronics and Communications in Japan*, 93, 12, 1-9, John Wiley and Sons, Inc., 2010.
- [19] Arai K., R. Mardiyanto, A prototype of electric wheel chair control by eye only for paralyzed student, *Journal of Robotics and Mechatronics*, 23, 1, 66-75, 2010.
- [20] Arai K. and K. Yajima, Robot arm utilized having meal support system based on computer input by human eyes only, *International Journal of Human Computer Interaction*, 2, 1, 120-128, 2011.
- [21] Arai K. and T. Herman, Automatic e-comic content adaptation, *International Journal of Ubiquitous Computing*, 1,1,1-11,2010
- [22] Arai K., T. Herman, "Method for Real Time Text Extraction from Digital Manga Comic", *International Journal of Image Processing*, 4, 6, 669-676, 2011.
- [23] Arai K., T. Herman, Module based content adaptation of composite e-learning content for delivering to mobile devices, *International Journal of Computer Theory and Engineering*, 3, 3, 381-386, 2011.
- [24] Arai K., T. Herman, Method for extracting product information from TV commercial, *International Journal of Advanced Computer Science and Applications*, 2, 8, 125-131, 2011
- [25] Arai K., T. Herman "Module Based Content Adaptation of Composite E-Learning Content for Delivering to Mobile Learners", *International Journal of Computer Theory and Engineering (IJCTE)*, Vol 3, No. 3, pp. 381-386, June 2011
- [26] Arai K., T. Herman, Efficiency improvements of e-learning document search engine for mobile browser, *International Journal of Research and Reviews on Computer Science*, 2, 6, 1287-1291, 2011.
- [27] Arai K., R. Mardiyanto, Evaluation of Students' Impact for Using the Proposed Eye Based HCI with Moving and Fixed Keyboard by Using EEG Signals, *International Journal of Review and Research on Computer Science(IJRRCS)*, 2, 6, 1228-1234, 2011

#### AUTHORS PROFILE

Kohei Arai, He received BS, MS and PhD degrees in 1972, 1974 and 1982, respectively. He was with The Institute for Industrial Science and Technology of the University of Tokyo from April 1974 to December 1978 and also was with National Space Development Agency of Japan from January, 1979 to March, 1990. During from 1985 to 1987, he was with Canada Centre for Remote Sensing as a Post Doctoral Fellow of National Science and Engineering Research Council of Canada. He moved to Saga University as a Professor in Department of Information Science on April 1990. He was a councilor for the Aeronautics and Space related to the Technology Committee of the Ministry of Science and Technology during from 1998 to 2000. He was a councilor of Saga University for 2002 and 2003. He also was an executive councilor for the Remote Sensing Society of Japan for 2003 to 2005. He is an Adjunct Professor of University of Arizona, USA since 1998. He also is Vice Chairman of the Commission A of ICSU/COSPAR since 2008. He wrote 26 books and published 327 journal papers.

# Algorithm for Design of Digital Notch Filter Using Simulation

Dr. Amit Verma

Professor, Chandigarh University,  
Ghauran

Naina

Electronics & Communication  
Engineering  
Ambedkar Institute of Advance  
Communication Technologies  
&Research (A.I.A.C.T&R)  
Delhi,India

Mrs. C.S. Vinitha

Electronics & Communication  
Engineering  
Ambedkar Institute of Advance  
Communication  
Technologies&Research  
(A.I.A.C.T&R)  
Delhi,India

**Abstract**—a smooth waveform is generated of low frequency signal can be achieved through the Digital Notch Filter. Noise can be easily eliminated from a speech signal by using a Notch filter. In this paper the design of notch filter using MATLAB has been designed and implemented. The performance and characteristics of the filter has been shown in the waveform in the conclusion part of the paper.

**Keywords**—Component; filters; design of filters; MATLAB etc

## I. INTRODUCTION

Signal Processing is the area of Engineering that deals with the processing of electrical signal either in discrete form or in continuous form. The signal need to be processed that the information that they contain can be converted ,displayed and analyzed to other form that may be used as a part of Analog signal processing is a part of signal processing where the continuous –time signal are to processed to get the desired results.

The area that deals with the discrete time signal in digitized form is known as Digital Signal Processing. Here a digitized signal as a number sequences at discrete time. There are many reasons why the digital signal processing of an actual (naturally analog) signal may be preferable. Programmability features of digital signal processing technique is one of the most important merit the make it superior to its analog counterpart. Other important features are accuracy and precision.

The subject of Digital Signal Processing is very wide. It consists of study of various mathematical tools like Fourier-Transform, Z-Transform, DFT, FFT etc. In addition to sound understanding of the simulation tools such as: MATLAB .A very important area of Digital Signal Processing, where huge numbers of efforts is being invested is the area of realized filter. Efficient techniques and algorithms are being worked out and are widely available in literature .in this paper we shall see that the realization of a digital notch filter and also see that the how removing noise from a speech signal by using GUI Model in MATLAB software and how the noise easily removed by using inverse filtering.

In this paper we shall know that how we can design a filter byusing a MATLAB software .There are many types of filters are available.

## II. DIGITAL TECHNOLOGY

First of all, we discuss about the Digital Technology that how significant is that in our life. 1) Digital signals can be represented by electronics ON-OFF switches.2) coding helps maintaining secrecy in transmission.3) Data-compression techniques helps in effective economy in transmission.4) signal enhancement and signal reduction can be effected by introducing 1's and 0's appropriate places, as required.5)one of the major advantage of digital transmission of signal is its ability to reduce noise . In transmission of signal, noise gets added to the signal in the form of amplitude disturbances. Since, the binary signals have only two levels (1's and 0's) ofoperation; we can reduce noise by limiting the amplitude. 6) Modern VLSI and ULSI technologies have made circuit complexities a simple affair. They have introduced high –speed digital processor into the open market at affordable prizes. This has resulted in the popularity of DSP among common man.

## III. TYPES OF FILTERS

Filters are the networks that process signal in frequency dependent manner. The basic concept of a filter can be explained by examining the frequency dependent nature of the Impedance of capacitors and inductors. There are main two types of Filters are:1) Analog Filters and 2) Digital Filters. The Analog Filters are like Low Pass Filter, High Pass Filters, Band Pass Filters and Band Reject Filters. And the Digital filters like Impulse Invariant Response (IIR) Filters and Finite Impulse Response (FIR) Filters.

## IV. DESIGN OF DIGITAL FILTERS

The procedure presented here for the design of digital filter is based on these some steps:

We first developed the expression for H(s) based on the analog filterdesign and then modify it in an appropriate fashion to suit the digital domain.

As an example consider the expression for the H(s) of the second order analog filter:

$$H(s) = \frac{\omega_c^2}{s^2 + 2\delta\omega_c s + \omega_c^2}$$

Where  $\omega_c$  = cut of frequency and  $\delta$  =damping factor. To get transfer function desired digital filter, we first take the inverse Laplace Transform of above equation to convert frequency domain expression of H(s) into its time domain equivalent h(t).

After h(t) is obtained we used Z-Transform to convert it into H(Z) , we construct the required digital filter . This type of design is called “impulse invariant design”.

We may also convert H(s) directly from s-domain into H(z) in z-domain by means of what is known as Bilinear Transformation. Once the H(z) is obtained , we proceed in the same way as in the case of impulse –invariant-design method to construct the desired digital filter.

#### A. Design of Digital Infinite Impulse Response (IIR) Filters

There are several methods to designing the digital IIR Filters.

##### 1) BUTTERWORTH IIR FILTER

The design of Butterworth filters design with the design of its analog Counter Part from the analog design Step. We find expression for H(s). From H(s) we find H(z) either by direct conversion or with the help of a suitable transformation . Then using H(z) we can construct the desired filter structure.

Normalized the frequency-To normalize the frequency we use the equation:

$$\omega = 2\pi f$$

##### 2) CHEBYSHEV FILTER

There are two types of Chebyshev IIR filters. They are type-I(regular) chebyshev filter and the type-II (inverse) chebyshev filters, which is characterized by pass band containing no ripples and stop band containing ripple.The chebyshev design makes use of chebyshev polynomials, given by:

$$|H(\omega)| \text{ in dB} = -10\log(1 + \varepsilon^2 c_n^2)$$

Where  $\varepsilon$  = amount of ripple in the magnitude, and =

Coefficient  $C_n$  is given by:

$$c_n = \cosh\left\{n \cosh^{-1} \frac{\omega}{\omega_c}\right\}, \quad \text{if } \frac{\omega}{\omega_c} \geq 1$$

##### 3) BILINEAR TRANSFORMATION

THE Bilinear or Tustin Transformation IS A mathematical relation by which we can convert an s-domain equation directly into its equivalent in the z-domian.The expression of the bilinear transformation is given by S= :

$$\frac{2(1 - z^{-1})}{T(1 + z^{-1})}$$

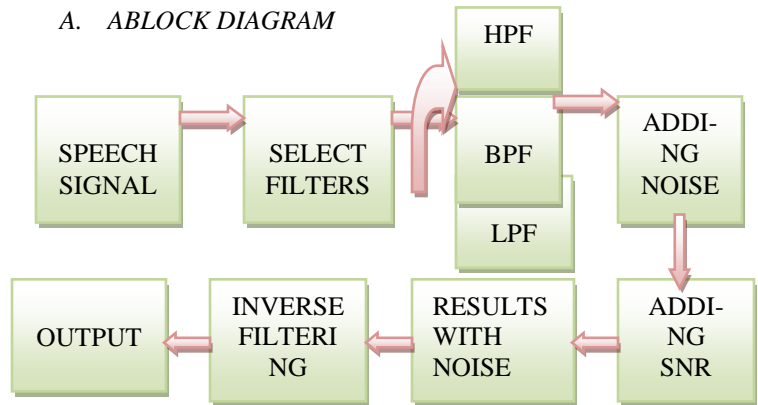
Where T= sampling interval

#### B. Design of Digital Finite Impulse Response (FIR) Filters

There are many methods of designing FIR filter like window Techniques .these techniques are like: rectangular window, Hamming window, Hanning window ,Blackman window ,Bartlett window and Kaiser window .

### V. PROPOSED ALGORITHM

#### A. BLOCK DIAGRAM



Above block diagram shows complete process of the system according to this block diagram .this process is done in MATLAB software. First of all, we will take an input of speech signal or an audio signal.

Then we select a filter like low pass, high pass or band pass and select the frequency of the selected filter and proceeding further and can see the waveform and spectrum of a speech signal and after that we have to add the noise as per user choice and then we can see the result of a noisy signal which is not our output. For eliminating noise from the speech signal we have to do the inverse filtering or denoising of the signal. After that we can get the eliminated noise speech signal. We can get a noise free speech signal only then when we denoising the signal or doing inverse filtering.

#### B NOTCH FILTER

The NOTCH FILTER is a filter that passes all the frequencies except those in a stop band centered on a centered frequency. A closely related knowledge item discusses the concept of the Q filter. The amplitude response of a notch filter is flat at all frequencies except for the stop band on either side of the centered frequency. The standard reference point for the roll-off on each side of the stop band are the points where the amplitude decreased by 3 db to 70.7% of its original amplitude. Many people think that the higher the Q then deeper the notch this is not true. The depth of a notch depends on the matching of components

#### C MATLAB SOFTWARE

This process we are doing on MATLAB software. For eliminating the noise from our speech signal we are using GUI

Tool in Matlab program. This is the mathematical tool which is used for all type of mathematical calculations or mathematical process. This software is used widely in these days and this software can be easily applicable on digital processing, image processing, signal processing, and control engineering many more fields.

## VI. RESULTS

### A. RESULTS WHEN WE UPLOAD A SPEECH SINPUT

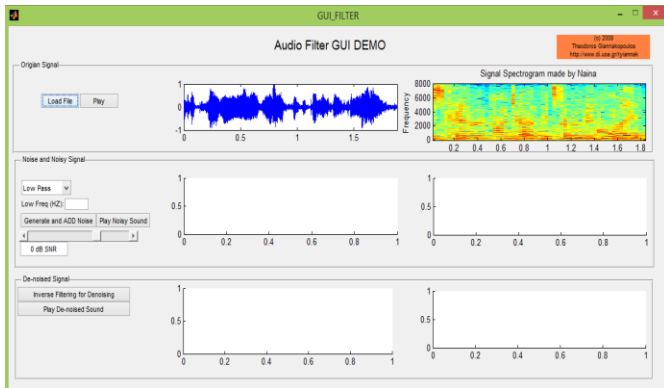


Fig.1. AUDIO FILTER GUI DEMO OF A SPEECH SIGNAL

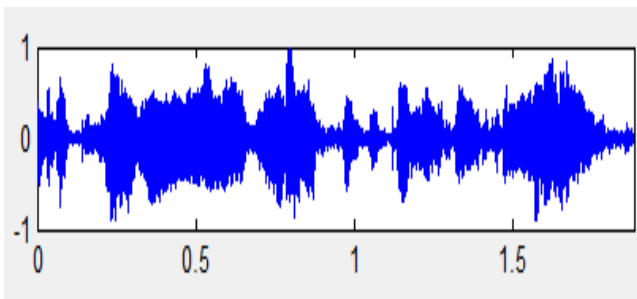


Fig.2. Waveform of original speech signal

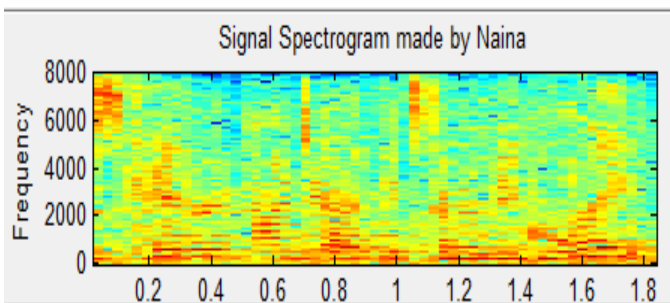


Fig.3. Spectrum of a speech signal

### B. RESULTS WHEN NOISE IS ADDED TO THE SIGNAL

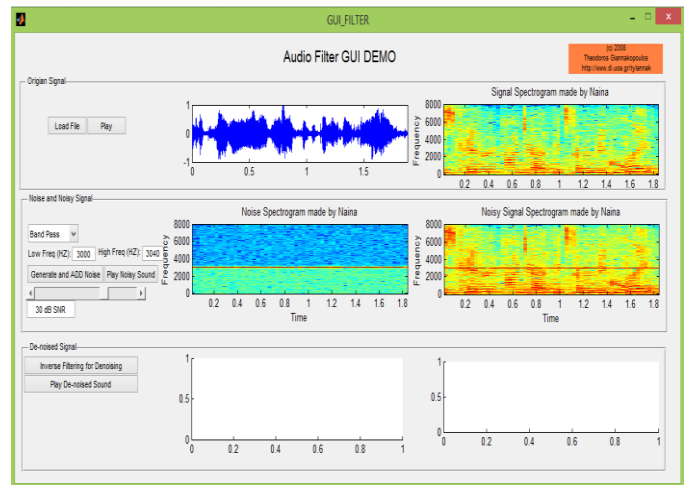


Fig.4. AUDIO FILTER GUI DEMO WHEN NOISE IS ADDED IN THE SPEECH SIGNAL

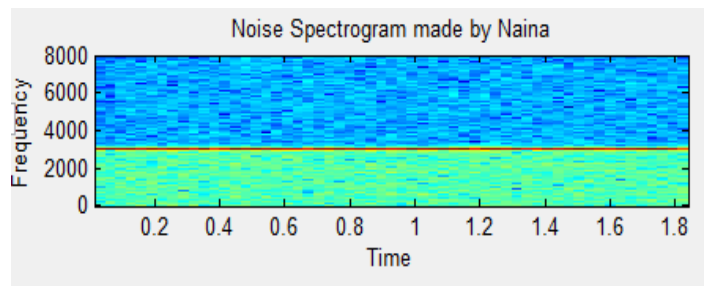


Fig.5. Waveform of the speech signal after adding the noise

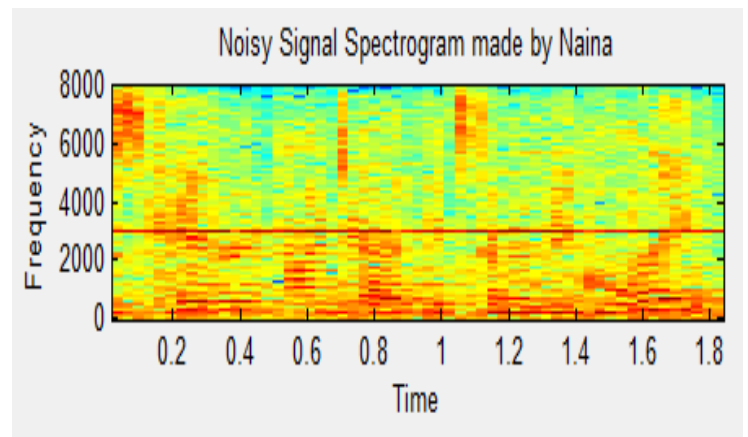


Fig.6. Spectrum of a signal when noise is added to the speech signal

### C. RESULTS AFTER INVERSE FILTERING FOR DENOISING THE SPEECH SIGNAL

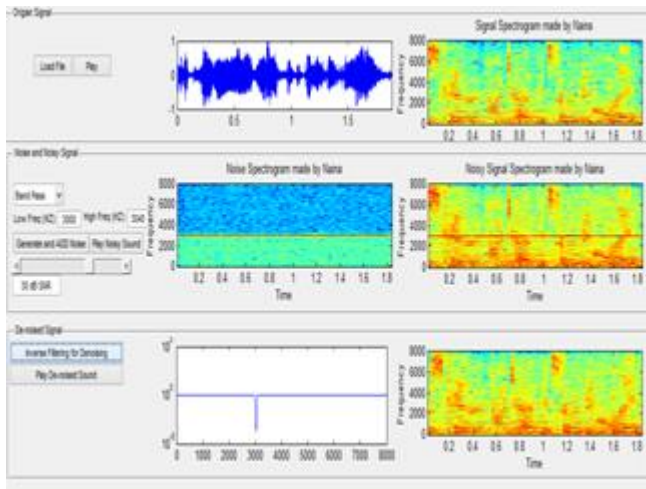


Fig.7. Audio filter GUI demo after inverse filtering for denoising the speech signal

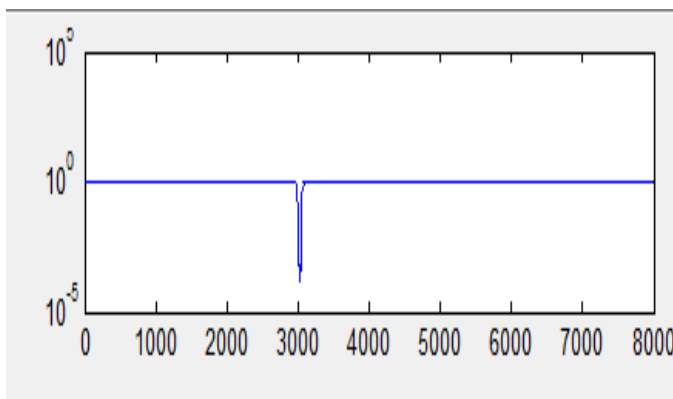


Fig.8. Noise eliminated by using the notch filter

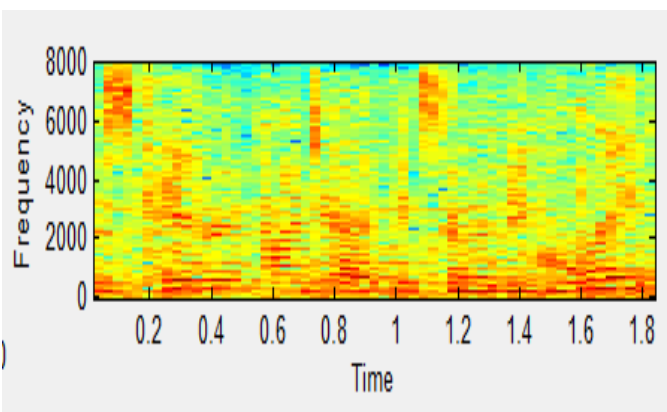


Fig.9. Spectrum of a notch filter after Denoising the speech signal

### VII. CONCLUSION

In this paper we have seen that how we can easily eliminated the noise from the speech signal or a random signal by using a GUI Tool in MATLAB software .and also seen the

design of notch filter by doing inverse filtering. This technique can easily use in speech signal processing for eliminating the noise from the random or a speech signal. We can test this process that weather is it correct or not? for the testing of this system we have to see the spectrum signal of an original speech signal and the spectrum after denoising the noised speech if we get the exact replica or a same spectrum that we are having at the time of an original signal so our system is correct if we don't get the exact replica so our system is not correct. As we have seen in above results here, the spectrum after denoising the speech signal is same as we have the spectrum of an original speech signal it means our results and systems is correct.

### REFERENCES

- [1] S. Schilt, L. Thevenaz, M. Nikles, L. Emmenegger, and C. Huglin, "Ammonia monitoring at trace level using photoacoustic spectroscopy in industrial and environmental applications," *Spectrochimica. Acta. Part A: Mol. Biomol. Spectrosc.*, vol. 60, no. 14, pp. 3259-3268, Dec. 2004.
- [2] H. Huszar, A. Pogany, Z. Bozoki, A. Mohacsi, L. Horvath, and G. Szabo, "Ammonia monitoring at ppb level using photoacoustic spectroscopy for environmental application," *Sensors and Actuators B: Chemical*, vol. 134, no. 2, pp. 1027-1033, Sep. 2008.
- [3] J. Li, X. Gao, W. Li, Z. Cao, L. Deng, W. Zhao, M. Huang, and W. Zhang, "Near-infrared diode laser wavelength modulation-based photoacoustic spectrometer," *Spectrochimica. Acta. Part A*, vol. 64, no. 2, pp. 338-342, May 2006.
- [4] J. P. Besson, S. Schilt, and L. Thevenaz, "Multi-gas sensing based on photoacoustic spectroscopy using tunable laser diodes," *Spectrochimica. Acta. Part A*, vol. 60, no. 14, pp. 3449-3456, Dec. 2004.
- [5] J. Li, X. Gao, L. Fang, W. Zhang, and H. Cha, "Resonant photoacoustic detection of trace gas with DFB diode laser," *Opt. Laser Technol.*, vol. 39, no. 6, pp. 1144-1149, 2007.
- [6] M. McCurdy, Y. Bakhirkin, G. Wysocki, R. Lewicki, and F. Tittle, "Recent advances of laser-spectroscopy based techniques for applications in breath analysis", *Journal of Breath Research*, vol. 1, pp. R1-R12, 2007.
- [7] C. Du, J. Zhou, H. Wang, X. Chen, A. Zhu, and J. Zhang, "Determination of soil properties using Fourier transform mid-infrared photoacoustic spectroscopy," *Vibrational Spectroscopy*, to be published.
- [8] S. Schilt, A. Vicet, R. Werner, M. Mattiello, L. Thevenaz, A. Salhi, Y. Rouillard, and J. Koeth, "Application of antimonide diode laser in photoacoustic spectroscopy," *Spectrochimica Acta Part A*, vol. 60, no. 14, pp. 3431-3436, Dec. 2004.
- [9] S. Schilt and L. Thevenaz, "Wavelength modulation photoacoustic spectroscopy: Theoretical description and experimental results," *Infrared Physics & Technology*, vol. 48, no. 2, pp. 154-162, Jun. 2006.
- [10] M. Angelmahr, A. Miklos, and P. Hess, "Wavelength- and amplitudemodulation photoacoustics: comparison of simulated and measured spectra of higher harmonics," *Applied Optics*, vol. 47, no. 15, pp. 2806- 2812, May 2008.
- [11] J. Besson, S. Schilt, and L. Thevenaz, "Sub-ppb ammonia detection based on photoacoustic spectroscopy," *17th International Conference on Optical Fibre Sensors, Proceedings of SPIE*, vol. 5855, pp. 415-418, May. 2005.
- [12] google search
- [13] wikipedia
- [14] Digital Signal processing (theory analysis and design filter design) by B. Somanathan Nair.
- [15] Digital signal processing By S. Saliwahanan & A. Vallavraj.

# Memetic Algorithm with Filtering Scheme for the Minimum Weighted Edge Dominating Set Problem

Shada N. Abdel-Aziz  
Dept. of Computer Science  
Faculty of Computers & Information  
Assiut, Egypt

Abdel-Rahman Hedar  
Dept. of Computer Science  
Faculty of Computers & Information  
Assiut, Egypt  
Email: hedar@aun.edu.eg

Adel A. Sewisy  
Dept. of Computer Science  
Faculty of Computers & Information  
Assiut, Egypt

**Abstract**—The minimum weighted edge dominating set problem (MWEDS) generalizes both the weighted vertex cover problem and the problem of covering the edges of graph by a minimum cost set of both vertices and edges. In this paper, we propose a meta-heuristic approach based on genetic algorithm and local search to solve the MWEDS problem. Therefore, the proposed method is considered as a memetic search algorithm which is called Memetic Algorithm with filtering scheme for minimum weighted edge dominating set, and called shortly (MAFS). In the MAFS method, three new fitness functions are invoked to effectively measure the solution qualities. The search process in the proposed method uses intensification scheme, called “filtering”, beside the main genetic search operations in order to achieve faster performance. The experimental results proves that the proposed method is promising in solving the MWEDS problem.

**Keywords:** Minimum weight edge dominating set, Graph theory, Genetic algorithm, Memetic algorithm, Local search.

## I. INTRODUCTION

The Minimum Edge Dominating Set (MEDS) is a subset of edges of minimum cardinality, where each edge is be in the edge dominating set, or adjacent to some edges in the edge dominating set [11], [12], [24]. The weighted version of MEDS seeks to find an edge dominating set with a minimum total weight [9]. The MEDS problem is a hard combinatorial problem, classified as NP-hard [24], and in general cannot be solved exactly in polynomial time. The MEDS problem is one of the fundamental covering problems in graphs; edge cover, vertex cover, dominating set and edge dominating set. These domination problems in graphs have been subject of many studies in graph theory, and have many applications in operations research, resource allocation and network routing, as well as in coding theory [4], [11], [12], [25].

There are many algorithms proposed for solving MWEDS. Although these algorithms guarantee the optimality of the solutions they find, they may fail to give a solution within reasonable time for large instances. As the size of the problem increases, these methods become futile. Meta-heuristics are powerful search methods which can be efficiently in providing satisfactory solutions to large and complex problems such as vertex cover [20], dominating set [14] and edge coloring [16] in a reasonable time. However, up to the authors’ knowledge, there are no studies up to day used meta-heuristic techniques for solving the MWEDS problem.

Genetic Algorithms (GAs) are the most popular meta-heuristic algorithms that have been employed in wide variety of problems [3]. Actually, GAs are able to incorporate other techniques within its framework to produce a hybrid method that brings more promising one. One direction of such hybridization is to use local search which can accelerate the search process in a pure GA. This modification yields another search approach which is called the Memetic Algorithm (MA) [17].

Several meta-heuristic methods have been developed to solve different problems in graph theory and combinatorial optimization [2], [19]. However, the number of contributions that deal with the graph domination problems is very limited. In this paper, we propose a memetic algorithm with filtering scheme for finding the minimum edge dominating set, called shortly MAFS. It uses a 0-1 variable representation of solutions in searching for the MWEDS, and invokes three new fitness functions to measure the solution qualities. Intensification search and filtering schemes are used beside local search in order to enhance the performance of the MAMEDS method.

The paper is organized as follows. The next section gives a brief description about the MWEDS problem as preliminaries needed throughout the paper, and highlights the related works in solving the considered problem. Section 3 describes the proposed method steps in details. Section 4 reports numerical experiments and results. Finally, the conclusions make up Section 5.

## II. PROBLEM FORMULATION AND RELATED WORKS

Given an undirected weighted graph  $G = (V, E, W)$ , without loops and multiple edges, where  $V$  is the set of nodes (or vertices),  $E$  the set of edges, and  $W$  is the set of positive edge weights represented by variables  $w_1, w_2, \dots, w_m$ , (where each  $w_i$  corresponds to an edge  $i = (u, v) \in E$ ). An edge  $(u, v)$  of  $G$  is said to dominate itself and any edge adjacent to it in  $G$ . An edge dominating set (EDS) is a set of edges which is collectively dominate all the other edges in the graph  $G$ . The Minimum Weight Edge Dominating Set (MWEDS) problem seeks to find an edge dominating set  $EDS$  of minimum total weight  $\sum_{e \in D} w(e)$ .

The edge dominating set problem is a basic problem introduced in Garey and Johnson’s work [10] on NP-completeness. Yannakakis and Gavril [24] proved that the edge dominating set problem is NP-hard even in planar or bipartite graphs

of maximum degree 3. Although the EDS has important application in areas such as telephone switching networks, a very little work was known about the weighted version of the problem.

For the EDS problem, Randerath and Schiermeyer [8] presented the first exact algorithm of time complexity  $O(1.4423^n)$  algorithm and Fomin et al. [6] improved this to  $O(1.4082^n)$ . Rooij and Bodlaender [21] got an  $O(1.3226^n)$  algorithm by using the “measure and conquer” method, which was further improved to  $O(1.3160^n)$  [23], where  $n$  is the number of vertices. From the point of approximation algorithm, the best known result was proposed in [18], which gave a 2-approximation algorithm for WEDS problem. Recently, parameterized computation theory was applied to solve the EDS and WEDS problems. Fernau [5] presented parameterized algorithms of time complexity  $O(2.62^k)$  for EDS and WEDS problem respectively. The above result was further reduced by Fomin [7], which gave a parameterized algorithm of time  $O(2.4181^k)$ . For the first time Wang [22] presented an enumeration algorithm of time complexity  $O(5.6^{2k}k^4z^2 + 4^{2k}nk^3z)$  for WEDS problem. Although these algorithms provide the optimal solution, they are too slow on graphs with few hundreds of nodes. Therefore, when deals with a very large graphs, these algorithm become impractical. This motivates us to consider meat-heuristics to design more efficient algorithm to solve the MWEDS problem.

### III. PROPOSED METHOD

In this section, we describe the components of the MAFS method, and then state its formal algorithm at the end of this section. The MAFS method is an evolutionary algorithm, therefore, we first start by describing the solution representation and the fitness function. Then, the genetic operators; selection, crossover and mutation are defined. The main memetic search element, local search, is stated after that. Finally, our intensification schemes are explained.

#### A. Graph Representation

The graph represented as  $n_V \times n_V$  adjacency matrix  $A$ , where  $n_V$  is the number of vertices in the graph. The non-diagonal entry  $a_{ij} = w_e$ , where  $w_e$  is an integer weight associated with each edge  $e$  connected the vertex  $i$  to vertex  $j$ . Form an adjacency matrix we create edges matrix  $E_m$  which include all edges in the graph. Edge matrix dimension is  $n_E \times 3$ , where  $n_E$  is the number of edges in the graph. The first two columns are the vertex numbers which represent the endpoints of edges and the third columns represent the weights of each edge in the graph.

#### B. Solution Representation

A solution  $s$  will be represented as a bit vector with size equal to the number of edges in the graph. Therefore,  $s$  is equal to  $(s_1, s_2, \dots, s_{n_E})$ , as shown in Figure 1. The subscript numbers  $1, 2, \dots, n_E$ , are related to the corresponding edges in  $E_m$ . If a component  $s_i$  of  $s$ ,  $i = 1, \dots, n_E$ , has the value 1, then the edge represented by the  $i$ -th row in  $E_m$  is contained in the edge subset represented by solution  $s$ . Otherwise, the solution  $s$  does not contain the  $i$ -th edge.

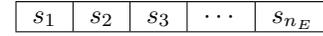


Fig. 1. Solution Representation

#### C. Fitness Function

Fitness function  $fit$  is a function designed to measures the quality of a solution which plays a major role in the selection process. The main idea in designing the fitness function is that better solutions will have a higher fitness function value than worse one. Three fitness functions are invoked to effectively measure the solution qualities.

$$fit_1(s) = \rho_d + \frac{1}{sum_w(s) \times n_E}, \quad (1)$$

$$fit_2(s) = \rho_d + (1 - \sqrt[\kappa]{\frac{sum_w(s)}{T_{sum}}}), \quad (2)$$

$$fit_3(s) = \alpha\rho_d + (1 - \alpha)(1 - \sqrt[\kappa]{\frac{sum_w(s)}{T_{sum}(s)}}), \quad (3)$$

where  $0 \leq \alpha \leq 1$ ,  $\kappa > 1$  is an integer, and  $\rho_d$ ,  $T_{sum}(s)$  and  $sum_w(s)$  are calculated by

$$\rho_d = \frac{n_D}{n_E},$$

$$T_{sum}(s) = \sum_{e \in E} w(e),$$

$$sum_w(s) = \sum_{e \in D} w(e),$$

where  $n_D$  is the number of edges dominated by the subset of edges  $D$  represented by the solution  $s$  and  $n_E$  the number of edges in the graph. All three fitness function consist of two parts, the first part  $n_D/n_E$ , reflects the size of domination on  $G$  by  $s$ . If  $s$  represents an edge dominating set, then this part is equal to 1. On the other hand, the second part distinguishes between solutions that have the same values of the first part based on the sum of weights associated with each edge contained in each of them. It is worthwhile to mention that the second term is designed to make  $fit(s_1) < fit(s_2)$  in only two cases:

- $x_1 < x_2$ , where  $x_1$  and  $x_2$  are the numbers of edges covered by  $s_1$  and  $s_2$  respectively, or
- $x_1 = x_2$  and  $sum_w(s_1) > sum_w(s_2)$ .

The parameter  $\kappa$  is set equal to 4 to highly distinguish between solutions that have the same domination number.

#### D. Genetic Operators

The parent selection mechanism first produces an intermediate population, say  $P'$  from the initial population  $P$ :  $P' \subseteq P$  as in the canonical GA. For each generation,  $P'$  has the same size as  $P$  but an individual can be present in  $P'$  more than once. The individuals in  $P$  are ranked with their fitness function values based on the *linear ranking selection mechanism* [1], [13]. Indeed, individuals in  $P'$  are copies of individuals in  $P$  depending on their fitness ranking: the higher fitness an individual has, the more the probability that it will be copied is. This process is repeated until  $P'$  is full while an already chosen individual is not removed from  $P$ .

The crossover operation has an exploration tendency, and therefore it is not applied to all parents. First, for each individual in the intermediate population  $P'$ , the crossover operation chooses a random number from the interval  $(0, 1)$ . If the chosen number is less than the crossover probability  $p_c \in (0, 1)$ , the individual is added to the parent pool. After that, two parents from the parent pool are randomly selected and mated to produce two children  $c_1$  and  $c_2$ , which are then replacing their parents in  $P'$ . These procedures are repeated until all selected parents are mated. The standard one-point crossover [15] is used in MAFS to compute children.

For each gene each in all individuals in the intermediate population  $P'$ , a random number from the interval  $(0, 1)$  is associated. If the associated number is less than the mutation probability  $p_m$ , then the individual is mutated using the standard uniform mutation operation [15].

#### E. Local Search

In *LocalSearch* mechanism, we add or delete some edges to improve the best solution  $s^{best}$  found so far, and this process is repeated  $n_l$  times. The formal description of this mechanism is shown in Procedure 1.

##### Procedure 1: (LocalSearch)

- 1) Set a suitable value to  $n_l$ .
- 2) Repeat the following Steps (2-6)  $n_l$  times.
- 3) Set  $\tilde{s}^{best} = s^{best}$ .
- 4) If  $\rho_d \geq 1$ , select a component  $\tilde{s}_i^{best}$  with value 1. This selection is randomly and proportional to the weight of its corresponding edge. Set  $\tilde{s}_i^{best} = 1 - \tilde{s}_i^{best}$ .
- 5) If  $\rho_d < 1$ , select a component  $\tilde{s}_i^{best}$  with value 0. This selection is randomly and inversely proportional to the weight of its corresponding edge. Set  $\tilde{s}_i^{best} = 1 - \tilde{s}_i^{best}$ .
- 6) If  $fit(\tilde{s}^{best}) > fit(s^{best})$ , set  $s^{best} = \tilde{s}^{best}$ .

In our numerical experiments, the number  $n_l$  of local search iterations is set equal to  $0.1 \times n_E$  in order to save computational costs.

#### F. Intensification Schemes

The intensification mechanism which called “*Filtering*” is used in MAFS to reduce the cost of the solution computed. This mechanism basically checks if an edge contained in  $s^{best}$  can be removed without losing the coverage.

##### Procedure 2: (Filtering)

- 1) If  $\rho_d < 1$ , return.
- 2) Compute the set  $X = \{x_1, \dots, x_{n_E}\}$  of all positions of value one in  $s^{best}$ .
- 3) Repeat the following Steps (4-5) for  $j = 1, \dots, n_E$ .
- 4) Set  $s_{x_j}^{best} = 0$ , and compute the new fitness value.
- 5) If the fitness value is increased, update  $s^{best}$ .

#### G. MAFS Algorithm

MAFS starts with an initial population of chromosomes  $P_0$  generated randomly. Each chromosome represents a trial solution to the MWEDS problem. During each generation, the quality of each chromosome in the population is evaluated by using three fitness functions (see Equations 1,2 and 3). MAFS applies Procedure 1 to improve the best solution. In each generation, the population is updated through genetic operators. Linear ranking selection algorithm uses to select parents for standard one-point crossover and uniform mutation to generate members of the new population [14]. MAFS invokes Local Search Procedure to update the current population. If a certain number of consecutive generations without improvement is achieved, MAFS invokes Procedure 2 to improve the best edge dominating set  $s^{best}$  obtained so far, if it exists. The search will be terminated if the number of generations exceeds  $g_{max}$ , or the number of consecutive generations without improvement exceeds a pre-specified number.

##### Algorithm 3: (MAFS)

- 1) **Initialization.** Set values of  $P_{size}$ ,  $g_{max}$ . Set the crossover and mutation probabilities  $p_c \in (0, 1)$  and  $p_m \in (0, 1)$ , respectively. Set *WEDS* to be an empty set. Generate an initial population  $P_0$  of size  $P_{size}$ .
- 2) **Local Search.** Evaluate the fitness function of all chromosomes in  $P_0$  by using the Equations 1, 2 or 3, and then apply Procedures 1 to improve the best trial solution in  $P_0$ . Set the generation counter  $t := 0$ .
- 3) **Parent Selection.** Select an intermediate population  $\hat{P}_t$  from the current population  $P_t$  using the linear ranking selection.
- 4) **Crossover.** Apply the standard one-point crossover to chromosomes in  $\hat{P}_t$ , and update  $\hat{P}_t$ .
- 5) **Mutation.** Apply the standard uniform mutation to chromosomes in  $\hat{P}_t$ , and update  $\hat{P}_t$ .
- 6) **Survival Selection.** Evaluate the fitness function of all generated children in the updated  $\hat{P}_t$ , and set  $P_{t+1} = \hat{P}_t$ . If the best solution in  $P_{t+1}$  is worse than the best solution in  $\hat{P}_t$ , then replace the worst solution in  $\hat{P}_{t+1}$  by the best solution in  $\hat{P}_t$ .
- 7) **Local Search.** Apply Procedure 1 to improve the  $s^{best}$ , update *WEDS*.
- 8) **Filtering.** If  $s^{best}$  represents a weight edge dominating set, then apply Procedure 2 to improve it, update *WEDS*.
- 9) **Stopping Condition.** If  $t > g_{max}$ , then terminate. Otherwise, set  $t := t + 1$ , and go to Step 3.

#### IV. NUMERICAL EXPERIMENTS

The MAFS algorithm was programmed using MATLAB. In this experimental section, we technically discuss the

implementation of the MAFS code as well as its results. This section also shows how the test graphs used in the numerical simulations are generated.

### A. Graph Generation

In order to measure the performance of MAFS we apply it on number of graphs with different sizes. The previous works in solving MWEDS did not implemented for special types of graphs. Thus, the graphs which we used in our experiments are randomly generated with a known edge domination number  $\hat{\gamma}(G)$  and optimal total weight  $op_w$ . The following algorithm describe how these graphs are constructed.

#### Algorithm 4: (Graph Generation)

- 1) Set the maximum number of edges  $max_E = n_V \times (n_V - 1)/2$ , and the number of edges  $n_E = max_E \times d$ , where  $d$  is the density of edges in the graph which is set to be in  $(0, 1)$ , and  $n_V$  is the number of vertices.
- 2) Divide the vertices into two groups:
  - $V_{ED}$  with size equal to  $\hat{\gamma}(G) \times 2$ , and has vertices incident to dominant edges. Therefore, each pair of them is connected.
  - $V_E$  with size equal to  $n_V - (\hat{\gamma}(G) \times 2)$ , and has vertices not incident to dominant edges.
- 3) Add edges to connect the graph vertices to reach the edge density  $d$ . This edge adding process should satisfy the following condition in order to maintain the edge domination number equal to  $\hat{\gamma}(G)$ .
  - No edge connects two vertices belong to different pairs in  $V_{ED}$ .
- 4) Set the weights  $w_e$  randomly for each edge in  $G$  such that  $0 < w_e \leq l_1$  for each dominant edge and  $l_1 < w_e \leq l_2$  for the remaining edges.

In our numerical experiments, the parameters  $l_1$  and  $l_2$  is set equal to  $\hat{\gamma}(G)$  and  $n_E$ , respectively.

MAFS was applied to 15 instances of MWEDS problems created from the five graphs G1-G5, see Table I. These three graphs generated randomly with a number  $n_V$  of vertices and different number  $n_E$  of edges depending on the density number  $d$  for each instance. For each problem instance, the edge domination number  $\hat{\gamma}(G)$  and the optimal total weight  $op_w$  was known and the code was run 10 times.

### B. Parameter Setting

Table II summarizes all parameters setting used in MAFS with their assigned values. These chosen values are based on our numerical experiments.

### C. Comparison Results

In this section, we study the performance comparison of the proposed MAFS with three fitness functions that we introduce in Equations 1, 2 and 3. We have two comparison results, the first comparison of MAFS with  $(fit_1)$  against MAFS with  $(fit_2)$ , and the results of this comparison are reported in Table

TABLE I. TEST PROBLEMS

Test graphs	$n_V$	$n_E$	$d$	$\hat{\gamma}(G)$	$op_w$
$G_{0.1}^{20}$	20	19	0.1	4	4
$G_{0.3}^{20}$	20	57	0.3	4	4
$G_{0.5}^{20}$	20	95	0.5	4	4
$G_{0.1}^{30}$	30	44	0.1	8	8
$G_{0.3}^{30}$	30	131	0.3	8	8
$G_{0.5}^{30}$	30	218	0.5	8	8
$G_{0.1}^{50}$	50	123	0.1	15	15
$G_{0.3}^{50}$	50	368	0.3	15	15
$G_{0.5}^{50}$	50	613	0.5	15	15
$G_{0.1}^{100}$	100	495	0.1	28	28
$G_{0.3}^{100}$	100	1485	0.3	28	28
$G_{0.5}^{100}$	100	2475	0.5	28	28
$G_{0.1}^{200}$	200	1990	0.1	46	46
$G_{0.3}^{200}$	200	5970	0.3	46	46
$G_{0.5}^{200}$	200	9950	0.5	46	46

TABLE II. MAMEDS PARAMETER SETTING

Parameter	Definition	Value
$P_{size}$	Population size	100
$p_c$	Crossover probability	0.8
$p_m$	Mutation probability	0.01
$n_{EDS}$	Max number of the best weight edge dominating sets used to update WEDS	10
$g_{max}$	Max number of generations	100

III. The second performance comparison of MAFS with  $(fit_2)$  against MAFS with  $(fit_3)$ , and the results of this comparison are reported in Table IV. To measure the performance of each method, two quantities are used in the comparisons which are computed as follows.

- 1) *Average Number (Ave.)*. This measure gives the average of the optimal solution values found in the independent runs.
- 2) *Rate Number (rate)*. The rate shows how many times MAFS acquires an optimal solution  $op_w$ .

1) *Performance Comparison of MAFS with  $(fit_1)$  and  $(fit_2)$* : The results of this comparison are reported in Table III. The results show that MAFS with  $(fit_1)$  could not acquire the optimal total weight  $op_w$  for all instances of the MWEDS problem especially when the number of edges increased proportionally with the graph size. MAFS with  $(fit_2)$  achieve significant improvement in the average results and in acquiring the optimal total weight  $op_w$  for all instances. However it has a low rate (*rate*) for instances with large number of edges.

2) *Performance Comparison of MAFS with  $(fit_2)$  and  $(fit_3)$* : In this comparison, we compared MAFS with  $(fit_2)$  against MAFS with  $(fit_3)$ . The results of this comparison are reported in Table IV. To achieve the best performance of the MAFS, the  $fit_2$  was moderated by adding weights  $\alpha$ , and  $(1 - \alpha)$  to get a new fitness function  $fit_3$  in 3. The weight parameters  $\alpha$  is set equal to 0.4, which is used to efficiently trade-off between the trail solutions. The comparison results confirm a superior performance of MAFS with  $fit_3$  in both terms (*Ave.*) and (*rate*) against the other two fitness functions.

In Table V the instances generated by algorithm 4 with modifications in the role of edge weights such that the dominant edges assigned weights  $w_e$  from  $\{1, 2, \dots, \hat{\gamma}(G)\}$ , and for the remaining edges the set  $\{\hat{\gamma}(G) + 1, \hat{\gamma}(G) + 2, \dots, \hat{\gamma}(G) + 30\}$ . MAFS with  $fit3$  applied for these instances. The results show that when the dominant edges have different weights

TABLE III. RESULTS OF MAFS ON G1-G5 USING TWO FITNESS FUNCTIONS  $fit_1$  AND  $fit_2$

Graph no	$n_E$	MAFS with $fit_1$			MWEDS with $fit_2$		
		$op_w$	Ave.	rate	$op_w$	Ave.	rate
$G_{0.1}^{20}$	19	4	4	10	4	4	10
$G_{0.3}^{20}$	57	4	4	10	4	4	10
$G_{0.5}^{20}$	95	4	4	10	4	4	10
$G_{0.1}^{30}$	44	8	18.5	3	8	10.8	9
$G_{0.3}^{30}$	131	8	36.9	4	8	9.2	8
$G_{0.5}^{30}$	218	8	40.2	1	8	9.2	8
$G_{0.1}^{50}$	123	15	146	3	15	25.2	6
$G_{0.3}^{50}$	368	15	180	0	15	33.9	3
$G_{0.5}^{50}$	613	15	197	0	15	32.2	4
$G_{0.1}^{100}$	495	28	169	1	28	42.9	4
$G_{0.3}^{100}$	1485	28	187	1	28	47.2	4
$G_{0.5}^{100}$	2475	28	210.9	0	28	50	3
$G_{0.1}^{200}$	1990	46	270	0	46	115	1
$G_{0.3}^{200}$	5970	46	320	0	46	132.2	2
$G_{0.5}^{200}$	9950	46	536	0	46	197	2

TABLE IV. RESULTS OF MAFS ON G1-G5 USING TWO FITNESS FUNCTIONS  $fit_2$  AND  $fit_3$

Graph no	$n_E$	MAFS with $fit_2$			MAFS with $fit_3$		
		$op_w$	Ave.	rate	$op_w$	Ave.	rate
$G_{0.1}^{20}$	19	4	4	10	4	4	10
$G_{0.3}^{20}$	57	4	4	10	4	4	10
$G_{0.5}^{20}$	95	4	4	10	4	4	10
$G_{0.1}^{30}$	44	8	10.8	9	8	8	10
$G_{0.3}^{30}$	131	8	9.2	8	8	8	10
$G_{0.5}^{30}$	218	8	9.2	8	8	8	10
$G_{0.1}^{50}$	123	15	25.2	6	15	15	10
$G_{0.3}^{50}$	368	15	33.9	3	15	15	10
$G_{0.5}^{50}$	613	15	32.2	4	15	15	10
$G_{0.1}^{100}$	495	28	42.9	4	28	28	10
$G_{0.3}^{100}$	1485	28	47.2	4	28	28	10
$G_{0.5}^{100}$	2475	28	50	3	28	28	10
$G_{0.1}^{200}$	1990	46	115	1	46	46	10
$G_{0.3}^{200}$	5970	46	132.2	2	46	46	10
$G_{0.5}^{200}$	9950	46	197	2	46	46	10

and near of that in non dominant edges the solutions will be more difficult to be acquired in every time. Moreover, the MAFS method exhibits very promising performance to obtain MWEDS of graphs.

### V. CONCLUSION

The minimum weight edge dominating set problem in graph theory has been studied in this paper. We proposed a memetic-based method to solve this problem called Memetic Algorithm with Filtering Scheme (MAFS). Intensification

TABLE V. RESULTS OF MAFS ON G1-G5 USING FITNESS FUNCTIONS  $fit_3$

Graph no	$n_E$	$op_w$	Ave.	rate
$G_{0.1}^{20}$	19	10	10	10
$G_{0.3}^{20}$	57	10	10	10
$G_{0.5}^{20}$	95	10	10	10
$G_{0.1}^{30}$	44	36	36	10
$G_{0.3}^{30}$	131	36	36.8	9
$G_{0.5}^{30}$	218	36	36.5	7
$G_{0.1}^{50}$	123	120	121.8	8
$G_{0.3}^{50}$	368	120	122.5	7
$G_{0.5}^{50}$	613	120	127.8	8
$G_{0.1}^{100}$	495	406	420	8
$G_{0.3}^{100}$	1485	406	427.8	8
$G_{0.5}^{100}$	2475	406	433.8	7
$G_{0.1}^{200}$	1990	1081	1150	7
$G_{0.3}^{200}$	5970	1081	1220	8
$G_{0.5}^{200}$	9950	1081	1300	6

scheme used beside the genetic and local search methodologies in order to achieve better performance. Three new fitness functions invoked to maximize the performance of the proposed method. These fitness functions consider different ways to balance between two objectives; edge dominating and weight minimizing. Specifically, two of these fitness functions use absolute additions of valued functions that measure the considered objectives while the third one uses a weighted addition way. Numerical experiments of MAFS using the three fitness functions on various test graphs show that the MAFS with a weighted fitness function outperform the MAFS with the other two fitness functions. In addition, the proposed method show very promising performance to obtain minimum weighted edge dominating sets for different graphs used in the numerical experiments.

### REFERENCES

- [1] James E. Baker. Adaptive selection methods for genetic algorithms. In *Proceedings of the 1st International Conference on Genetic Algorithms*, pages 101–111, Hillsdale, NJ, USA, 1985. L. Erlbaum Associates Inc.
- [2] Christian Blum and Andrea Roli. Metaheuristics in combinatorial optimization: Overview and conceptual comparison. *ACM Computing Surveys (CSUR)*, 35(3):268–308, 2003.
- [3] Lance D Chambers. *Practical handbook of genetic algorithms: complex coding systems*, volume 3. CRC press, 2010.
- [4] Zhifang Feng, Wensheng Li, Huaming Xing, and Qiongyu Ma. On the upper bounds of local inverse signed edge domination numbers in graphs. In *Information Computing and Applications*, pages 368–372. Springer, 2012.
- [5] Henning Fernau. Edge dominating set: Efficient enumeration-based exact algorithms. In *Parameterized and Exact Computation*, pages 142–153. Springer, 2006.
- [6] Fedor V Fomin, Serge Gaspers, Saket Saurabh, and Alexey A Stepanov. On two techniques of combining branching and treewidth. *Algorithmica*, 54(2):181–207, 2009.
- [7] Fedor V Fomin, Serge Gaspers, Saket Saurabh, and Alexey A Stepanov. On two techniques of combining branching and treewidth. *Algorithmica*, 54(2):181–207, 2009.
- [8] Fedor V Fomin, Fabrizio Grandoni, and Dieter Kratsch. Measure and conquer: domination—a case study. In *Automata, Languages and Programming*, pages 191–203. Springer, 2005.
- [9] Toshihiro Fujito and Hiroshi Nagamochi. A 2-approximation algorithm for the minimum weight edge dominating set problem. *Discrete Applied Mathematics*, 118(3):199–207, 2002.
- [10] Michael R Garey and David S Johnson. *Computers and intractability*, volume 174. freeman New York, 1979.
- [11] Teresa W Haynes, Stephen T Hedetniemi, and Peter J Slater. *Domination in graphs: advanced topics*, volume 40. Marcel Dekker New York, 1998.
- [12] Teresa W Haynes, Stephen T Hedetniemi, and Peter JB Slater. *Fundamentals of Domination in Graphs*, volume 208. CRC Press/ Llc, 1998.
- [13] Abdel-Rahman Hedar and Masao Fukushima. Minimizing multimodal functions by simplex coding genetic algorithm. *Optimization Methods and Software*, 18(3):265–282, 2003.
- [14] Abdel-Rahman Hedar and Rashad Ismail. Hybrid genetic algorithm for minimum dominating set problem. In *Computational Science and Its Applications—ICCSA 2010*, pages 457–467. Springer, 2010.
- [15] Francisco Herrera, Manuel Lozano, and Jose L. Verdegay. Tackling real-coded genetic algorithms: Operators and tools for behavioural analysis. *Artificial intelligence review*, 12(4):265–319, 1998.
- [16] Tiago Januario, Sebastián Urrutia, Belo Horizonte, and Minas Gerais-Brazil. An edge coloring heuristic based on vizings theorem. In *Sejam bem-vindos aos pr-anais XVI CLAIO*. Conference Proceedings, 2012.
- [17] Pablo Moscato, Carlos Cotta, and Alexandre Mendes. Memetic algorithms. In *New optimization techniques in engineering*, pages 53–85. Springer, 2004.

- [18] Ojas Parekh. *Polyhedral techniques for graphic covering problems*. PhD thesis, Department of Mathematical Science, Carnegie Mellon University, 2002.
- [19] El-Ghazali Talbi. *Metaheuristics: from design to implementation*, volume 74. Wiley, 2009.
- [20] Onur Ugurlu. New heuristic algorithm for unweighted minimum vertex cover. In *IV International Conference "Problems of Cybernetics And Informatics"*. Conference Proceedings, 2012.
- [21] Johan MM Van Rooij and Hans L Bodlaender. Exact algorithms for edge domination. In *Parameterized and Exact Computation*, pages 214–225. Springer, 2008.
- [22] Jianxin Wang, Beiwei Chen, Qilong Feng, and Jianer Chen. An efficient fixed-parameter enumeration algorithm for weighted edge dominating set. In *Frontiers in Algorithmics*, pages 237–250. Springer, 2009.
- [23] Mingyu Xiao and Hiroshi Nagamochi. A refined exact algorithm for edge dominating set. In *Theory and Applications of Models of Computation*, pages 360–372. Springer, 2012.
- [24] Mihalis Yannakakis and Fanica Gavril. Edge dominating sets in graphs. *SIAM Journal on Applied Mathematics*, 38(3):364–372, 1980.
- [25] Yancai Zhao, Lianying Miao, Haichao Wang, and Wenyao Song. Maximal matching and edge domination in complete multipartite graphs. *International Journal of Computer Mathematics*, (to appear), 2013.